



Cambrian–Ordovician magmatism of the Ikh-Mongol Arc System exemplified by the Khantaishir Magmatic Complex (Lake Zone, south-central Mongolia)



Vojtěch Janoušek ^{a,*}, Yingde Jiang ^b, David Buriánek ^a, Karel Schulmann ^a, Pavel Hanžl ^a, Igor Soejono ^{a,c}, Alfred Kröner ^{d,e}, Battushig Altanbaatar ^f, Vojtěch Erban ^a, Ondrej Lexa ^c, Turbat Ganchuluun ^g, Jan Košler ^{h,1}

^a Czech Geological Survey, Klárov 3, 118 21 Prague 1, Czech Republic

^b State Key Laboratory of Isotope Geochemistry, Guangzhou Institute of Geochemistry, Chinese Academy of Sciences, Guangzhou 510640, China

^c Institute of Petrology and Structural Geology, Charles University, Albertov 6, 128 43 Prague 2, Czech Republic

^d Department of Geosciences, University of Mainz, D-55099 Mainz, Germany

^e Beijing SHRIMP Centre, Chinese Academy of Geological Sciences, 26 Baiwanzhuang Road, 100037 Beijing, China

^f Institute of Paleontology and Geology, Mongolian Academy of Sciences, P.O. Box 45/650, Ulaanbaatar 15160, Mongolia

^g School of Geology and Mining Engineering, MUST, P.O. Box 654, Ulaanbaatar, Mongolia

^h Department of Earth Science, University of Bergen, Allégaten 41, 5007 Bergen, Norway

ARTICLE INFO

Article history:

Received 6 December 2016

Received in revised form 17 August 2017

Accepted 12 October 2017

Available online 18 October 2017

Handling Editor: S.J. Liu

Keywords:

Subduction

Lake Zone

Whole-rock geochemistry

Zircon dating

Ikh-Mongol Arc System

ABSTRACT

The Khantaishir Magmatic Complex (KMC) (south-central Mongolia) exposes a section of a magmatic system consisting of deep crustal, ultramafic cumulates (coarse-grained Amp gabbros and hornblendites; c. 0.35–0.5 GPa) to shallower crustal levels dominated by Amp–Bt tonalites (c. 0.1–0.2 GPa). The magmatic rocks were emplaced during most of the Cambrian (c. 538–495 Ma) and are mostly geochemically primitive (Mg# ~50), Na-rich and metaluminous. The (normal-) calc-alkaline signature and characteristic trace-element enrichment in hydrous-fluid mobile large-ion lithophile elements (LILE) relative to high-field strength elements (HFSE) suggest an origin within a magmatic arc. Multiple intrusions of basic magma derived from a subduction-modified depleted mantle developed by fractional crystallization and/or accumulation of (Ol, Cpx) Amp + Bt, later joined by Pl. Magma mixing with, or without, exchange of xenocrysts between compositionally dissimilar melt batches was also important. Over time, partial melting of older, lower crustal metabasic rocks became increasingly significant, again with a strong subduction signature. The lack of zircon inheritance in the magmatic products and rather high zircon ε_{Hf}^t values (all >+3, but for most samples >+8) as well as whole-rock Sr–Nd isotopic compositions imply that the arc was not founded on mature continental crust. It was probably located at the margin of the Baydrag microcontinent, dominated by accreted metabasic rocks of an older (early Tonian?) island arc covered by a thin layer of subordinate metasediments containing detrital zircons with Tonian and ill-defined Palaeoproterozoic ages. The KMC represents a small vestige of an extensive Cambrian–Ordovician subduction system (termed here the Ikh-Mongol Arc System), bordering the western margin of a chain of Precambrian microcontinents (Tuva-Mongolia, Zabkhan and Baydrag) that, together with accreted Neoproterozoic marginal basins (the Lake Zone), defines the external part of the Mongolian orocline.

© 2017 International Association for Gondwana Research. Published by Elsevier B.V. All rights reserved.

1. Introduction

The timescales and key mechanism(s) driving crustal growth are of fundamental geotectonic importance and thus justly a subject of heated debate in the current literature. The inferred composition of the average continental crust – in particular its intermediate silica contents, calc-

alkaline chemistry and characteristic strong enrichment of Large Ion Lithophile Elements (LILE) relative to the High Field Strength Elements (HFSE) – resembles that of many Phanerozoic magmatic arcs (e.g., Rudnick and Gao, 2003; Taylor and McLennan, 2009; Weaver and Tarney, 1984). This is taken as evidence that at least post-Archaean continental crustal growth occurred mainly in such arcs (e.g., Jagoutz and Schmidt, 2012; Kelemen, 1995), an idea that is still a matter of discussion, though (Condie and Kröner, 2013).

The average crust is relatively siliceous (andesitic ± dacitic: see Taylor and McLennan, 2009 for review) and poor in ferromagnesian

* Corresponding author.

E-mail address: vojtech.janousek@geology.cz (V. Janoušek).

¹ Deceased.

components (Rudnick and Gao, 2003; Taylor, 1967; Taylor and McLennan, 1995). However, the net juvenile input into arcs, as a product of partial melting of mantle peridotite, would be characterized by low SiO₂, high FeOt + MgO, and Mg#, i.e. significantly different from bulk continental crust estimates. This so-called ‘continental crust paradox’ has attracted explanations that can be subdivided into two broad groups (Castro et al., 2013; Jagoutz and Kelemen, 2015; Tatsumi, 2005).

The first group of models invokes rather silicic, high-Mg andesitic parental magmas (Taylor, 1967). These can be generated by slab melting (Rapp et al., 2010; Yogodzinski et al., 2001), by partial melting of previously depleted, but subsequently metasomatised, hydrous mantle peridotite (Grove et al., 2012), or by reaction between ascending melts and mantle peridotite (Kelemen, 1995). From mantle domains contaminated by subducted oceanic crust the material can be transported into the melting region by mixed mantle wedge diapirs (Castro and Gerya, 2008; Castro et al., 2013).

The second possibility is that some additional open-system process comes into play, transforming the primary basaltic magma into andesitic/dacitic continental crust:

- (1) Hybridization between a mafic melt and crustally-derived felsic magma, including the early metabasic products of arc activity melted by subsequent basaltic injections (Annen et al., 2006; Atherton and Petford, 1993; Huppert and Sparks, 1988). Arcs often provide ample evidence for the operation of magma mixing/mingling in the form of variously hybrid mafic enclaves or larger igneous units, whole-rock geochemical and isotopic variation as well as microtextural record for chemical and thermal disequilibria and exchange of xenocrysts (Didier and Barbarin, 1991a; Bateman, 1995; Hibbard, 1995; Janoušek et al., 2004; Wiebe, 1996).
- (2) Extensive fractionation of basaltic magma or partial melting of metabasic lower crust produces hydrous melts which have low viscosity and thus ascend to shallower crustal levels (e.g., Annen et al., 2006; Lee and Bachmann, 2014). These two processes are inevitably connected with formation of dense mafic cumulates or basic granulitic residua dominated by hornblende, clinopyroxene ± garnet. The mass balance requires subsequent foundering of the lowermost, garnet-bearing crust into the asthenospheric mantle (Arndt and Goldstein, 1989; Jagoutz and Behn, 2013; Kay and Kay, 1993; Lee and Anderson, 2015; Zandt et al., 2004).
- (3) Relamination of deeply recycled felsic crustal material at the bottom of the arc crust (Castro et al., 2013; Hacker et al., 2011, 2015; Kelemen and Behn, 2016; Schulmann et al., 2014). Such recycling may include subduction of sediments deposited on the oceanic slab, arc/forearc subduction, subduction erosion of the overriding plate and deep underplating of felsic continental crust during continent–continent collision (Carswell and Compagnoni, 2003; Dobrzhinetskaya et al., 2011; Chopin, 1984; Hacker et al., 2011). However, the significance, applicability and details of the crustal relamination model still largely remain to be investigated (Dymkova et al., 2016; Guy et al., 2015; Kusbach et al., 2015; Maierová et al., 2016).

The gigantic (c. 9 mil. km²) Central Asian Orogenic Belt (CAOB) represents the product of unprecedented late Mesoproterozoic–Phanerozoic continental growth, the exact mechanism of which is still poorly understood (e.g., Kröner et al., 2014; Xiao and Santosh, 2014). In any case, Neoproterozoic to Carboniferous magmatic arcs form an essential component of the CAOB (Şengör and Natal'ın, 1996) and have been variably interpreted as Andean-type or purely intra-oceanic (Kröner et al., 2014; Xiao et al., 2015). These giant magmatic units are of great interest as they can be used to characterize the plate configuration, polarity and spatio-temporal evolution of migrating Palaeo-Asian subduction zones (Şengör et al., 1993; Wilhem et al., 2012; Windley et al., 2007).

This paper deals with Cambrian magmatic arc rocks located in the Lake Zone of Mongolia (Fig. 1a), a region critical for the Neoproterozoic to early Palaeozoic evolution of the CAOB. We describe a more or less continuous section from deep crustal ultramafic cumulates to shallower arc levels, built by quartz diorites to tonalites in the eastern Khantaishir Range (south-central Mongolia, Fig. 1b). Moreover, we present petrological, whole-rock geochemical and Sr–Nd isotopic data, as well as *in-situ* zircon U–Pb and Hf isotopic data. These datasets are integrated to provide an insight into the nature, likely petrogenesis and geotectonic setting of the arc magmas.

The Khantaishir Magmatic Complex (KMC) provides an excellent opportunity to study the important Cambrian period of arc-related magmatism and crustal growth in the Mongolian CAOB as well as the anatomy and internal workings of immature continental magmatic arcs in general. We demonstrate that the Khantaishir Magmatic Complex forms a part of the largest arc system in the Mongolian and Russian tracts of the CAOB, termed here the Ikh-Mongol Arc System. Its character varies from Andean-type to purely intra-oceanic along the strike of the Tuva–Mongolian continental ribbon (Yakubchuk, 2004) (Fig. 1a).

2. Geological setting

2.1. Central Asian Orogenic Belt (CAOB)

The CAOB (Mossakovskiy et al., 1994; Yanshin, 1965) developed between the Siberian, Tarim and Sino-Korean blocks in latest Mesoproterozoic to early Triassic times (Fig. 1a) (e.g., Dergunov, 2001; Şengör et al., 1993; Xiao et al., 2009a). The Mongolian tract of the CAOB formed by accretion of Neoproterozoic, Cambrian, Ordovician and Devonian–Carboniferous arcs, back-arcs and accretionary wedges (Badarch et al., 2002; Kröner et al., 2007; Lamb and Badarch, 2001; Windley et al., 2007) to Archaean to early Tonian microcontinents (Tuva–Mongolian, Zabkhan, and Baydrag) (Bold et al., 2016; Buriánek et al., 2017; Demoux et al., 2009a; Kozakov et al., 2007; Kuzmichev et al., 2001; Rojas-Agramonte et al., 2011). This so-called Mongolian collage (Xiao et al., 2015) is thought to having been shaped by three major accretionary events: the late Proterozoic and early Palaeozoic, forming a tectonic province in the north, and the Late Devonian to Early Carboniferous, during which vast oceanic domains evolved in the south (Xiao et al., 2004; Zonenshain, 1973; Zonenshain et al., 1976).

In detail, the Mongolian collage consists of several Precambrian continental fragments of both Siberian (Barguzin; Gladkochub et al., 2008) and Gondwanan (Tuva Mongol, Zavkhan, Baydrag and Erguna, Parfenov et al., 2003) provenance that have been amalgamated to the north-eastern margin of Siberian Continent during Baikalian orogenic cycle at 560–540 Ma (Dobretsov et al., 2003). The intervening oceanic domains were accreted to both Siberian margin and to Precambrian fragments in form of several ophiolite sheets and accretionary oceanic arc complexes forming the Lake Zone (Khain et al., 2003; Kovach et al., 2011). Altogether, thus freshly formed Mongolian collage was affected by ca. 500 Ma magmatic and HT/LP metamorphic event during the second, late Cambrian–early Ordovician cycle (Dobretsov et al., 2003; Kozakov et al., 2015). The Devono–Carboniferous orogenic cycle represented a specific accretionary convergent event that was responsible for shortening of external oceanic units (Lehmann et al., 2010). It is only later (in Carboniferous to Permian times) when the whole system was rotated clockwise to the current position, together with opening of the Mongol–Okhotsk Ocean (Domeier and Torsvik, 2014) and formation of Mongolian ribbon continent orthogonal to the Siberian margin (Zorin, 1999). Finally, in Permian to Jurassic the whole Mongolian ribbon system was compressed in between jaws of Siberian and North China cratons in course of the Mongol–Okhotsk oceanic basin closure (Lehmann et al., 2010).

The early Cambrian accretion in the CAOB could be interpreted as a consequence of thrusting of oceanic fragments of Neoproterozoic age over the southern margin of the Siberian Craton (Khain et al., 2003) or accretion of Neoproterozoic ophiolitic sequences onto the peri-Siberian

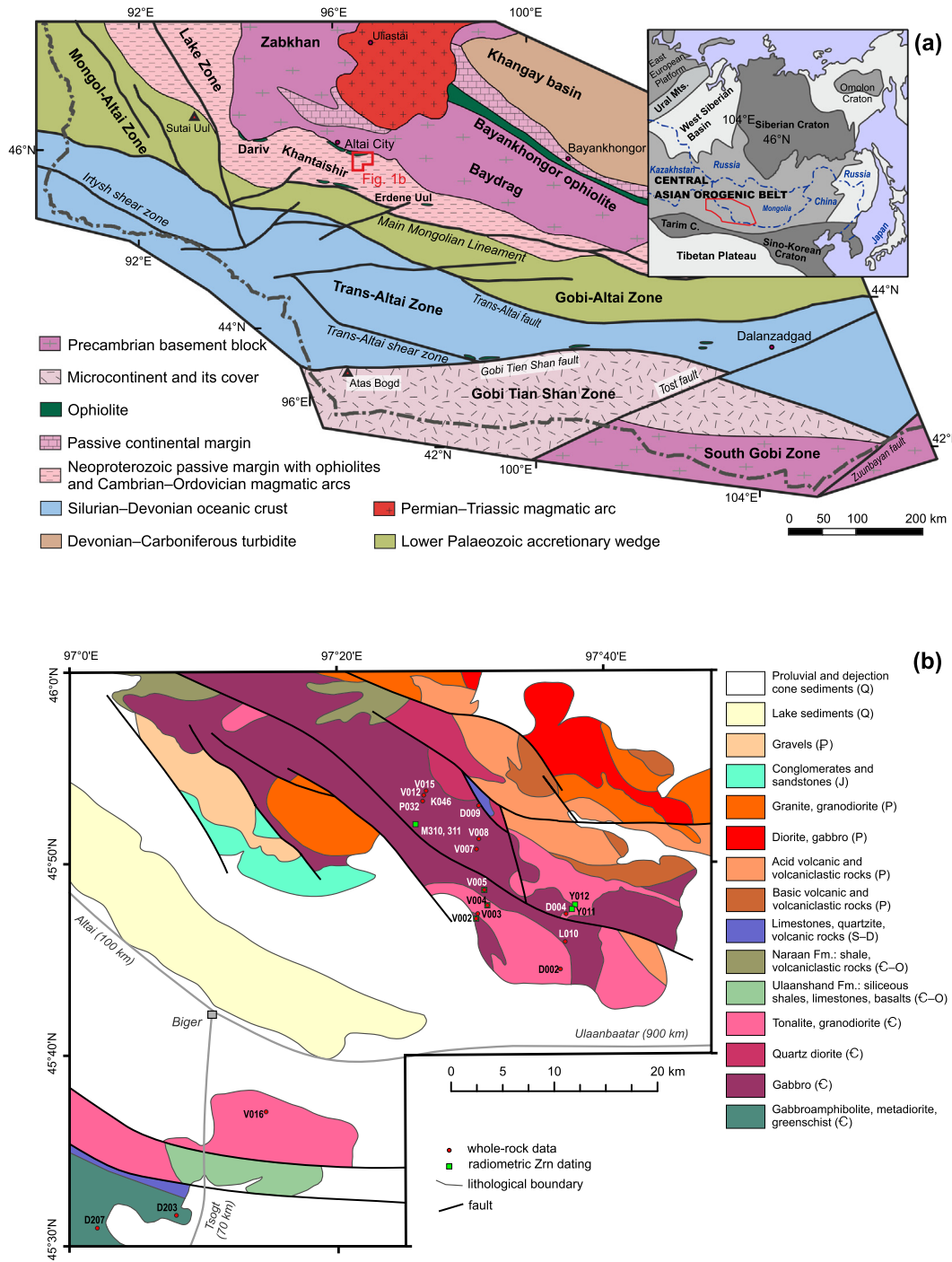


Fig. 1. (a) – Simplified map of the major tectonic zones of SW Mongolia with location of the study area. Inset shows location of the CAOB in the frame of adjacent tectonic elements. Modified from Kröner et al. (2010) and Buriánek et al. (2017). (b) – Geological sketch map of the Khantaishir Magmatic Complex based on Czech Geological Survey field work with sample locations shown.

Tuva–Mongolian continental ribbon (Domeier and Torsvik, 2014; Štípká et al., 2010). In any case, this event hallmark the onset of convergence between the “Palaeo-Asian” oceanic plate and the Siberian Continent after break-up of the Rodinia supercontinent (Domeier and Torsvik, 2014; Wilhem et al., 2012). A relatively well preserved early Palaeozoic suture is represented by isolated occurrences of ophiolitic sequences in central Kazakhstan (Khain et al., 2003), the Gorny Altai of Russia (Buslov and De Grave, 2015; Volkova and Sklyarov, 2007; Wilhem et al., 2012), and in the Lake Zone of northwestern and south-central Mongolia (Jian et al., 2014 and references therein).

2.2. Lake Zone

The Lake Zone is a narrow, continuous belt decorating the western and southern rims of the Zabkhan and Baydrag microcontinents; its southern boundary with the late Palaeozoic units of the Gobi Altai and Mongolian Altai ranges is known as the Main Mongolian Lineament (Badarch et al., 2002; Marinov et al., 1973). The Lake Zone was interpreted by Badarch et al. (2002) as a Neoproterozoic accretionary wedge (Kovach et al., 2011 Windley et al., 2007) composed of volcanic, volcano-sedimentary and sedimentary sequences with

imbricated ophiolitic remnants (Buchan et al., 2002; Dijkstra et al., 2006; Jian et al., 2014; Zonenshain and Kuzmin, 1978).

The Dariv ophiolite has been dated as late Neoproterozoic using the U-Pb and Pb-Pb methods on zircon: 571 ± 4 Ma (Khain et al., 2003), 573 ± 6 Ma (Kozakov et al., 2002) and 515 ± 8 Ma (Dijkstra et al., 2006). Recent SHRIMP dating of zircon yielded $^{206}\text{Pb}/^{238}\text{U}$ ages of 568 ± 5 Ma, 567 ± 4 Ma, 560 ± 8 Ma (Jian et al., 2014). Likewise, the plagiogranites from the Khantaishir ophiolite gave U-Pb and Pb-Pb zircon ages of 568 ± 4 Ma (Khain et al., 2003), 573 ± 8 Ma and 566 ± 7 Ma (SHRIMP $^{206}\text{Pb}/^{238}\text{U}$ ages of Jian et al., 2014).

During the early Cambrian, the ophiolites were thrust over the continental basement in the hanging wall of eclogitic units (Štípká et al., 2010), described from the Zambyn Nuruu (Buriánek et al., 2017) and the Dariv (Dijkstra et al., 2006) mountain ranges. These high-pressure units are interpreted as remnants of subduction channels which sampled a sedimentary matrix scraped off the Ediacaran to early Cambrian cover of the Baydrag and Zabkhan continental blocks (Buriánek et al., 2017). The related phengite-bearing foliation in eclogite and high-pressure fabrics in the associated metapelites yielded $^{40}\text{Ar}/^{39}\text{Ar}$ cooling ages of c. 540 Ma (Štípká et al., 2010), timing the overthrusting. In any case, thrusting took place before intrusion of a syn- to post-tectonic diorite in the Dariv ophiolite, dated at 514.7 ± 7.6 Ma (U-Pb SHRIMP on zircon, Dijkstra et al., 2006).

Deformed but unmetamorphosed upper Cambrian to Ordovician siliciclastic sequences rest upon the metamorphic rocks and ophiolites in the Erdene Uul-Zambyn Nuruu area (Hrdličková et al., 2010; Kröner et al., 2010).

The Lake Zone is characterized by an abundance of mostly Cambrian mafic to intermediate plutons which can be traced from the Zambyn Nuruu Range (Buriánek et al., 2017) towards the NW to the Khantaishir (Matsumoto and Tomurtagoo, 2003 and the current paper) and the Dariv ranges (Dijkstra et al., 2006), where they were described as ophiolite-related (Jian et al., 2014). Exposures of Cambrian to Ordovician plutons in the northwestern continuation of the Lake Zone were reported, among others, by Rudnev et al. (2009, 2013b), Yarmolyuk et al. (2011) and Soejono et al. (2016). However, Cambrian arc-related magmatic complexes are also known from the underlying continental blocks (e.g., Sal'nikova et al., 2001).

3. Materials and methods

Please note that this is just an abbreviated version focusing mostly on data interpretation; full analytical details are given in the Electronic Appendix 1.

3.1. Sampling, petrology and mineral chemistry

The studied magmatic complex was described in the eastern Khantaishir Mountain Range (NE of Biger, southern-central Mongolia, Fig. 1b) during the Czech Geological Survey (CGS) expedition in 2012. Twenty-four samples of the major igneous rock types selected for petrological study are listed in Electronic Appendix 2, and their locations are shown in Fig. 1b.

Electron-microprobe analyses (EMPA) were performed using the Cameca SX-100 instrument at Masaryk University (Brno, Czech Republic). The empirical formulae of feldspars and micas were recalculated to 8 and 22 oxygen atoms, respectively. The amphibole formulae were obtained on the basis of 23 oxygen atoms (Leake et al., 1997). The $\text{Fe}^{2+}/\text{Fe}^{3+}$ ratios in amphiboles were estimated assuming the cation sum of 13 without Ca, Na and K (13 eCNK). Pyroxenes are classified according to Morimoto (1988); the formulae were obtained on the basis of 4 cations and the ferric iron estimated after Droop (1987). The abbreviations of the mineral names are taken from Whitney and Evans (2010).

3.2. Whole-rock geochemistry

In total, 19 whole-rock samples, each 5–10 kg in weight, were obtained in the field (see Fig. 1b for locations). After conventional crushing and homogenization, the powders produced in an agate mill were analyzed at ActLabs (Vancouver, Canada), using the 4Lithoresearch procedure (<http://www.actlabs.com>). Major-element concentrations were obtained by Inductively-Coupled Plasma Optical Emission Spectrometry (ICP-OES) and trace-element concentrations by Inductively-Coupled Plasma Mass Spectrometry (ICP-MS), following lithium metaborate/tetraborate fusion and weak nitric acid dissolution. Such a procedure ensures that the entire sample is digested, including refractory phases such as zircon and sphene.

Recalculation and plotting were facilitated using the R software package *GCDkit* (Janoušek et al., 2006). In this work, the Mg number ($\text{Mg}\#$) is defined as $100 \frac{\text{MgO}}{\text{FeO} + \text{MgO}} [\text{mol}\%]$ and the A/CNK index (Shand, 1943) as $\frac{\text{Al}_2\text{O}_3}{\text{CaO} + \text{Na}_2\text{O} + \text{K}_2\text{O}} [\text{mol}\%]$. For description of chondrite-normalized REE patterns serves the Eu/Eu^* ratio, reflecting the magnitude of the Eu anomaly ($\frac{\text{Eu}}{\text{Eu}^*} = \frac{\text{Eu}_N}{\sqrt{\text{Sm}_N \text{Gd}_N}}$), where N refers to concentrations normalized to chondritic abundances (Boynton, 1984). Moreover, their curvature is expressed using the Dy/Dy^* parameter (Davidson et al., 2013) defined as $\frac{\text{Dy}}{\text{Dy}^*} = \frac{\text{Dy}_N}{\text{La}_N^{4/13} \text{Yb}_N^{9/13}}$. The magnitude of the Ti anomaly on the NMORB-normalized plots is quantified by the Ti/Ti^* ratio. Note that while the overall philosophy of the Ti/Ti^* parameter calculation follows Davidson et al. (2013), our calculation formula is different: $\frac{\text{Ti}}{\text{Ti}^*} = \frac{\text{Ti}_N}{\text{Gd}_N^{4/5} \text{Sm}_N^{1/5}}$, where N refers to values normalized to average NMORB of Sun and McDonough (1989).

3.3. Whole-rock Sr-Nd isotopic compositions

Isotopic analyses of Sr and Nd were performed on a Finnigan MAT 262 thermal ionization mass spectrometer housed at CGS. The decay constants applied to age-correct the isotopic ratios are from Steiger and Jäger (1977 – Sr) and Lugmair and Marti (1978 – Nd). The ε_{Nd} values were obtained using Bulk Earth parameters of Jacobsen and Wasserburg (1980). In order to compensate for the effects of crystal accumulation upon the $^{147}\text{Sm}/^{144}\text{Nd}$ ratios, we calculated not only single-stage ($T_{\text{DM},1\text{stg}}^{\text{Nd}}$) but also two-stage Depleted Mantle Nd model ages ($T_{\text{DM},2\text{stg}}^{\text{Nd}}$), using the Depleted Mantle parameters and the general approach of Liew and Hofmann (1988). However, the $^{147}\text{Sm}/^{144}\text{Nd}$ ratio of the intermediate average reservoir has been set to 0.138 in order to better reflect the basic sources involved.

3.4. U-Pb geochronology

Except for samples M310 and M311, zircon dating used an ArF excimer 193 nm laser ablation system (Resolution M-50), coupled with a Nu Plasma HR MC-ICP-MS at the Department of Earth Sciences, University of Hong Kong, following the analytical procedure of Xia et al. (2011). The age calculations and concordia plots were performed using ISOPLOT (version 3.0, Ludwig, 2003). Individual analyses are presented with 1σ error in the concordia diagrams, and uncertainties in mean age calculations are quoted at the 95% level (2σ).

For measurement of U/Pb and Pb/Pb isotopic ratios in zircons from samples M310 and M311, a Thermo-Finnigan Element 2 sector field ICP-MS, coupled to a 193 ArF Excimer laser (Resonetech RESolution M50-LR) at Bergen University, Norway was used following the technique described by Košler et al. (2002). Details of raw data reduction and corrections are described in Košler et al. (2002) and Košler and Sylvester (2003). The calculations and plotting on concordia diagrams were done using Isoplot 4.15 (Ludwig, 2012).

3.5. Zircon Lu-Hf isotope analyses

In-situ zircon Lu-Hf isotopic analyses were carried out on a Neptune Plus multi-collector ICP-MS equipped with a Resolution M-50-LR laser-ablation system at the Guangzhou Institute of Geochemistry, Chinese Academy of Sciences. Detailed instrumental settings and analytical procedures were described by Zhang et al. (2015).

All Hf-in-zircon isotopic data were calculated with the decay constant of $1.867 \times 10^{-11} \text{ yr}^{-1}$ (Söderlund et al., 2004). The chondritic

values of $^{176}\text{Hf}/^{177}\text{Hf} = 0.282772$ and $^{176}\text{Lu}/^{177}\text{Hf} = 0.0332$ reported by Blichert-Toft and Albaréde (1997) were employed for the calculation of $\varepsilon_{\text{Hf}}^t$ values. The depleted-mantle evolution line is defined by present-day $^{176}\text{Hf}/^{177}\text{Hf}$ of 0.28325 and $^{176}\text{Lu}/^{177}\text{Hf}$ of 0.0384 (Griffin et al., 2000). A “crustal” Hf model age ($T_{\text{DM}}^{\text{HfC}}$) is considered to be more meaningful for the studied rocks than a depleted mantle model age. This model age ($T_{\text{DM}}^{\text{HfC}}$) was calculated separately for each zircon grain, assuming a mean basaltic $^{176}\text{Lu}/^{177}\text{Hf}$ ratio of 0.022 for the 2nd stage of the model (Lancaster et al., 2011). In the calculation, $^{206}\text{Pb}/^{238}\text{U}$ ages were

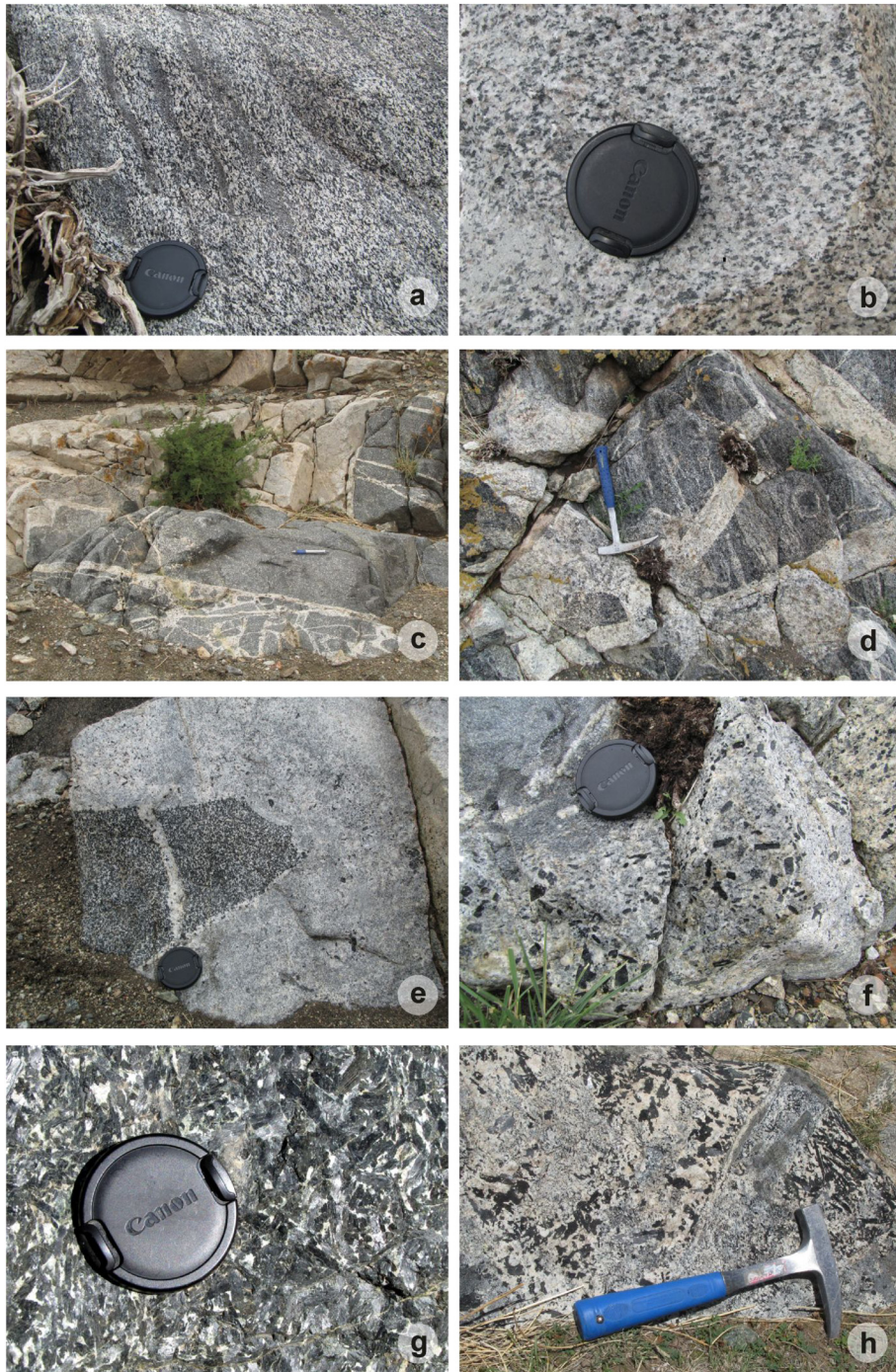


Fig. 2. (a) – Amp-Bt tonalite showing strong fabric and intensely deformed MME (site V008); (b) – Coarse-grained Amp leucodiorite (sample V004); (c) – Angular fragments of coarse-grained Amp quartz diorite to gabbro, net veined by felsic magma also Amp-bearing; the top-left part of the photo occupies a younger felsic dyke with a stepped contact (site V009); (d) – Angular xenoliths of cumulate quartz gabbros (sample V008a) showing distinct layering broken by, and enclosed in, fresh leucocratic intrusion, the latter also Amp-bearing; (e) – Large angular xenolith of coarse-grained Amp gabbro enclosed by Amp-Bt tonalite (site V008); (f) – Resorbed amphibole xeno/anecrusts in later intrusion of leucocratic Amp-Bt tonalite (sample V008c); (g) – Coarse-grained amphibole-dominated cumulate (site V012); (h) – Pegmatoid facies with unidirectional solidification structure, indicating strong undercooling (site V012).

used for analyses younger than 1.0 Ga, and $^{207}\text{Pb}/^{206}\text{Pb}$ ages for older grains.

4. Results

4.1. Structural setting and field relations

The Khantaishir Magmatic Complex (Fig. 1b) is exposed along both sides of the Cenozoic Biger Basin, in the central part of the Neoproterozoic accretionary wedge of the Lake Zone. It is underthrust southwards beneath the Palaeozoic volcano-sedimentary prism of the Gobi Altai Zone (Lehmann et al., 2010). All magmatic rocks show variably developed NNE–SSW trending, sub-vertical magmatic fabric defined by mafic minerals. The deepest gabbroic cumulates exhibit a weak shape-preferred orientation of amphiboles which is parallel to a locally strong mineral foliation developed in tonalites higher up in the section (Fig. 2a).

The KMC is mainly composed of several types of gabbro/hornblendite and, higher up in the sequence, quartz diorite and tonalite. Mingling textures are commonly observed between mafic and more felsic lithologies. Hybrid mafic microgranular enclaves (MME; Didier and Barbarin, 1991b) of variable shapes and sizes are locally abundant (Fig. 2a), whereas elsewhere the felsic rocks are pristine and homogeneous (Fig. 2b). The MME often cluster into monogenic enclave swarms (Didier and Barbarin, 1991b); rarely, load-cast structures were observed at the bottom of mafic layers along mafic/felsic interfaces (Wiebe and Collins, 1998; Žák et al., 2009). Some MME exhibit lobate contacts and/or chilled margins against their host; others contain xenocrysts derived from the surrounding granitoid such as mantled plagioclases and rapakivi K-feldspars (Hibbard, 1991, 1995).

The mafic rocks, hornblendites and hornblende gabbros, often display cumulate textures and conspicuous magmatic layering, pointing to a predominant amphibole accumulation. Numerous syn-magmatic shear zones and mafic or felsic veins cut the layering (Fig. 2c–d). Late dykes (up to c. 1 m wide) of aplite and pegmatite are dominated by plagioclase, with <10 vol% of hornblende (Fig. 2c).

In places, the already solidified hornblendite/gabbro of the layered mafic complex was broken into angular fragments and net veined by the invading felsic magma (Fig. 2c–d). Some mafic blocks were arrested in the process of fragmentation, and the contacts are accentuated by felsic rims (Fig. 2e). The felsic rocks contain variable amounts of relatively large, prismatic hornblende crystals that have been resorbed in the host magma (Fig. 2f) and thus seem to be xenocrystic in origin. The texture of the mafic rocks varies from microgabbro to coarse-grained gabbro (columnar amphibole crystals up to a few centimetres long) in the more homogeneous, isolated mafic bodies (Fig. 2g).

In one of the valleys cutting the KMC N of Biger, spectacular comb layering (Moore and Lockwood, 1973) was observed. This Unidirectional Solidification Texture (UST) is defined by large feather-like amphibole crystals growing perpendicular to the margins of late, otherwise fine-grained (quenched) sheets that cut the Amp-rich gabbro-hornblendite; plagioclase forms large grains but is only interstitial (Fig. 2h).

4.2. Petrology and mineral chemistry

Representative electron-microprobe analyses of amphibole, plagioclase, olivine, pyroxenes and biotite are given in Electronic Appendix 3a–c.

Amphibole–biotite tonalites are commonly medium-grained, grey to reddish rocks. They are composed of plagioclase, quartz, biotite, amphibole, clinopyroxene and minor K-feldspar (Fig. 3a). Typical accessories are monazite, apatite, zircon, titanite and magnetite.

Subhedral to euhedral plagioclase (52–59 vol%) from tonalite V005 is usually oscillatory-zoned andesine ($\text{An}_{36–42}$); however plagioclase in tonalite D002 is unzoned oligoclase ($\text{An}_{21–22}$). The content of anhedral K-feldspar ($\text{Ab}_{4–8} \text{Or}_{92–96}$) varies from 2 to 4 vol%. Biotite (7–

12 vol%) occurs as aggregates up to 3 mm or as single flakes up to 1 mm across and exhibits a fairly wide range of chemical composition ($\text{Fe}/(\text{Fe} + \text{Mg}) = 0.39–0.49$; $^{IV}\text{Al} = 2.29–2.43 \text{ apfu}$). These chemical characteristics are typical of biotite in I-type calc-alkaline granitoids from volcanic arcs (Abdel-Rahman, 1994). Subhedral amphibole (5–10 vol%) is classified as magnesiohornblende ($\text{Si} = 6.69–7.24 \text{ apfu}$; $\text{Mg}/(\text{Fe} + \text{Mg}) = 0.59–0.75$; Fig. 4a). Anhedral diopside ($\text{Fe}/(\text{Fe} + \text{Mg}) = 0.21–0.24$) is pushed back by magnesiohornblende (Fig. 3a). Biotite slightly altered to pale green-brown chlorite occurs locally. Secondary white mica appears as inclusions in the central parts of plagioclase grains. A replacement of plagioclase by secondary interstitial K-feldspar is seen in the reddish tonalite (sample D002).

Biotite–amphibole to amphibole–clinopyroxene quartz diorites (Fig. 3b) are medium-grained, equigranular, grey rocks composed of plagioclase (55–61 vol%), amphibole (22–27 vol%), quartz (7–11 vol%), biotite and/or clinopyroxene (5–12 vol%). Texturally the quartz diorites resemble the tonalites. Locally they contain amphibole or clinopyroxene-rich layers, 5 to 10 cm thick (Fig. 3b). Typical accessories are monazite, apatite, zircon, titanite and magnetite. Slightly altered plagioclase and chloritized biotite are locally present.

The main rock types of the KMC are medium- to coarse-grained biotite–amphibole gabbro to hornblendite which locally pass into amphibole gabbro with olivine or pyroxene. These mafic to ultramafic rocks chiefly consist of amphibole and variable amounts of plagioclase (Fig. 3c–f). Subordinate biotite, clinopyroxene and/or olivine are also present. Magnetite, apatite, ilmenite, rutile, chalcopyrite and spinel are common accessory minerals.

Biotite–amphibole gabbros to hornblendites are usually massive or layered with a cumulate texture. Massive gabbro is dominantly hypautomorphic granular (Fig. 3c). Very common are several cm to dm thick layers with variable proportions of amphibole (36–94 vol%) and plagioclase (63–5 vol%). Felsic mesocumulate to adcumulate layers consist of euhedral to subhedral plagioclase crystals (Fig. 3d) with interstitial amphibole, whereas mafic adcumulates consist of columnar or polygonal amphibole crystals with small amounts of interstitial plagioclase (0–12 vol%) and/or biotite (0–5 vol%). The plagioclase crystals usually show normal zoning ($\text{An}_{89–93}$). The amphiboles (pargasite; $\text{Si} = 6.21–6.35 \text{ apfu}$; $\text{Mg}/(\text{Fe} + \text{Mg}) = 0.74–0.76$; Fig. 4b) occur as subhedral crystals, either individually or in aggregates. Apatite, magnetite and ilmenite usually form inclusions in amphibole. Late feldspar-rich felsic veins cutting mafic cumulate (Y011) in places also break or wrap up the mafic cumulate layers.

Amphibole gabbros with olivine and/or pyroxene display hypautomorphic granular, poikilitic or orthocumulate textures. Columnar amphibole (pargasite; $\text{Si} = 6.15–6.37 \text{ apfu}$; $\text{Mg}/(\text{Fe} + \text{Mg}) = 0.67–0.86$; Fig. 4b) is often preferentially oriented (Fig. 3e). The cores of plagioclase grains usually show normal zoning ($\text{An}_{77–94}$) but rarely are replaced by younger oligoclase (An_{24}). Diopside ($\text{Fe}/(\text{Fe} + \text{Mg}) = 0.17$) is only present in the amphibole gabbro as strongly resorbed relicts in centres of amphibole crystals (Fig. 3e). Olivine ($\text{Fo}_{74–76}\text{Fa}_{24–25}\text{Tp}_1$) is a rare early phase of the gabbros (V013). Olivine is completely surrounded by amphibole (Fig. 3f) and often rimmed by small magnetite, spinel and/or enstatite grains, next to small relicts of plagioclase. Enstatite ($\text{Fe}/(\text{Fe} + \text{Mg}) = 0.20–0.21$) is present as up to 0.1 mm thick layers adjacent to olivine, locally in association with small anhedral grains of spinel ($\text{Sp}_{58–59}\text{Hc}_{31–32}$) and magnetite. Spinel and clinopyroxene do not form inclusions in olivine. Large magnetite grains are in direct contact with small anhedral grains of ilmenite, whereas fine trellis ilmenite lamellae sometimes occur in magnetite. Magnetite and chalcopyrite are also present as interstices of olivine and/or amphibole. Secondary Fe-Ti oxides occur as alteration products of ilmenite and magnetite. Symplectites of rutile and hematite after ilmenite are very common.

Olivine is often partially replaced by thin veins of a serpentinite group mineral and magnetite grains. Biotite and amphibole are partially altered to chlorite (rarely also K-feldspar, hematite and prehnite) and plagioclase to sericite and/or zoisite, albite and prehnite.

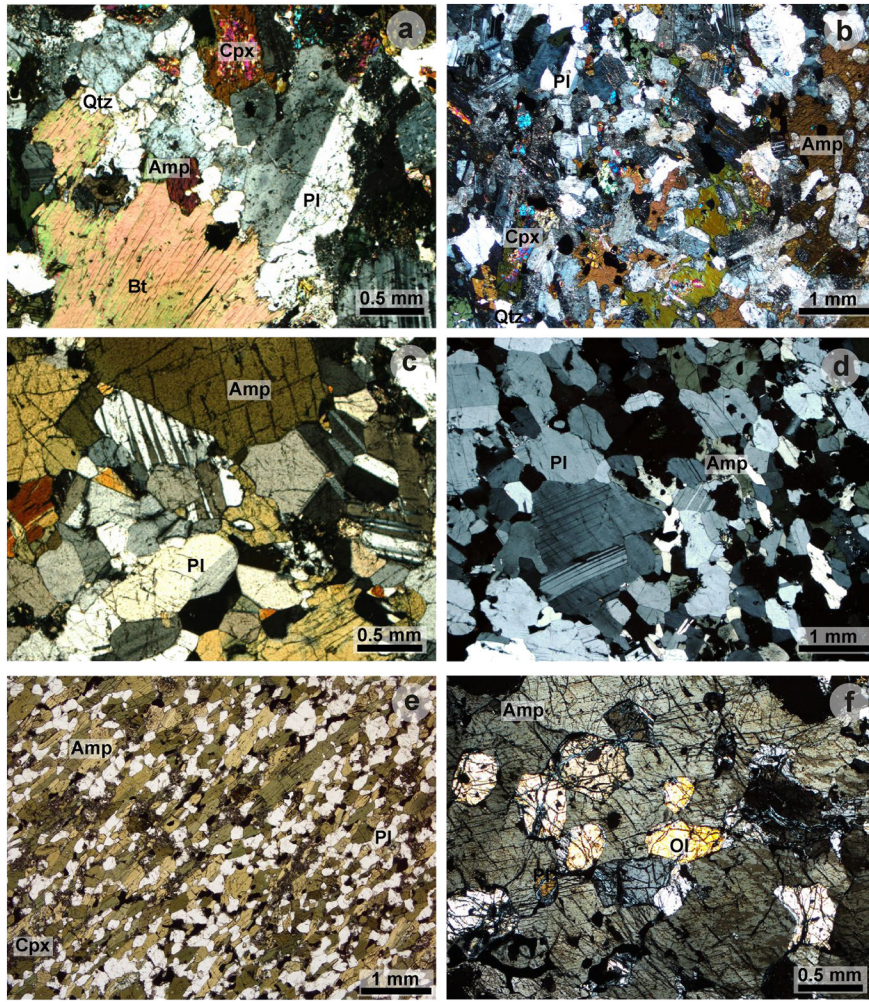


Fig. 3. Photomicrographs in cross-polarized light (XPL, except panel e) showing typical petrology and textures in rocks of the KMC: (a) – Incomplete replacement of clinopyroxene by amphibole in Amp-Bt tonalite with Cpx (D002); (b) – Contact between clinopyroxene and amphibole-rich layers in Cpx-Amp quartz diorite (D009b); (c) – Subhedral amphibole in Amp gabbro (D016); (d) – Plagioclase crystals with interstitial amphibole in Amp gabbro with a mesocumulate texture (D015); (e) – Magmatic foliation subparallel to layering in cumulate Cpx-Amp gabbro (P032); (f) – Olivine phenocrysts enclosed in amphibole of Amp-Ol gabbro (V013).

4.3. Thermobarometry

According to the thermobarometer of Ridolfi et al. (2010), amphiboles from gabbros to hornblendites were equilibrated at higher P-T conditions (0.35–0.51 GPa and 931–976 °C; Table 1) than those from tonalites ($P = 0.11\text{--}0.20$ GPa and 808–844 °C) (Fig. 4c). The amphibole-plagioclase barometry of Molina et al. (2015) provided slightly higher pressure estimates for gabbros to hornblendites (0.49–0.53 GPa; Table 1) and a wider range of generally similar pressures (0.08–0.13 GPa) for tonalite sample D002. For the tonalite sample V005, however, this calculation yielded unrealistically low results. Temperatures calculated using the Holland and Blundy (1994) edenite-richertite (model B) plagioclase-amphibole thermometer are comparable to the results of Ridolfi et al. (2010) formulation for the gabbros to hornblendites (914–1098 °C). Again, we obtained only 664–725 °C for the tonalites, probably due to subsolidus reequilibration during cooling (e. g., Cornejo and Mahood, 1997).

Disequilibrium texture between olivine and plagioclase (V013) explains the formation of spinel-enstatite-magnetite rims as a result of sub-solidus reactions (Claeson, 1998; Mongkoltip and Ashworth, 1983; Turner and Stüwe, 1992). Temperatures of formation of orthopyroxene and spinel in the olivine rims were estimated at 725 to 742 °C (Table 1), using the orthopyroxene geothermometer (Witt-Eickschen and Seck, 1991).

4.4. Oxygen fugacity and water contents in the magma

The Ridolfi et al. (2010) formulation also provides an estimate of oxygen fugacity during crystallization of amphibole. For gabbros to hornblendites, it varies from $\log f_{\text{O}_2} = -10.7$ to 9.2 (± 0.4 log units; equal to NNO +0.4 to +1.0) and for tonalites from $\log f_{\text{O}_2} = -13.1$ to −12.3 (± 0.4 log units; equal to NNO +0.2 to +1.8). The water content in the magma was evaluated using the amphibole compositions (Ridolfi et al., 2010) and is higher for the ultrabasic to basic rocks (7.1–8.4 wt%) than for the tonalites (4.2–6.2 wt%) (Fig. 4d).

Additionally, temperatures and f_{O_2} were estimated using the ilmenite-magnetite geothermometer and oxygen geobarometer (Andersen et al., 1993) and range from 517 to 534 °C and −22.5 to −23.9, respectively. The observed ilmenite-magnetite intergrowths suggest a eutectic relationship. Low calculated temperatures probably reflect subsolidus reequilibration during cooling.

4.5. U-Pb zircon ages and in-situ Hf isotopes

4.5.1. Zircon internal structures

Zircons from three quartz diorite-tonalite samples (V002, V003 and V004) display mutually similar morphological and internal structures. They form clear, euhedral and long prismatic crystals, mainly ranging from 250 to 450 µm in length. These zircons commonly show clearly igneous-related oscillatory zoning without inherited cores in CL images

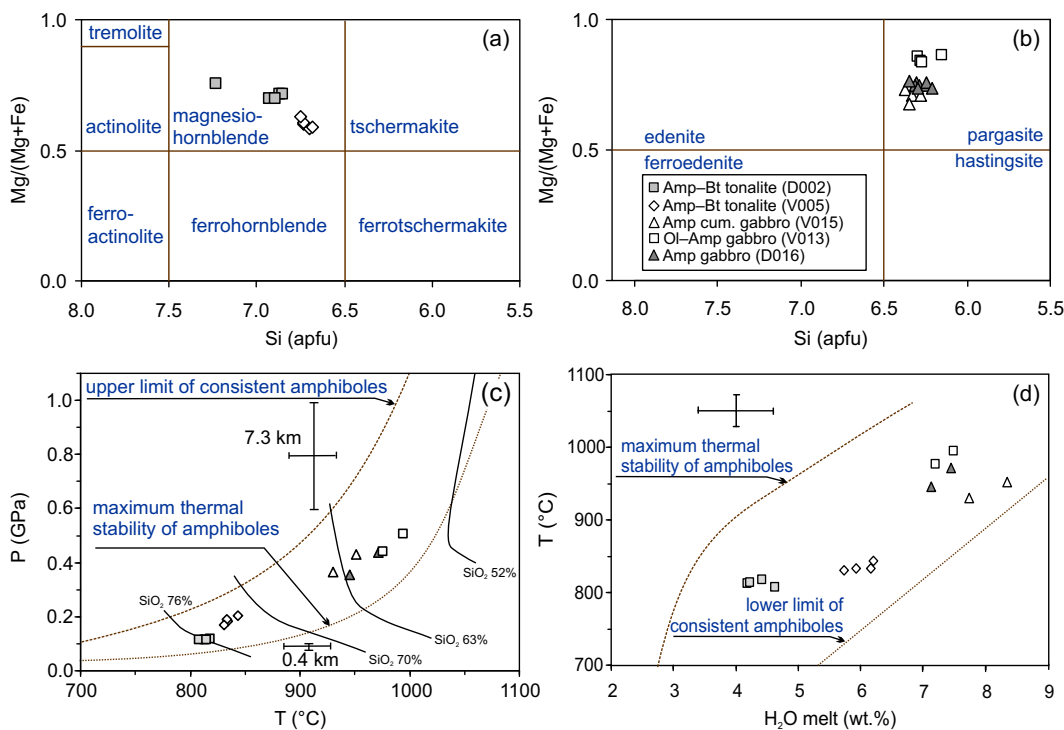


Fig. 4. (a–b) – Si vs. Mg/(Mg + Fe²⁺) classification plot for calcic amphiboles (Leake et al., 1997); (c) – P-T diagram; isopleths show anhydrous SiO₂ (wt%) content of the melt and consistent amphiboles are defined according to Ridolfi et al. (2010); (d) – H₂O in melt diagram vs. T. Error bars represent the expected uncertainty in T (± 22 °C), for H₂O in the melt (± 1 wt%), and representative errors for P, indicating the variation in accuracy.

(Fig. 5a–c). Zircons from the tonalite V005 are dominated by euhedral and stubby prismatic crystals, ranging from 150 to 300 µm in length with a length/width ratio lower than 2:1. These grains also show concentric oscillatory zoning, suggesting an igneous origin (Fig. 5d).

Zircons from the gabbro Y011 are euhedral and short-prismatic. These grains vary between 150 and 300 µm in length and most clearly display igneous growth zoning in CL images (Fig. 5e). The majority of zircons

from the leucogabbro M310 are long-prismatic with slightly rounded terminations, but short, stubby grains also occur. The CL images reveal broad, striped zonation (Fig. 6a) due to high-T crystallization typical of gabbroic rocks (Corfu et al., 2003). Some grains have very narrow high-luminescence (low-U) rims or embayments, indicating metamorphic overgrowth or partial recrystallization. The zircons of the quartz diorite dyke M311 are similar in morphology, but their terminations are mostly well

Table 1
Composition of amphiboles, estimated P-T conditions, oxygen fugacities and water contents for rocks from the KMC.

Rock	Gabbroic dyke	Hornblendite	Amp gabbro	Cpx–Amp tonalite	Bt–Amp tonalite
Sample	V015	V013	D016	D002	V005
Mineral assemblage	Amp, Pl, Mgt, Ap	Amp, Ol, Pl, Opx, Ilm, Mgt, Ap	Pl, Amp, Ilm, Rt, Mgt, Ap, Ccp	Pl, Bt, Amp, Qtz, Cpx, Kfs, Mgt, Ttn, Ap, Ccp	Pl, Qtz, Amp, Bt, Mgt, Ttn, Ap
Secondary minerals	Sericite, Zo		Hem		
Amphibole					
X _{Mg}	0.67 to 0.73	0.83 to 0.86	0.74 to 0.76	0.70 to 0.75	0.58 to 0.63
Si	6.28 to 6.37	6.15 to 6.30	6.21 to 6.35	6.85 to 7.24	6.69 to 6.75
Amp thermobarometry (Ridolfi et al., 2010)					
T (°C)	931 to 952	976 to 995	945 to 971	808 to 818	831 to 844
Uncertainty (σ_{est})	22	22	22	22	22
P (GPa)	0.36 to 0.43	0.44 to 0.51	0.35 to 0.43	0.11 to 0.12	0.17 to 0.20
Uncertainty (max error)	0.04	0.05	0.04	0.01	0.04 to 0.05
log fO ₂	-10.7 to -10.5	-9.2 to -9.6	-10.3 to -10.2	-13.1 to -12.3	-12.8 to -12.7
Uncertainty (σ_{est})	0.4	0.4	0.4	0.4	0.4
H ₂ O melt (wt%)	7.7 to 8.4	7.2 to 7.5	7.1 to 7.5	4.2 to 4.6	5.7 to 6.2
Uncertainty (σ_{est})	1.2 to 1.3	1.1	1.1	0.4	0.4
Pl–Amp thermometry (Holland and Blundy, 1994); pressure according Amp barometry (Ridolfi et al., 2010)					
T (°C) ± 32 °C	914 to 939	1030 to 1052	954 to 1098	664 to 699	683 to 725
Amp barometry (Molina et al., 2015); temperature according to Amp thermometry (Ridolfi et al., 2010)					
P (GPa)	0.49 to 0.50	0.50 to 0.53	0.52 to 0.53	0.08 to 0.13	-
Al in Opx geothermometer (Witt-Eickschen and Seck, 1991)					
T (°C)	-	725 to 742	-	-	-
Fe–Ti two-oxide geothermometer and oxygen barometer (Andersen et al., 1993)					
T (°C)	-	517 to 534	-	-	-
log fO ₂	-	-22.5 to -23.9	-	-	-

rounded (Fig. 6b). Striped zonation is also abundant, and some grains show very homogeneous domains. As in sample M310, very narrow low-U rims occur on some grains.

Zircons from the migmatite Y012 (Fig. 7a) are dominated by euhedral and stubby to elongated prismatic crystals (100–200 µm long), some with variably corroded surfaces. In CL images, they can broadly be subdivided into two groups. One generally exhibits simple oscillatory zoning but commonly with dull luminescence in the narrow outermost part, whereas the other shows core–rim structures with corroded, angular or rounded cores surrounded by weakly zoned, low-luminescent rims (Fig. 7b–c).

4.5.2. Zircon U–Pb ages and Hf isotopic compositions

4.5.2.1. Quartz diorites–tonalites. Bt–Amp tonalite V002c: thirty-one analyses were made on oscillatory zoned zircons. Except for three

discordant ones, the remaining twenty-eight points form a cluster with $^{206}\text{Pb}/^{238}\text{U}$ ages between 484 and 505 Ma. Their weighted mean age of 495 ± 3 Ma (Electronic Appendix 4; Fig. 5a) is interpreted as timing the magmatic crystallization.

Bt–Amp quartz diorite V003: twenty-eight zircons with oscillatory zoning were selected for U–Pb isotopic analyses. Nearly all the data are concordant (Fig. 5b), yielding $^{206}\text{Pb}/^{238}\text{U}$ ages between 477 and 512 Ma. Their weighted mean age of 494 ± 3 Ma is interpreted to reflect the crystallization of the quartz diorite.

Leucocratic Bt–Amp quartz diorite V004: a total of thirty-one zircon grains were analyzed, twenty-nine of which were concordant. These concordant analyses gave $^{206}\text{Pb}/^{238}\text{U}$ ages ranging from 502 Ma to 525 Ma, defining an age cluster with a weighted mean of 511 ± 2 Ma (Fig. 5c). This is considered to represent the crystallization age of the quartz diorite.

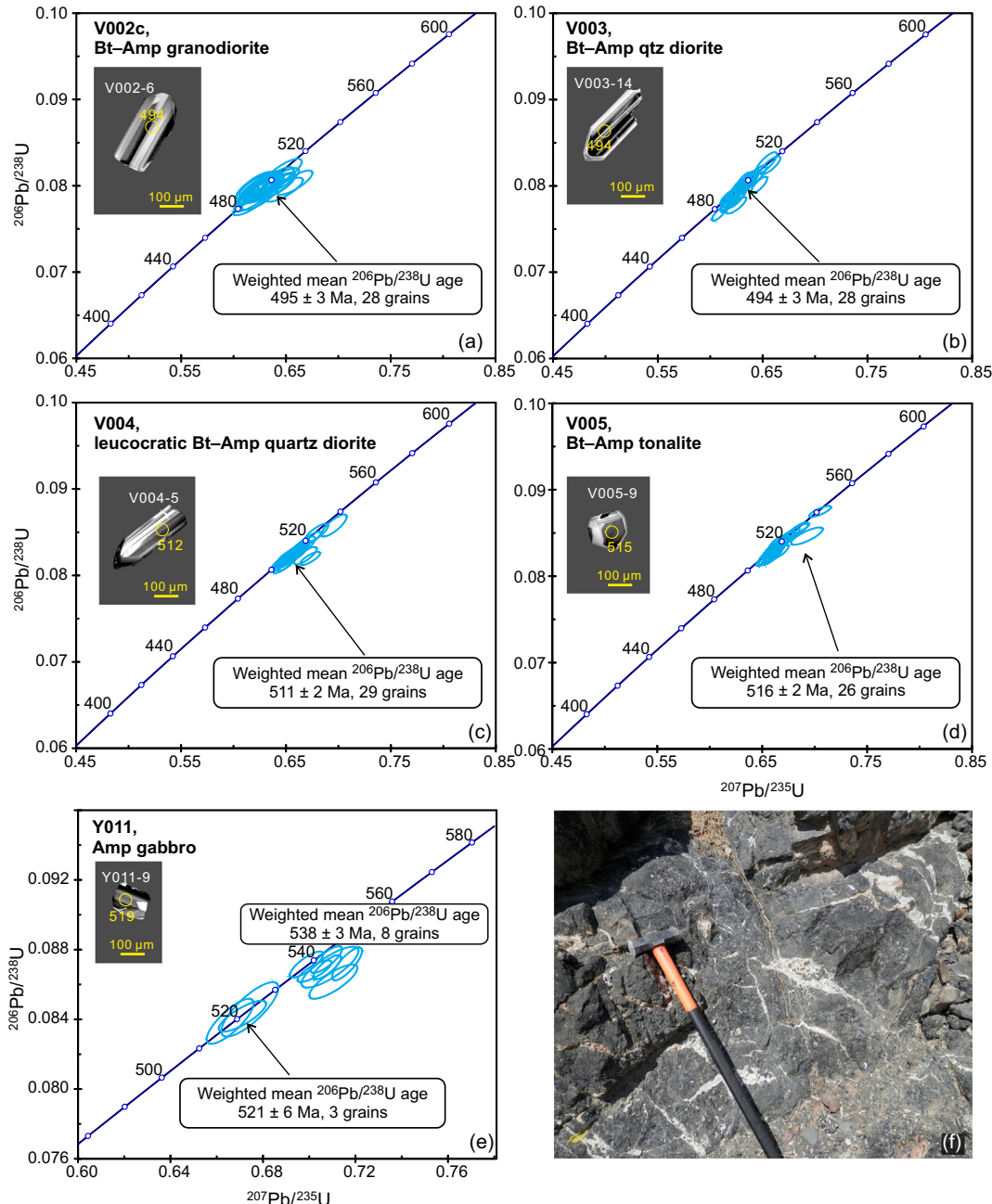


Fig. 5. (a–e) U–Pb concordia plots for studied zircons from igneous samples of the KMC (dated at the University of Hong Kong). Insets: characteristic CL images. (f) Field photograph of the outcrop situation of the sample Y011.

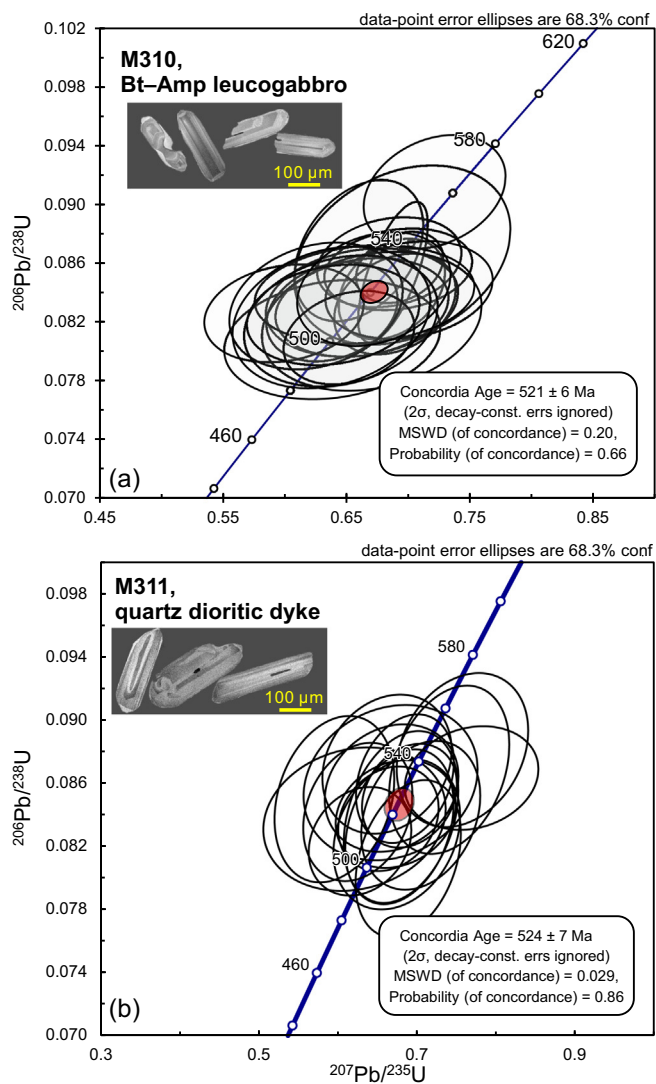


Fig. 6. U-Pb concordia plots for studied zircons from basic magmatic rocks of the KMC (dated at the University of Bergen).

Bt-Amp tonalite V005: zircons from this sample show well-defined magmatic oscillatory zoning; thirty of them were selected for U-Pb isotopic analyses. Twenty-eight analyses gave $^{206}\text{Pb}/^{238}\text{U}$ ages ranging from 508 Ma to 541 Ma, twenty-six of which define an age cluster with a weighted mean age of 516 ± 2 Ma (Fig. 5d). We interpret this age to reflect the crystallization of the tonalite.

Although zircons from these four samples yielded consistent ages, they show large variations in their initial $^{176}\text{Hf}/^{177}\text{Hf}$ ratios. In general, Hf isotopic compositions from the tonalite (V002c) and two quartz diorites (V003 and V004) exhibit similar Hf isotopic characteristics, with strongly positive initial $\epsilon_{\text{Hf}}^{\text{t}}$ values (+8.4 to +14.3) and young $T_{\text{DM}}^{\text{Hf}}$ model ages (0.59–1.12 Ga) (Electronic Appendix 5; Fig. 8a–c; Fig. 9). This may imply derivation through (near) closed-system fractionation from little modified, depleted-mantle derived magmas. In contrast, zircons in the Bt-Amp tonalite V005 yield less radiogenic Hf isotopic characteristics ($\epsilon_{\text{Hf}}^{\text{t}} = +2.5$ to +6.2; $T_{\text{DM}}^{\text{Hf}} = 1.34$ –1.67 Ga, Fig. 8d; Fig. 9). This may indicate an origin from a distinct, less depleted or perhaps slightly metasomatised mantle domain or, more likely, by remelting of pre-existing, but still rather juvenile, metabasic crust.

4.5.2.2. Gabbro. Net-veined gabbro Y011 yielded two zircon populations, 521 ± 6 Ma and 538 ± 3 Ma, although these show similar features in CL images (Fig. 5e). The *in-situ* Hf initial isotopic ratios vary widely ($\epsilon_{\text{Hf}}^{\text{t}} =$



Fig. 7. Zircon age data for migmatite from roof of the KMC (sample Y012). (a) Field appearance of the migmatite. (b) U-Pb concordia plot, including detail at around the presumed migmatitization age (~750 Ma) (d) (dated at the University of Hong Kong).

+4.3 to +13.3; Fig. 8e). The zircons contain both, the more and less radiogenic, Hf components distinguished in the more siliceous samples (Fig. 9a). However, there seems to be no simple relation between the ages of individual zircon grains and their Hf isotopic compositions (Fig. 9a). The $T_{\text{DM}}^{\text{Hf}}$ crustal model ages in the gabbro Y011 again vary widely between 0.70 and 1.52 Ga, almost covering the range of all the more siliceous samples studied (Fig. 9b).

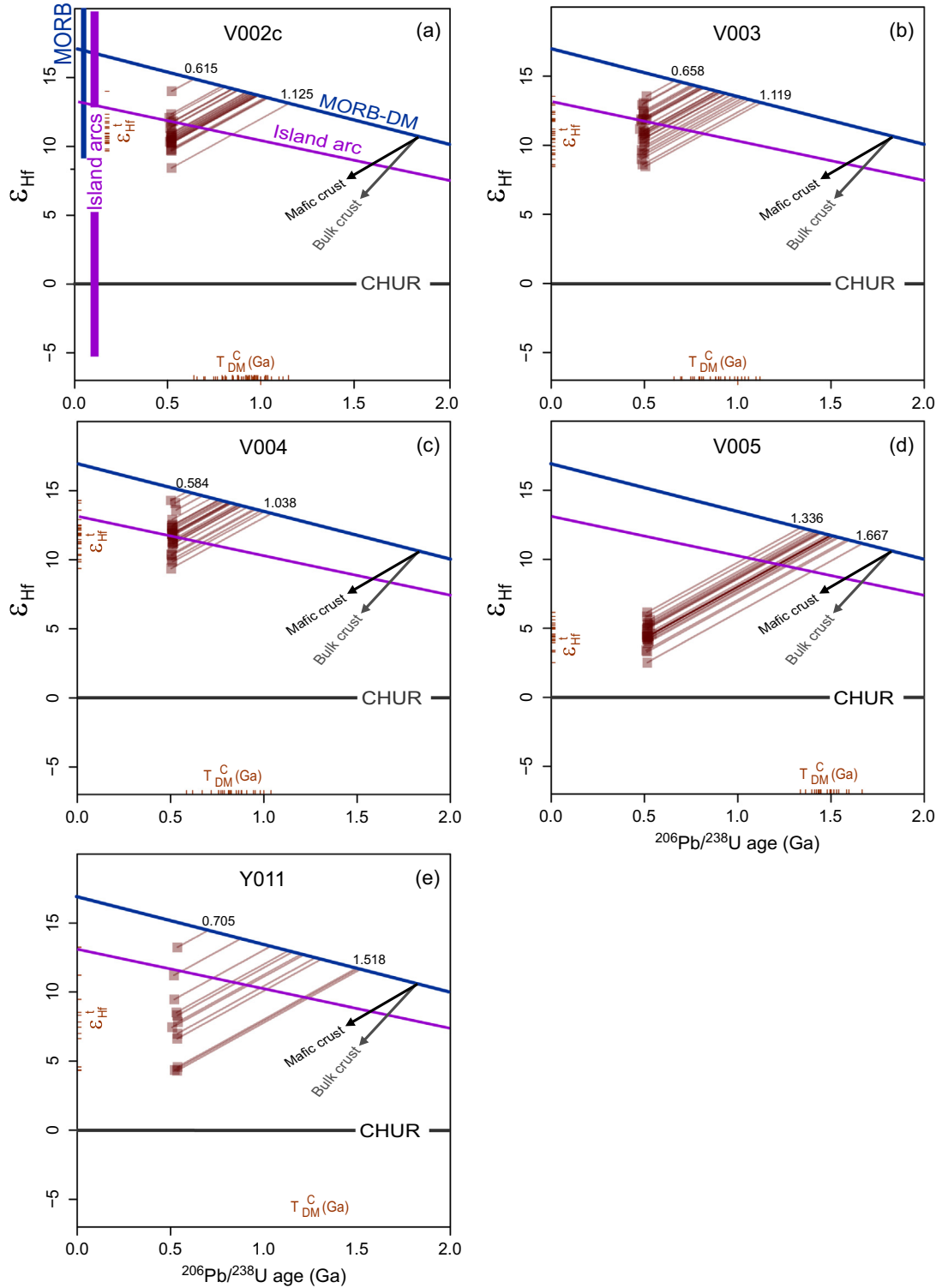


Fig. 8. Two-stage Hf evolution diagram for dated zircons from samples V003, V004, V005 and Y011 (a–d). The Depleted Mantle line is after Griffin et al. (2000) and Belousova et al. (2010), the composition of CHUR from Blichert-Toft and Albaréde (1997). The evolution line for the average mantle source to modern island-arc magmas, as well as intervals ϵ_{Hf}^t of modern Mid-Ocean Ridge Basalt (MORB) and Island-Arc Basalts are from Kemp and Hawkesworth (2014 and references therein).

Twenty-eight analyses of zircons from leucogabbro sample M310 produced well-grouped results with a concordia age of 521 ± 6 Ma (Fig. 6a) that we interpret to reflect the time of gabbro crystallization. Similarly, 19 analyses of zircons from quartz diorite vein M311 also yielded a tight cluster of error ellipses with a concordia age of 524 ± 7 Ma (Fig. 6b), identical, within error, to the gabbro data. These ages may imply that the two rocks were coeval, and thus perhaps also cogenetic.

4.5.2.3. Migmatite. The U-Pb analyses of the oscillatory-zoned zircon grains of migmatite sample Y012 (Fig. 7b–c) yielded ages clustering around 750 Ma (751 ± 5 Ma, $n = 7$; Electronic Appendix 4). The narrow dull outermost rims were too thin to be analyzed. Given the lack of younger ages, the near-euhedral shape, oscillatory zoning and high Th/U ratios (0.65–2.21) of these zircons, they can be theoretically interpreted as igneous, resulting from crustal melting during the

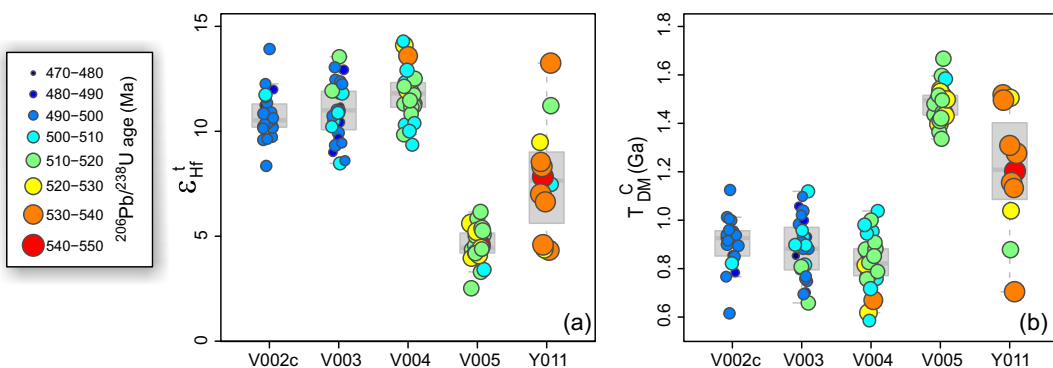


Fig. 9. 'Strip box plots' (Janoušek et al., 2016) illustrating the statistical distribution of ϵ_{Hf}^t values (a) and "crustal" model ages ($T_{\text{DM}}^{\text{HFC}}$) for individual zircons in each of the dated samples (b). The variously sized and coloured circles depict the distribution of intrusive $^{206}\text{Pb}/^{238}\text{U}$ ages. For calculation of crustal model ages ($T_{\text{DM}}^{\text{HFC}}$), a basaltic $^{176}\text{Lu}/^{177}\text{Hf}$ ratio of 0.022 (Lancaster et al., 2011) was employed.

migmatitization. However, the ~750 Ma zircons can equally well be viewed as an igneous, detrital component in the sediment whose migmatitization was younger than 750 Ma and remained undetected by the U-Pb dating.

The remaining zircon population in Y012 is characterized by rather complicated core-rim structures. Dating the zircon cores mostly provided old $^{207}\text{Pb}/^{206}\text{Pb}$ ages, typically discordant due to Pb-loss or partial re-crystallization. They vary between 1.6 Ga and 2.5 Ga and this scatter is taken as a consequence of metamorphic disturbance. Again, no ages could have been obtained from the rather narrow rims.

4.6. Whole-rock geochemistry

In the following section, the dataset will be split into four groups based on the silica contents, differences in appearance, petrology, the salient geochemical signatures and likely genesis as follows: Group 1: ultrabasic cumulates ($\text{SiO}_2 < 42$ wt%), Group 2: gabbros ($42 < \text{SiO}_2 < 50$ wt%), Group 3: quartz diorites ($50 < \text{SiO}_2 < 57$ wt%) and Group 4: tonalitic rocks ($\text{SiO}_2 > 57$ wt%).

4.6.1. Major and minor elements

The studied magmatic rocks are ultrabasic to intermediate in composition, rarely straddling the boundary of the acid domain ($\text{SiO}_2 = 40.2\text{--}63.6$ wt%; data from Electronic Appendix 6 recast on a volatile-free basis). They are geochemically rather primitive ($\text{Mg}^\# = 58\text{--}30$, but mostly constant at ~50) amphibole-bearing gabbros and hornblendites to Amp-Bt tonalites with quartz dioritic types prevailing (Fig. 10a). All samples are metaluminous to subaluminous (Fig. 10b), with A/CNK values (Shand, 1943) rising continuously from 0.61 to 0.98 with increasing SiO_2 (not shown).

Using the CIPW norm (Hutchison, 1975), the three ultrabasic samples (V015, V012a and P032) contain up to 9.5% normative Ne , together with Ol (Electronic Appendix 6). The more acidic compositions are characterized by the presence of normative Q , Hy and Pl ; only in samples D004 and L010b appears some normative Ol instead of Q . The bulk of the dataset is thus subalkaline, except for the ultrabasic types that are slightly alkaline.

As there is no significant change in FeOt/MgO during differentiation for most of the samples (Fig. 10c), they do not represent a tholeiitic but a calc-alkaline suite (Miyashiro, 1974). The rocks are all Na-rich ($\text{Na}_2\text{O} = 1.8\text{--}6.6$ wt%, $\text{Na}_2\text{O}/\text{K}_2\text{O} = 1.3\text{--}9.7$ by weight). They classify mostly as normal-K calc-alkaline in the diagram of Peccerillo and Taylor (1976) (Fig. 10d); only the most siliceous samples enter the high-K calc-alkaline field.

Harker plots show mostly negative correlations, except for those involving alkalis and phosphorus that have positive slopes (Fig. 11). For FeOt and CaO negative trends are well defined over the entire silica range. On the other hand, plots with TiO_2 and MgO display excess range. On the other hand, plots with TiO_2 and MgO display excess

scatter for the (ultra-) basic samples. The trend for Al_2O_3 is clearly inflexed; a strongly scattered positive correlation for (ultra-) basic samples gives way to a negative one at about 50 wt% SiO_2 and 19 wt% Al_2O_3 .

4.6.2. Trace elements

The complete trace-element data are presented in Electronic Appendix 7. The elemental concentrations were normalized to the average composition of Normal Mid-Ocean Ridge Basalt (NMORB) (Sun and McDonough, 1989) (Fig. 12) and chondrite (Boynton, 1984) (REE; Fig. 13). The former multi-element plots are invariably characterized by the presence of deep negative anomalies of Nb and Ta, and, except for the least siliceous samples, a fair enrichment in LILE (including K, Pb and Sr).

The **ultrabasic rocks (Group 1)** are extremely poor in many incompatible elements (Rb 1–3, Cs < 0.1, Th < 0.05–0.06, U 0.02–0.04, Nb < 0.2–0.3, Ta < 0.01–0.004 ppm). The Sr concentrations are somewhat elevated, leading to low Rb/Sr ratios of 0.001–0.004. The contents of transition metals are variable (Cr < 20, Ni < 20–50, Pb < 5 ppm but Co 43–62, Sc 34–99, and V 422–751 ppm). The NMORB-normalized patterns (Fig. 12a) show normalized contents, for most elements, significantly lower than unity (Th, Nb, Ta – if above the respective detection limits – as well as P, Zr, Hf, HREE) or approaching it (U, LREE + MREE). The only more abundant elements are Rb, Ba, K, Sr ± Ti.

The chondrite-normalized REE patterns for the three ultrabasic samples are concave down, with maxima reached at Sm and Eu (Fig. 13a). Hence, the Dy/Dy* values are high (1.35–1.58). Total REE contents are consistently low ($\Sigma\text{REE} = 26.8\text{--}28.3$ ppm). Normalized contents of La and Yb are mutually comparable ($\text{La}_N/\text{Yb}_N = 0.96\text{--}1.04$, $\text{Yb}_N = 5.6\text{--}6.1$), and the Eu anomaly is insignificantly positive ($\text{Eu/Eu}^* = 1.09\text{--}1.16$).

Compared with the previous group, three of the **Group 2 gabbros** (Fig. 12b) contain much higher LILE (Cs, Rb, Ba, K), LREE and HFSE (Nb, Ta, Ti, Zr, Hf). The normalized contents of the said elements mostly exceed unity. Still, the distribution pattern for the fourth sample V016 is more depleted and does not differ greatly from that of the ultrabasic group.

For the three gabbros, the total REE contents are higher than those in the Group 1 ($\Sigma\text{REE} = 51.0\text{--}107.7$ ppm), and the Eu anomalies are negligible to clearly negative ($\text{Eu/Eu}^* = 0.97\text{--}0.72$) (Fig. 13b). The sample V007 is very different, showing distinctly lower ΣREE of 31.8 ppm and a strong positive Eu anomaly ($\text{Eu/Eu}^* = 1.41$). The patterns of Group 2 invariably display weak LREE over HREE enrichment ($\text{La}_N/\text{Yb}_N = 2.26\text{--}6.05$, $\text{Yb}_N = 4.7\text{--}9.1$) and are gently concave up at Dy ($\text{Dy/Dy}^* = 0.93\text{--}0.80$).

The **Group 3 quartz diorites** yielded NMORB-normalized multi-element patterns that are strongly enriched in incompatible elements (particularly Cs and Rb; Fig. 12c); the contents of the most compatible elements are only slightly below unity. Superimposed on the patterns are strong spikes in Ba, K, Pb, Sr and P as well as deep troughs in Nb and Ta as well as – much less pronounced – Ti.

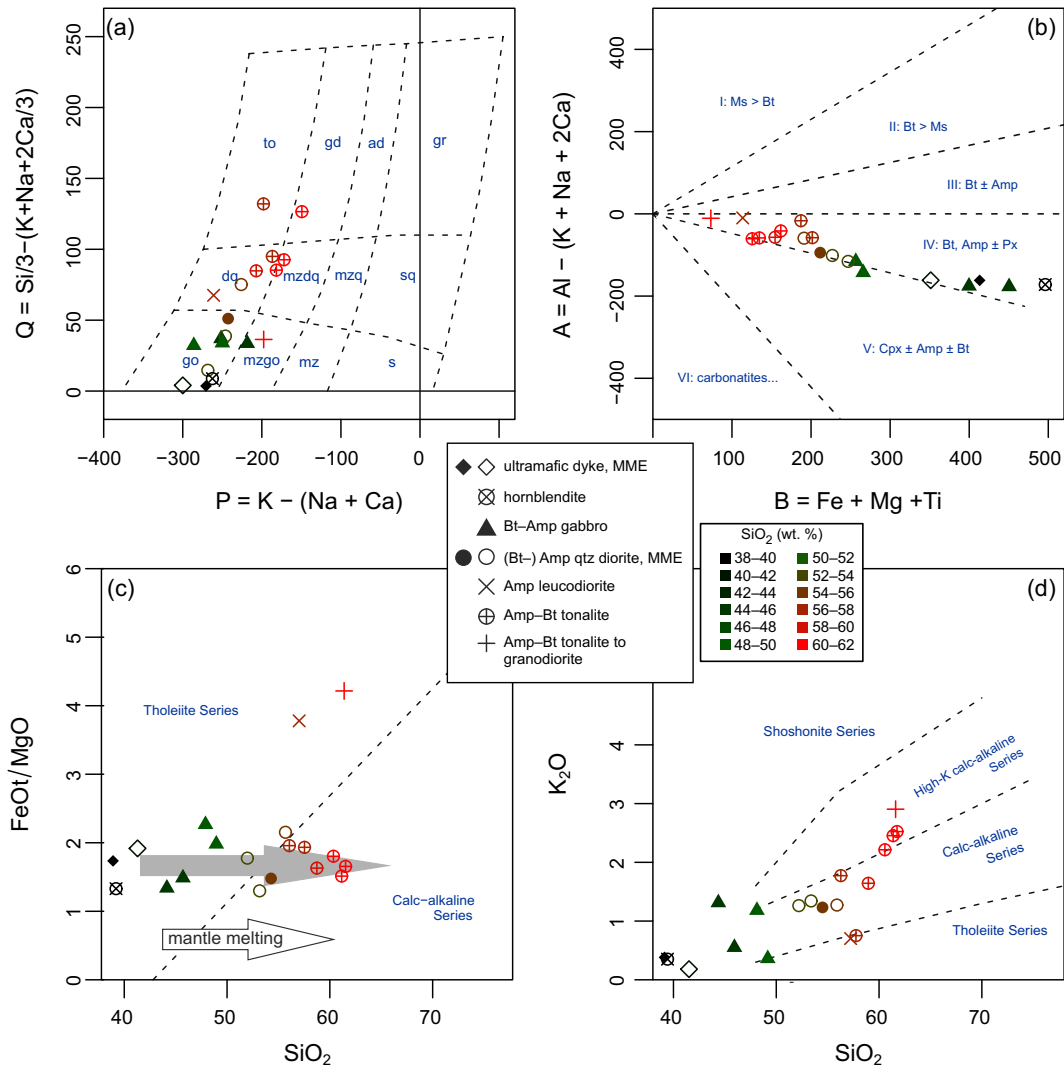


Fig. 10. Major-element based classification plots with the plotting symbols colour-coded according to silica contents. (a) Multicationic P–Q diagram of Debon and Le Fort (1983). gr = granite, ad = adamellite, gd = granodiorite, to = tonalite, sq = quartz syenite, mzq = quartz monzonite, mzdq = quartz monzodiorite, dq = quartz diorite, s = syenite, mz = monzonite, mzgo = monzogabbro, go = gabbro. (b) Multicationic B–A diagram of the same authors. Sectors (I–VI) reflect alumina balance of samples: I, muscovite > biotite; II, biotite > muscovite; III, biotite ± amphibole; IV, biotite, amphibole ± pyroxene; V, clinopyroxene ± amphibole ± biotite; VI, unusual mineral associations (carbonatites...). (c) Binary plot of SiO_2 vs. FeOt/MgO (wt%) of Miyashiro (1974) showing the calc-alkaline affinity of the KMC. The global mantle melting array is based on the compilation of Grove et al. (2012). (d) SiO_2 – K_2O plot with discrimination boundaries between the tholeiitic, calc-alkaline, high-K calc-alkaline and shoshonitic rocks of Peccerillo and Taylor (1976).

The REE patterns are subparallel for the entire group (Fig. 13c; $\text{La}_{\text{N}} = 4.94\text{--}9.10$). They exhibit no or slightly negative Eu anomalies ($\text{Eu}/\text{Eu}^* = 1.00\text{--}0.80$) and are clearly curved, concave up ($\text{Dy}/\text{Dy}^* = 0.72\text{--}0.65$). However, the total contents are variable ($\Sigma\text{REE} = 59.9\text{--}123.5$ ppm, $\text{Yb}_{\text{N}} = 6.8\text{--}10.8$).

The NMORB-normalized spiderplots for the felsic **Group 4** do not differ greatly from the previous one, even though the LILE enrichment reaches its highest values here. An interesting feature is a strong Zr and Hf enrichment in the felsic samples V002c and V008c as well as considerable variability in the HREE + Y contents of the whole group.

The REE patterns are very variable (Fig. 13d) in terms of total REE (62.8–191.8 ppm), the HREE contents ($\text{Yb}_{\text{N}} = 3.6\text{--}10.1$) and the degree of the LREE/HREE enrichment ($\text{La}_{\text{N}}/\text{Yb}_{\text{N}} = 6.45\text{--}20.14$). The magnitude of the Eu anomaly is also variable ($\text{Eu}/\text{Eu}^* = 1.24\text{--}0.78$), but all curves are clearly concave up ($\text{Dy}/\text{Dy}^* = 0.65\text{--}0.54$).

4.7. Sr–Nd isotopes

In order to shed more light on sources and subsequent development of the studied plutonic association, Sr–Nd isotopic analyses

were undertaken for seven representative whole-rock samples (Table 2, Fig. 14). In view of the newly obtained intrusive ages, the isotopic data were age-corrected to 500 Ma. Overall they show a rather narrow range of initial Sr isotopic compositions (${}^{87}\text{Sr}/{}^{86}\text{Sr}_{500} = 0.7034\text{--}0.7044$), but the Nd isotopic variability is significantly broader ($\varepsilon_{\text{Nd}}^{500} = +5.8$ to -4.9).

The most primitive, clearly Depleted Mantle-derived samples are the ultrabasic dyke V015, gabbro V007 and quartz diorite V003 (${}^{87}\text{Sr}/{}^{86}\text{Sr}_{500} = 0.7035\text{--}0.7038$, $\varepsilon_{\text{Nd}}^{500} = +4.7$ to $+3.5$). The hornblende V012a has slightly less radiogenic Nd (${}^{87}\text{Sr}/{}^{86}\text{Sr}_{500} = 0.7036$, $\varepsilon_{\text{Nd}}^{500} = +2.6$). Due to elevated ${}^{147}\text{Sm}/{}^{144}\text{Nd}$ ratios in the cumulate rocks, the two-stage Nd model ages represent only rather rough estimates ($T_{\text{DM}}^{\text{Nd},2\text{stg}} = 0.87\text{--}1.07$ Ga).

The more siliceous rocks represent a rather heterogeneous group. Two of these (leucocratic hybrid Amp–Bt tonalite V008c and Amp–Bt tonalite V005) show primitive Sr but immature crust-like Nd isotopic compositions (${}^{87}\text{Sr}/{}^{86}\text{Sr}_{500} = 0.7043$ and 0.7044 , $\varepsilon_{\text{Nd}}^{500} = -4.9$ and -0.6 , $T_{\text{DM},2\text{stg}}^{\text{Nd}} = 1.79$ and 1.38 Ga). On the other hand, coarse-grained leucocratic Amp–Bt quartz diorite V004 has a composition resembling the Depleted Mantle and is the least evolved among the samples investigated (${}^{87}\text{Sr}/{}^{86}\text{Sr}_{500} = 0.7034$, $\varepsilon_{\text{Nd}}^{500} = +5.8$, $T_{\text{DM}}^{\text{Nd},2\text{stg}} = 0.77$ Ga).

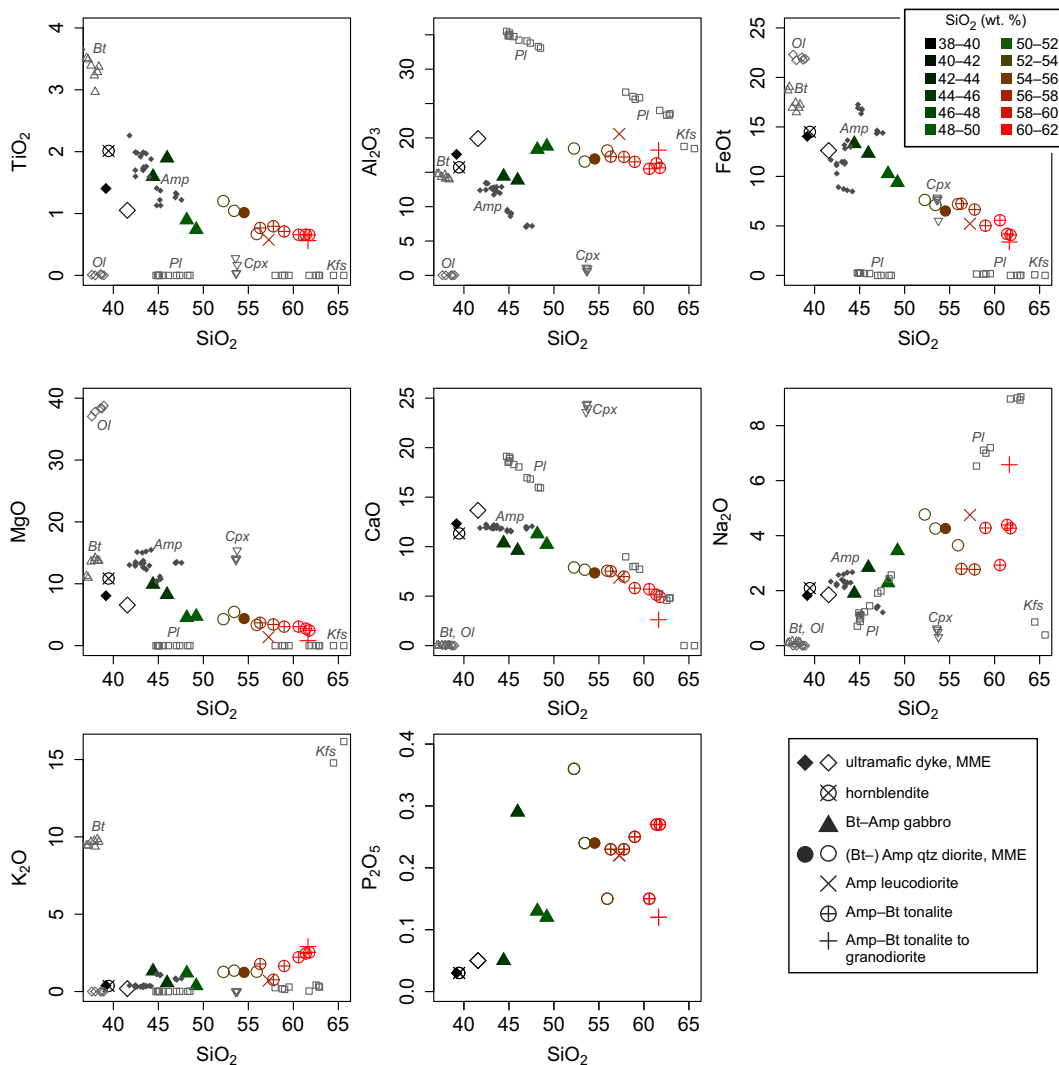


Fig. 11. Harker plots for the studied magmatic rocks from the KMC. Also plotted are typical electron-microprobe analyses of the main rock-forming minerals.

5. Discussion

5.1. Geotectonic context

The studied samples from the Khantaishir Magmatic Complex are mostly subalkaline, except for the ultrabasic types gradually becoming alkaline in character, most likely due to accumulation of amphibole crystals. The (normal-K) calc-alkaline chemistry of the more siliceous rock types, as well as characteristic trace-element enrichment in hydrous-fluid mobile LILE (Cs, Rb, Ba, K, Pb and Sr), with Th and U, relative to the “conservative” HFSE (Nb, Ta and Ti) suggest an origin within a magmatic arc (Fig. 12) (e.g., Pearce and Peate, 1995; Tatsumi and Eggins, 1995).

Indeed, in the Th-Hf/3-Ta ternary plot of Wood (1980) (Fig. 15a), the samples fall exclusively into the arc-related (CAB and IAT) fields. Also, the binary plots Ti–V of Shervais (1982) and Zr–Ti of Pearce (1982) demonstrate an arc affinity of the studied samples (Fig. 15b–c). In the binary diagram Nb/Yb vs. Th/Yb (Pearce, 2008, 2014) (Fig. 15d) all samples plot well above the ‘NMORB–OIB array’, into the region occupied by arc-related magmas. Moreover, this plot demonstrates that the arc was rather mature, producing magmas with relatively high Nb and Th contents.

One should be aware of possible limitations concerning the interpretation of geotectonic diagrams, though. Especially for the felsic igneous rocks, the Nb, Ta and Ti depletion and LILE enrichment may merely

imply remelting of older, arc-related crustal sources (Arculus, 1987; Förster et al., 1997; Janoušek et al., 2010; Roberts and Clemens, 1993). In fact, these characteristics are inherent to the continental crust as a whole (see Introduction). The chemistry of the magmatic rocks can also be profoundly modified by crystal accumulation, peritectic phase entrainment, assimilation or hybridization (e.g., Clemens and Stevens, 2012; Deering and Bachmann, 2010; Didier and Barbarin, 1991a). Still, the whole-rock geochemical signature for most of the KMC dataset (mafic–intermediate rocks) seems to consistently indicate an affinity to subduction-modified mantle melts, or their fractionates.

5.2. Petrogenesis of the Khantaishir Magmatic Complex

5.2.1. Magma evolution

As shown above, the Harker plots for non-cumulate rocks show negative correlations of TiO₂, Al₂O₃, FeOt, MgO and CaO with SiO₂ (Fig. 11), but the ultrabasic cumulates often define scattered oblique trends (e.g., Al₂O₃). Such a variation can be modelled by fractionation dominated by ferromagnesian phases (mainly amphibole) with, or without, their crystal accumulation. This is in line with the field and microtextural evidence that points to a particularly important role for amphibole accumulation (and hence also fractional crystallization) in the petrogenesis of the KMC.

Plagioclase was probably only a late crystallizing phase, as shown by distinct inflections at SiO₂ ~ 50 wt%, especially in the SiO₂–Al₂O₃ and

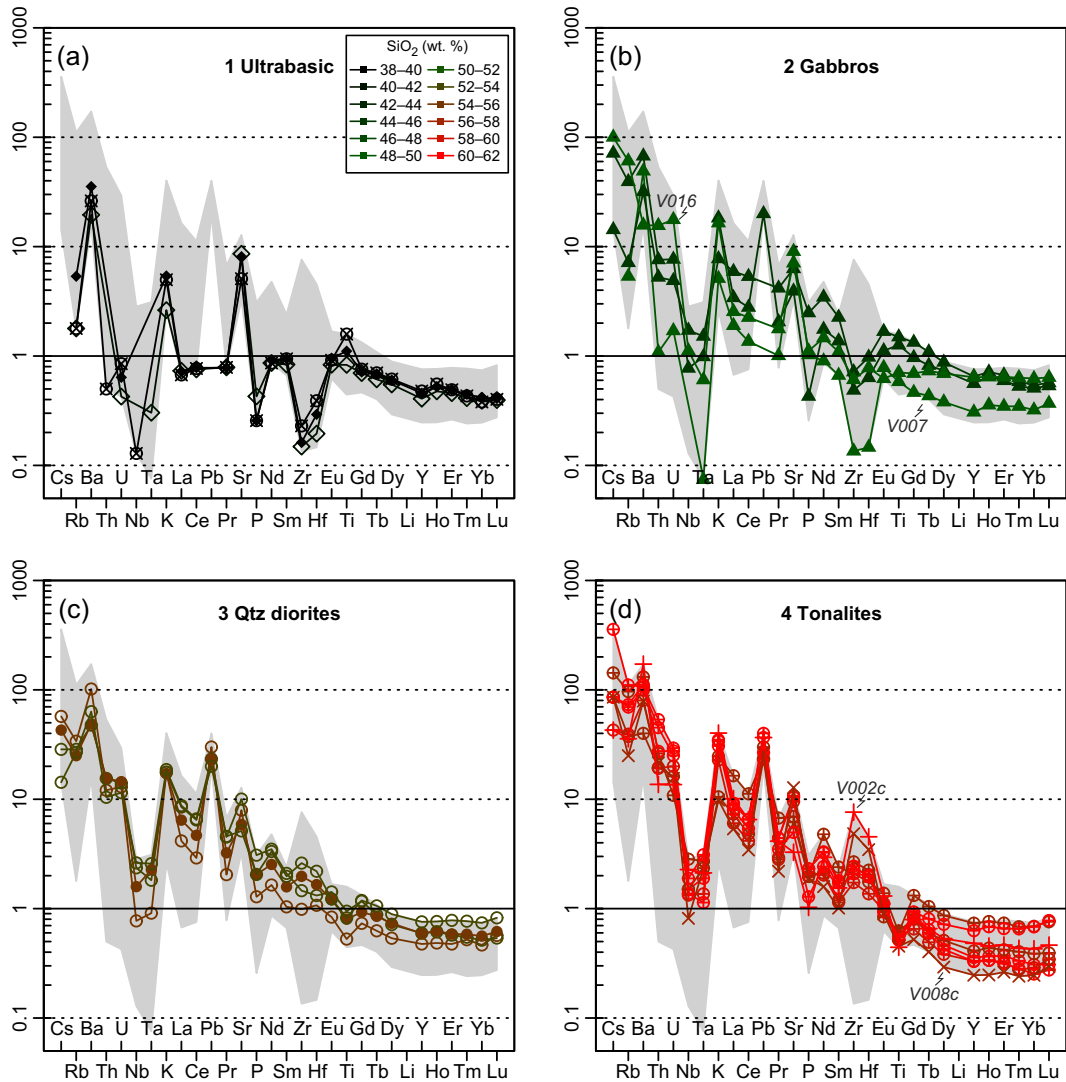


Fig. 12. Normal Mid-Ocean Ridge Basalt (NMORB) (Sun and McDonough, 1989) normalized spiderplots colour-coded by silica contents. The grey background field indicates the overall variability in the dataset. Plotting symbols as in Fig. 10.

SiO_2 -MgO plots (Fig. 11) as well as the general lack of Eu anomalies, especially in more mafic rock types (Fig. 13). Indeed, delayed crystallization of plagioclase is a common feature of water-rich calc-alkaline magmas at continental margins (Dessimoz et al., 2012; Grove et al., 2012).

Theoretically also garnet could have been involved during deep crustal crystallization (Alonso-Perez et al., 2009), or partial melting. Given the preference of amphibole and, to a lesser extent, clinopyroxene for the MREE and garnet for the HREE, the nature of the key ferromagnesian phase can be best assessed using the shapes of the REE patterns and their change in course of differentiation. In this context the observed positive SiO_2 - La_N/Yb_N correlation (Fig. 16a) is equivocal as it could be interpreted as being due to either garnet or amphibole control (Davidson et al., 2007).

Fortunately Dy/Dy^* and Ti/Ti^* , the parameters expressing the curvature of the MREE-HREE segments of the REE patterns (Fig. 13) and the magnitude of the Ti anomaly in the NMORB-normalized multi-element plots (Fig. 12), respectively, are capable of distinguishing between the two possibilities (Davidson et al., 2013). According to these authors, garnet fractionation should cause a rise in Dy/Dy^* (increasingly concave down patterns), but amphibole should have the opposite effect. In the KMC, all non-cumulate rocks are characterized by $\text{Dy}/\text{Dy}^* < 1$, further sharply decreasing with rising SiO_2 (Fig. 16b).

In addition, the amphibole control (\pm magnetite) should result in a progressively developing negative Ti anomaly in the NMORB-normalized multi-element plot (Fig. 12), and thus a positive Ti/Ti^* - Dy/Dy^* correlation. Therefore, the binary plots involving the Dy/Dy^* and Ti/Ti^* parameters (Fig. 16c-d) corroborate the amphibole control for most of the studied rocks. Moreover, they confirm that the amphibole-rich ultrabasic samples are truly cumulates (see e.g., the low SiO_2 , La_N/Yb_N , high $\text{Dy}/\text{Dy}^* (\gg 1)$ and Ti/Ti^*).

5.2.2. Water contents in the magma

As pointed out by Grove et al. (2012), primary arc magmas are commonly water-rich, with 6–8 wt% H_2O or more, bearing a witness to the profusion of water in their subduction-modified mantle sources. The major effect of H_2O is to suppress the crystallization of plagioclase at mid- to lower-crustal pressures in favour of Fe-Mg-rich silicates. Hence the distinctive enrichment in SiO_2 , typical of these magmatic suites, is primarily driven by the early crystallization of olivine, pyroxene and/or amphibole. Moreover, the late-crystallizing plagioclase is An-rich (and thus Ca-Al-rich and Si-poor), further promoting a rapid evolution to siliceous residual liquids rich in alkalis (Grove et al., 2012).

Using the amphibole compositions as a proxy (Ridolfi et al., 2010), the Khantaishir magma was probably water-rich; gabbros and hornblendites could have had c. 7.0 to 8.5 wt% H_2O , tonalites somewhat

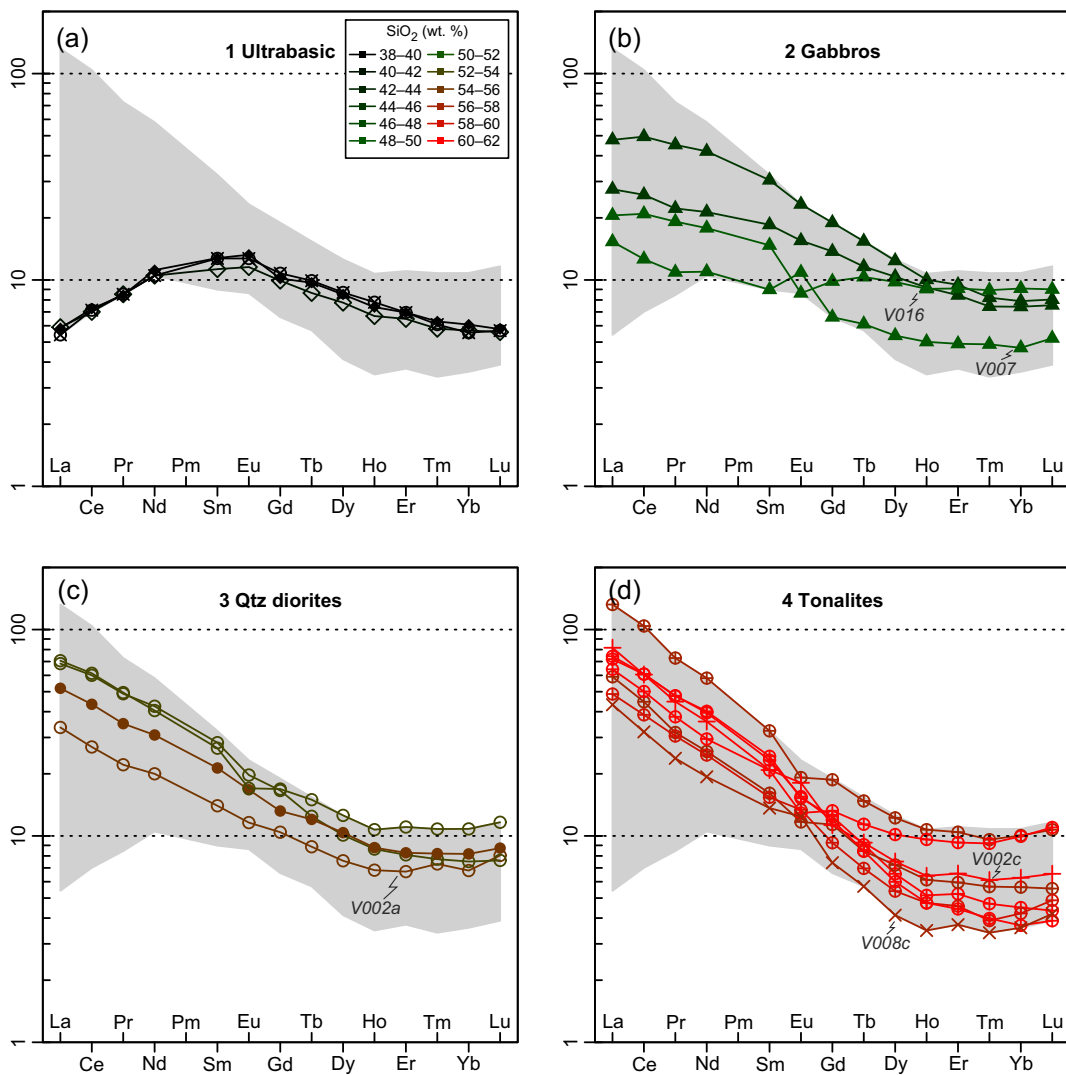


Fig. 13. Chondrite (Boynton, 1984) normalized REE patterns colour-coded by silica contents. The grey background field indicates the overall variability in the dataset. Plotting symbols as in Fig. 10.

less, down to 4 wt% (Table 1). The former values correspond to vapour saturation of a basaltic magma at depths of about 15–25 km (Plank et al., 2013), which is in good agreement with calculated pressures for the gabbros and hornblendites (Table 1).

Most parental magmas in subduction zones fractionate amphibole as a result of elevated H₂O during crystallization (Grove et al., 2012; Müntener et al., 2001). But this mineral could also be a product of a late-stage peritectic reaction of clinopyroxene with melt (hydrous melt + clinopyroxene + Fe-Ti oxides + Ca-rich plagioclase = amphibole + quartz + Na-rich plagioclase; Beard et al., 2004).

Still, high initial H₂O contents of the basic intrusions into the Khantaishir arc are confirmed by the occurrence of comb layering (Fig. 2h). Based on extensive experimental work, these textures have been explained by the loss of H₂O from the crystallizing mafic system (nearly) saturated in water into the adjacent water-poor (felsic) magma or wall rock (Pistone et al., 2015). In this model, the mafic part of the system would be ‘chemically quenched’ just by the H₂O loss, even if the loss was isothermal. The undercooling front migrates inwards, away from the interface between both domains. The nucleation takes place on the interface, and the steady undercooling regime promotes perpendicular, inward growth of large crystals, such as amphiboles in the present case.

The rock sequence in the KMC preserves evidence for a fractionation trend typical of arc magmas with early olivine crystallization, followed

by clinopyroxene and/or amphibole (e.g., Smith, 2014). Mainly at the more advanced stages, the crystallization produced assemblages with higher proportions of amphibole at the expense of clinopyroxene. The studied mafic or intermediate magmas would be saturated at 4 wt% H₂O at relatively shallow depths (~6 km) which is a common storage depth beneath arc volcanoes, based on geodetic and seismic observations (e.g., Cervelli et al., 2010; Lu et al., 2010; Plank et al., 2013).

Similar to our case, the importance of hornblende-dominated fractional crystallization in the production of intermediate arc magmas was emphasized by several authors (e.g., Davidson et al., 2007; Dessimoz et al., 2012; Lee and Bachmann, 2014). Clearly also in the KMC, the basic melts were responsible for H₂O transfer from a water-rich mantle wedge to the lower-middle arc crust, where they were subject to fractional crystallization forming the amphibole “sponge” sensu Davidson et al. (2007).

5.2.3. Depleted mantle contribution

The whole-rock geochemical and Sr-Nd isotopic signatures some of the (ultra-) basic samples, namely the ultrabasic dyke V015, microgabbro V007 and hornblendite V012a, requires direct fractionation (with variable degree of crystal accumulation) from primary melts derived from a depleted mantle wedge, overprinted by subduction fluids ($^{87}\text{Sr}/^{86}\text{Sr}_{500} = 0.7038$ to 0.7036 , $\varepsilon_{\text{Nd}}^{500} = +4.5$ to $+2.6$, $T_{\text{DM}, 2\text{stg}}^{\text{Nd}} = 0.89$ – 1.07 Ga).

Table 2
Whole-rock Sr–Nd isotopic data for selected samples of the KMC.

Sample ID	Petrology	SiO ₂ (wt%)	Rb (ppm)	Sr (ppm)	⁸⁷ Rb/ ⁸⁶ Sr	⁸⁷ Sr/ ⁸⁶ Sr ^a	2 se	⁸⁷ Sr/ ⁸⁶ Sr ₅₀₀ ^b	Sm (ppm)	Nd (ppm)	¹⁴⁷ Sr/ ¹⁴⁴ Nd ^a	¹⁴³ Nd/ ¹⁴⁴ Nd ^a	2 se	(¹⁴³ Nd/ ¹⁴⁴ Nd) ₅₀₀ ^b	$\varepsilon_{\text{Nd}}^{500}$	T _{DM,1stg} ^c	T _{DM,2stg} ^d
V015	Fine-grained ultrabasic dyke	39.18	3	728	0.0119	0.703911	0.000005	0.70383	2.49	6.7	0.2247	0.512907	0.000007	0.512117	+3.5	-6.69	0.99
V012a	Hornblendeite	39.47	1	458	0.0063	0.703588	0.000012	0.70364	2.48	6.3	0.2380	0.512908	0.000010	0.512113	+2.6	-1.97	1.07
V007	Fine-grained Amp gabbro from the mingling zone	49.21	3	813	0.0107	0.703707	0.000017	0.70363	1.75	6.6	0.1608	0.512753	0.000005	0.51223	+4.5	1.04	0.89
V003	Bi–Amp qtz diorite	54.53	14	530	0.0764	0.703997	0.000009	0.70345	4.16	18.5	0.1359	0.512679	0.000005	0.51223	+4.7	0.87	0.88
V008c	Leucocratic Amp–Bt tonalite with Amp xenocrysts	57.26	14	1149	0.0352	0.704530	0.000009	0.70428	2.66	11.6	0.1386	0.512197	0.000010	0.51174	-4.9	1.80	1.79
V005	Amp–Bt tonalite	60.59	62	448	0.4004	0.707260	0.000012	0.70441	4.06	17.7	0.1387	0.512419	0.000004	0.51196	-0.6	1.39	1.38
V004	Leucocratic Amp–Bt quartz diorite	61.77	41	936	0.1267	0.704275	0.000009	0.70337	4.54	23.7	0.1158	0.512669	0.000005	0.51229	+5.8	0.71	0.77

^a Followed by error (2 standard errors of the mean).

^b Subscripts 500 indicate age-corrected isotopic ratios.

^c Single-stage Nd model ages (Ga) using the Depleted Mantle parameters of Liew and Hofmann (1988).

^d Two-stage Nd model ages (Ga) using the Depleted Mantle parameters and the general approach of Liew and Hofmann (1988); however, ¹⁴⁷Sr/¹⁴⁴Nd_{CC} = 0.138 (metabasic crust).

However, the chemistry of the more siliceous samples is more equivocal. The crustal Hf model ages (T_{DM}^{Hf}) for the quartz diorite V003, leucocratic quartz diorite V004 and tonalite V002c are low, ranging between 0.59 and 1.12 Ga. Also, the whole-rock Sr–Nd isotopic signatures of the former two samples are in accord with a short crustal residence time of their source (⁸⁷Sr/⁸⁶Sr₅₀₀ ~ 0.7035, $\varepsilon_{\text{Nd}}^{500}$ = +4.7 and +5.8, T_{DM,2stg} = 0.88 and 0.77 Ga, respectively). The plausible genetic scenarios thus include remelting of a recently formed basaltic underplate at the bottom of the magmatic arc (Atherton and Petford, 1993), or direct fractionation from primary melts derived from a metasomatized depleted-mantle wedge. Another viable alternative is partial melting of a relatively young and geochemically primitive metabasic crust; given the HFSE depletion, it could have formed a recently accreted island-arc (Rapp and Watson, 1995).

5.2.4. Anatexis of pre-existing crust?

In contrast, the Hf and Nd isotopic compositions of the two remaining felsic samples disclose a longer crustal history of their sources. Tonalite V005 contains exclusively old Hf (T_{DM}^{Hf} = 1.34–1.67 Ga, median 1.5 Ga), and its Nd is significantly less radiogenic than in the more basic rock types ($\varepsilon_{\text{Nd}}^{500}$ = −0.6, T_{DM,2stg} = 1.38 Ga). Even more clear-cut is the case of tonalite V008c, which requires a crustal source with a still older Mesoproterozoic mean Nd residence age ($\varepsilon_{\text{Nd}}^{500}$ = −4.9, T_{DM,2stg} = 1.79).

At the same time, both samples do not have particularly high ⁸⁷Sr/⁸⁶Sr₅₀₀ ratios (~0.7044). This points to a source with low time-integrated Rb/Sr, such as metabasic rocks. In view of the Hf isotopic composition of the V005 zircons, as well as of the whole geochemical signature (esp. distinct HFSE depletion), the most likely candidate would again be previously accreted, significantly older island-arc rocks.

Nevertheless, there is also evidence for the presence of some, truly metasedimentary country rocks in the roof of the KMC. The migmatite sample Y012 gives c. 750 Ma ages for near-euhedral zircons that can be most plausibly interpreted as a detrital component in Neoproterozoic sediment deposited, after short transport, from a homogenous Tonian magmatic source. The migmatitization could have been of Cambrian age, being caused by the heat input from the voluminous mafic magmas of the KMC.

Even though the number of dated zircons from the migmatite is very limited, the strongly discordant inherited component with ill-defined upper intercept age(s) suggests an abundance of Palaeoproterozoic detritic zircon in the sedimentary source of its protolith, resembling the age spectra known from the nearby Baydrag Continent (e.g., Demoux et al., 2009a; Kozakov et al., 1993). This does not seem to imply that the Khantaishir arc was founded on an ancient crustal segment, though. The evidence to the contrary is provided by the lack of typical ('S-type') anatexitic granites in the KMC, its rather primitive Sr isotopic signature as well as (mostly) short crustal residence times shown by the whole-rock Nd and zircon Hf model ages. The migmatite is thus interpreted as a minor sedimentary component overlying the local, mostly metabasic crust. The sedimentary material of its protolith could have been transported from a Palaeoproterozoic core of the continent, perhaps not very far away. These metasediments, however, apparently played a negligible role in the genesis of the arc itself.

5.2.5. Mutual interaction of mantle- and crustally-derived magmas

Field and petrographic observations suggest that hybridization between crustal and mantle-derived melts was significant in the genesis at least some of the studied quartz diorites and tonalites. Its importance is documented by the abundance of MME commonly with lobate contacts and chilled margins (e.g., Barbarin, 2005; Didier and Barbarin, 1991a) as well as by the presence of some microtextures, most notably mantled plagioclases and rapakivi feldspars (e.g., Hibbard, 1991; Janoušek et al., 2004; Vernon, 1984).

The variation in the Sr–Nd isotopic data (Fig. 14) indicates heterogeneity of the sample set that can be interpreted in terms of contrasting

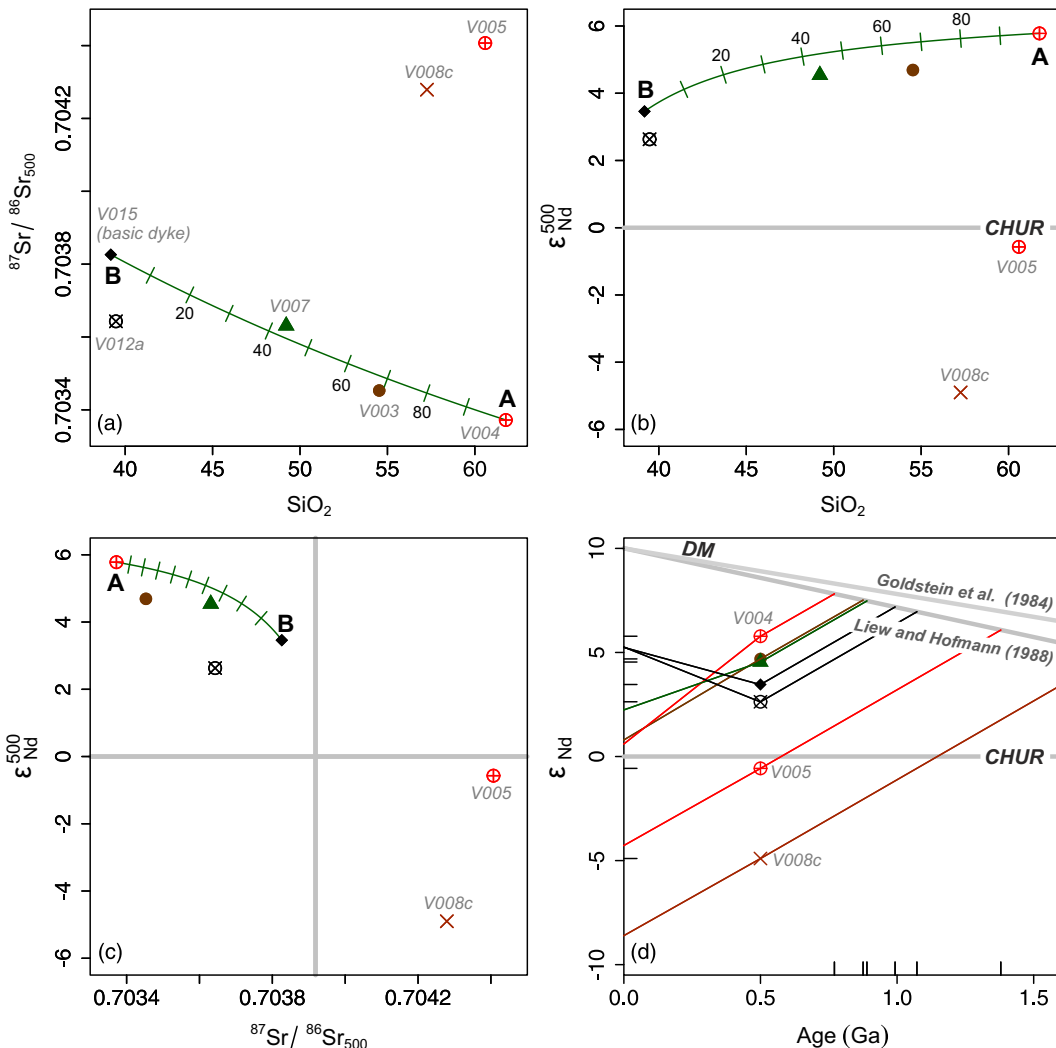


Fig. 14. Whole-rock Sr-Nd isotopic compositions. (a) – SiO_2 vs. $^{87}\text{Sr}/^{86}\text{Sr}_{500}$ plot. (b) – SiO_2 vs. $\varepsilon_{\text{Nd}}^{500}$ plot. (c) Binary plot of $^{87}\text{Sr}/^{86}\text{Sr}_{500}$ vs. $\varepsilon_{\text{Nd}}^{500}$ for KMC rocks. (d) Two-stage Nd evolution diagram. DM = Depleted Mantle evolution lines after Goldstein et al. (1984) and Liew and Hofmann (1988). The extra tick marks on the ordinate denote $\varepsilon_{\text{Nd}}^{500}$ values, on the abscissa the two-stage Depleted Mantle model ages, $T_{\text{DM-2stg}}^{\text{Nd}}$ (Liew and Hofmann, 1988). Plotting symbols as in Fig. 10. Binary mixing hyperbolae in (a–c) indicate weight proportions of assumed felsic end-member V004 (10% tick marks) mixed with a mafic magma with composition of dyke V015 (see Janoušek et al., 2016 for the principles and R code employed). Independent position of felsic samples V005 and V008c, probably derived by anatexis of older metabasic crust, is clearly visible. For explanation see text.

mantle and crustal sources for individual rock types. Moreover, the position of samples V015, V007, V003 and V004 in Fig. 14a–c does not seem fortuitous but rather reflects the operation of open-system processes. Rather curiously, strontium becomes less and neodymium more radiogenic with increasing silica in this sequence (Fig. 14a–b).

Assuming that the basic mantle-derived end-member had a composition of dyke V015 and the felsic crustal melt of leucocratic quartz diorite V004, binary mixing hyperbolae require that the microgabbro V007 contains c. 40 wt%, and the Bt-Amp quartz diorite V003 c. 70 wt% of the crustal component (Fig. 14a–c). The negligible curvature in the SiO_2 vs. $^{87}\text{Sr}/^{86}\text{Sr}_{500}$ plot makes it to appear nearly linear (Fig. 14a). Indeed, the two samples presumably dominated by the felsic component (V003 and V004) yielded exclusively low Hf model ages ($T_{\text{DM}}^{\text{Hf}}$) of 0.59 to 1.12 Ga, with medians at 0.8–0.9 Ga (Fig. 9b). The U-Pb dating proves that these two samples were contemporaneous at c. 495 Ma (late Cambrian).

Nonetheless, binary plots of SiO_2 vs. Al_2O_3 and MgO (Fig. 11) are clearly inflexed. On this basis, simple binary mixing, but also partial melting or fractional crystallization with a constant proportion of minerals in the residue/crystallizing cumulate can be discounted. These processes are all governed by mass balance, leading to simple linear relationships (Janoušek and Moyen, 2014). On this basis, as well as of

field, petrological and geochemical arguments given above, fractional crystallization had to be an important process, but there also had to be a major change in the fractionating assemblage (plagioclase in?) at c. $\text{SiO}_2 \sim 50$ wt%.

Taken together, neither simple binary mixing nor closed-system fractional crystallization alone can account for the observed Sr-Nd isotopic, major- and trace-element variations. Hence, the two mechanisms had to be coupled into a single process, such as Assimilation and Fractional Crystallization (AFC) (DePaolo, 1981; O'Hara, 1977) most likely with changing fractionating assemblages and thus also bulk distribution coefficients (Janoušek et al., 2000; Powell, 1984). The operation of complex multistage fractional crystallization/crystal accumulation in combination with variable open-system processes is typical of many magmatic arcs (Otamendi et al., 2012).

The amphibole gabbro Y011 contains two zircon populations of dissimilar ages (521 ± 6 and 538 ± 3 Ma), giving a broad range of *in-situ* $\varepsilon_{\text{Hf}}^t$ values (Fig. 9a). The field relations indicate that the already solidified mafic igneous rock has been invaded by younger, felsic magma (Fig. 5f). The likely mechanism thus appears to be recycling of c. 538 Ma xenocrysts/antecrusts from an earlier, more mafic magma pulse and mixing with the c. 521 Ma magmatic crystals from the more felsic system (e.g., Davidson et al., 2007; Larrea et al., 2013).

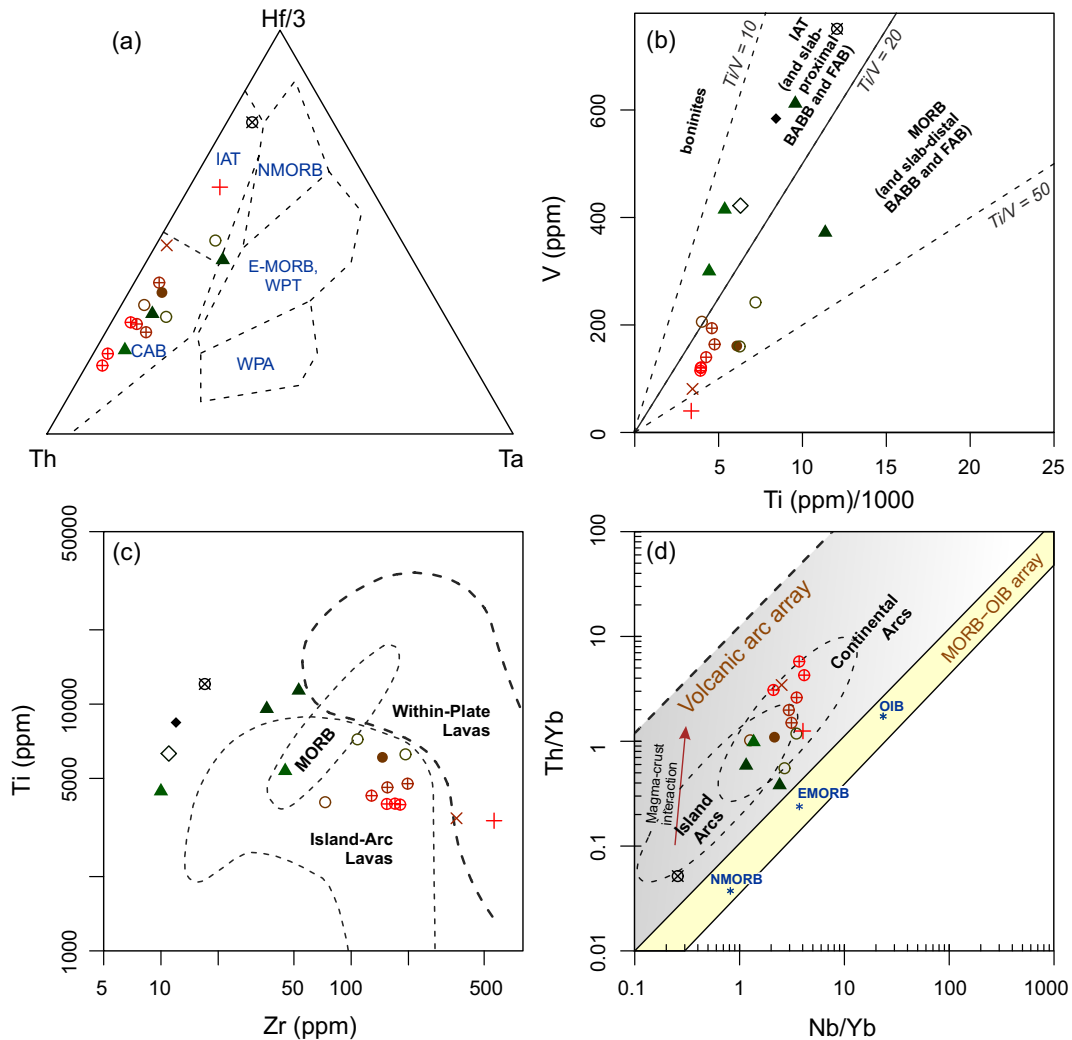


Fig. 15. Geotectonic diagrams based on whole-rock geochemical compositions. (a) – Triangular plot Th–Hf/3–Ta of Wood (1980). IAT – Island-Arc Tholeiites, CAB – Calc-Alkaline Basalts, NMORB – Normal Mid-Ocean Ridge Basalts, E-MORB – Enriched Mid-Ocean Ridge Basalts, WPT – Within-Plate Tholeiites, WPA – Within-Plate Alkali Basalts. (b) – Binary plot Ti–V of Shervais (1982) modified by Pearce (2014). IAT – Island-Arc Tholeiites, BABB – Back-Arc Basin Basalts, FAB – Fore-Arc Basalts. (c) – Binary plot Zr vs. Ti of Pearce (1982). (d) – Binary diagram Nb/Yb vs. Th/Yb (Pearce, 2008, 2014). The ‘MORB–OIB array’ is defined by average NMORB, EMORB and OIB compositions taken from Sun and McDonough (1989). Plotting symbols and colours as in Fig. 10.

The felsic samples V005 and V008c show a position different from the main trend in Fig. 14, having comparably radiogenic Sr and non-radiogenic Nd. In particular in the $^{87}\text{Sr}/^{86}\text{Sr}_{500} - \varepsilon_{\text{Nd}}^{500}$ plot (Fig. 14c), they fall on the other side of the magma mixing array compared to the inferred crustal end-member (V004). This is in line with the fact that their Nd model ages ($T_{\text{DM-2stg}}^{\text{Nd}}$) are Mesoproterozoic and that the former sample yields rather high $T_{\text{DM}}^{\text{Hf}}$ (1.34–1.67 Ga). The tonalite V005 was dated at 516 ± 2 Ma, but for the leucotonalite V008c we have no direct age information. However, based on field relations, sample V008c needs to be younger than the layered gabbro/hornblendite (Fig. 2d) because it contains amphibole xenocrysts/antecrysts derived from the gabbro (Fig. 2f). This can be taken as a field evidence for recycling of amphibole crystals from the older, more mafic into the younger, felsic members of the magmatic suite (e.g., Paterson et al., 2008; Solgadi and Sawyer, 2008).

5.3. Age and temporal development of the Khantaishir Magmatic Complex

The pressures for KMC rocks, estimated from the amphibole compositions (Ridolfi et al., 2010) are considerably higher for the ultrabasic cumulates and gabbros (c. 0.35–0.5 GPa) than for the quartz diorites and tonalites (c. 0.1–0.2 GPa). The former correspond to a depth of c. 13–19 km, the latter to c. 4–8 km. As the typical thickness of arc crust ranges

from 15 to 35 km (intra-oceanic arc) to 30–70 km (continental arc) (Spandler and Pirard, 2013), the studied amphibole-rich cumulates record crystallization at middle to lower crustal levels.

Field evidence, together with the whole-rock Sr–Nd isotopes, argue for the presence of several generations of (ultra-) basic magmas as well as magma mixing/mingling between some of the contrasting magma batches. However, among the samples dated by the U–Pb method on zircon, the most mafic rock types preceded somewhat the more siliceous magmatic activity. Sample Y011 shows two age populations, at 538 ± 3 and 521 ± 6 Ma. Leucogabbro sample M310 yielded a well-defined age of 521 ± 6 Ma, and the quartz diorite dyke M311 cutting it has an identical age, within error, of 524 ± 7 Ma. On the other hand, four quartz diorites to tonalites are on average younger, ranging between 516 ± 2 and 494 ± 3 Ma.

Such a temporal shift from deeper, mafic to shallower, more felsic magmatic activity may reflect upward growth of the magmatic arc (Otamendi et al., 2012). The growth would be linked to increasing importance of crustal melting with time, an inevitable consequence of progressive heating by, and/or water release from, the periodically incoming, hot and hydrous mantle-derived basaltic melts (Annen et al., 2006; Dufek and Bergantz, 2005; Hildreth and Moorbath, 1988). This could go hand in hand with the establishment of larger magma

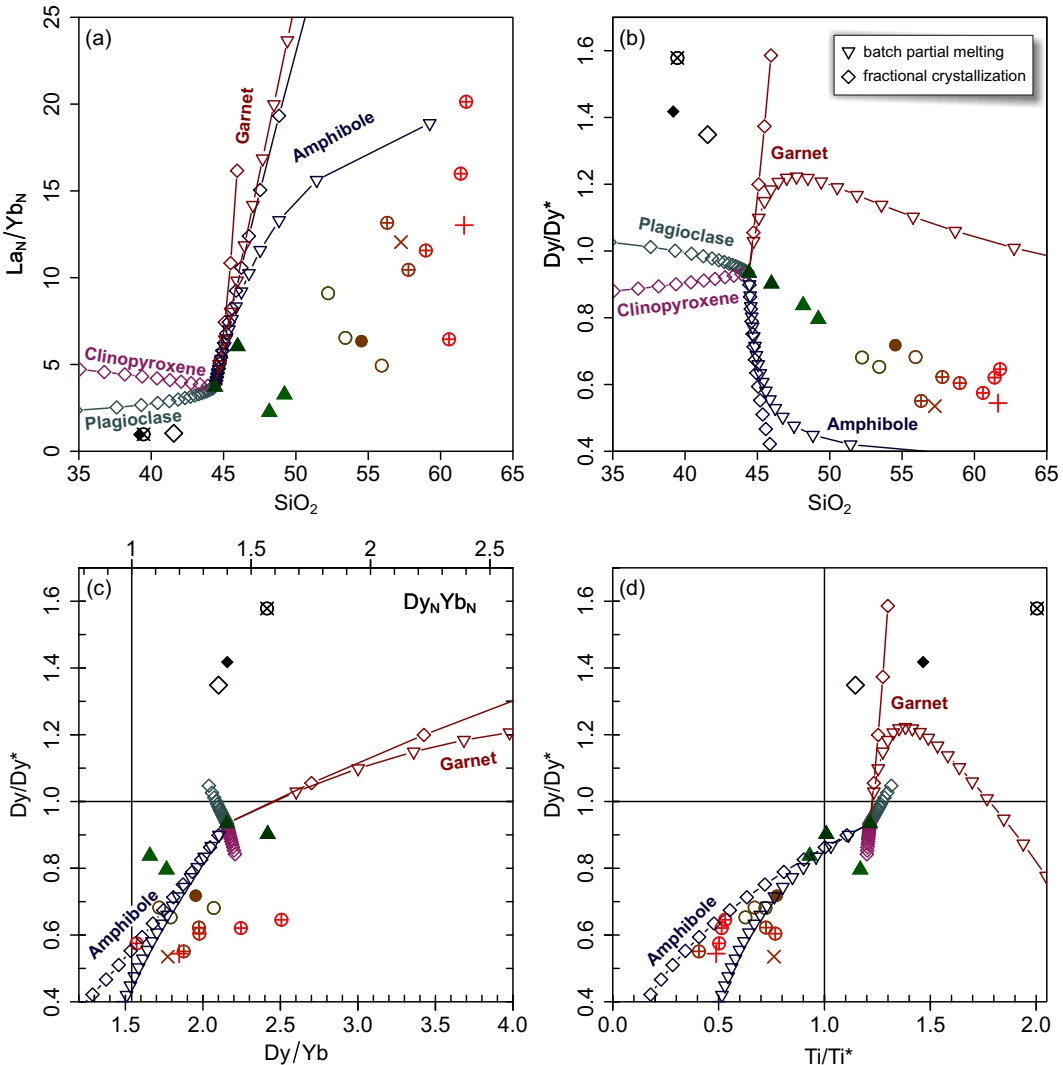


Fig. 16. Binary plots underlining the important petrogenetic role played by amphibole. (a) – SiO_2 (wt%) vs. the La_N/Yb_N ratio; (b) – SiO_2 (wt%) vs. the Dy/Dy^* parameter (Davidson et al., 2013); (c) – Dy/Yb vs. Dy/Dy^* ; (d) – Ti/Ti^* vs. Dy/Dy^* diagram. Plotting symbols as in Fig. 10. Please note that while the rationale of the Ti/Ti^* value follows Davidson et al. (2013), the calculation formula is different (see Analytical Techniques). For consistency with Figs 12 and 13, the normalizing values for Ti are based on average NMORB composition of Sun and McDonough (1989), and those for the REE are chondritic (Boynton, 1984). Also shown are trends of fractional crystallization (diamonds) and batch partial melting (triangles) (5% tick interval in both cases) for single mineral phases: amphibole, garnet, clinopyroxene and plagioclase. The partition coefficients are from Sisson (1994) (Amp), Johnson (1998) (Grt), Hart and Dunn (1993) with Johnson (1998) (Cpx) and McKenzie and O'Nions (1991) (Pl). For further discussion see text.

chambers that would have greater potential for fractionation and crustal contamination. However, it cannot be ruled out that this temporal evolution of compositions is just an artefact and that it simply reflects ongoing Cambrian erosion of the magmatic products down to the older arc roots, accompanied by contemporaneous intrusion by younger, inevitably shallower magma pulses. The former hypothesis still seems more likely thanks to the preserved vertical distribution of igneous rocks in a column > 1000 m high which is characterized by mafic cumulates in a deeply incised valley and tonalites close to the crest of the Khantaishir Mountain Range.

Apart from a few discordant analyses, most likely reflecting variable Pb loss, no older xenocrysts or cores were found in the studied zircons from the magmatic rocks. This seems to reflect the fact that the magmas were hot and mafic, with enhanced zircon solubility not favourable for unmelted zircon preservation (Janoušek, 2006; Watson and Harrison, 1983). Indeed Zr behaves incompatibly in the studied samples over the whole silica range, demonstrating that zircon saturation was never reached close to the liquidus. Thus the zircon grew relatively late in the dated samples. If present in the metabasic source, zircons were likely fully dissolved in the partial melt. In any case, substantial amounts of

zirconium could have been stored also in other phases, such as rutile, garnet, or hornblende (Kohn et al., 2015).

5.4. Regional correlation

Based on the petrologic, geochemical and age similarities, the newly discovered Cambrian arc-related magmatism in the Khantaishir Range could be correlated with similar occurrences in adjacent regions of Mongolia and Russia. The Cambrian subduction-related magmatic complexes can be traced through terranes bordering the Precambrian Tuva-Mongolia, Zabkhan, and Baydrag microcontinental segments (Badarch et al., 2002; Buslov et al., 2001; Demoux et al., 2009a; Kröner et al., 2011; Kuzmichev et al., 2001), as well as the southern and southwestern margin of the Siberian Craton (in present coordinates) (Fig. 17).

The north-easternmost occurrences of Cambrian magmatic-arc complexes (Fig. 18a) in the eastern CAOB are the Uda-Vitim island arc (Gordienko et al., 2010), the Tsagan-Zaba Complex in the Olkhon Terrane (Gladkochub et al., 2014) and the Dzhida Zone (Gordienko et al., 2006, 2007, 2015) of Transbaikalia. These complexes have been interpreted as parts of an island-arc system that bordered the southern

margin of the Siberian Craton (Gladkochub et al., 2014; Gordienko et al., 2006, 2010).

The second, separate group of arc-related magmatic bodies occurs in the eastern part of the Gorny Altai (Glorie et al., 2011; Kruk et al., 2007; Rudnev et al., 2008), considered as components of an Ediacaran–Cambrian island arc (named Kuznetsk–Altai arc) formed along the Siberian margin (Buslov et al., 2001, 2013; Dobretsov et al., 2004; Kruk et al., 2010, 2011; Ota et al., 2007). Fragments of island arcs of comparable age are also exposed in the Gornya Shoria and West Sayan (Rudnev et al., 2005, 2013a), in the Tannu-Ola Zone (c. 520 Ma, Mongush et al., 2011) and in the Kaakhem Batholith (563–535 Ma, Rudnev et al., 2006) of eastern Tuva (Fig. 18a).

A similar situation has been reported from other areas in western and southwestern Mongolia. In the Lake Zone, numerous island-arc complexes of Cambrian age have been described from the Kharanur and Sharatologoi plutons (Rudnev et al., 2009), Ureg Nuur area (Izokh et al., 2011), Bumbat-Hairhan Pluton, Bayan-Tsagaan-Nuur Ridge (Rudnev et al., 2012), Dariv Range (Kovalenko et al., 2014), Tugrik Pluton (Rudnev et al., 2013b) and the Bayan-Khairkhan Massif (Yarmolyuk et al., 2011).

Another similar age of c. 540 Ma from the Zambyn Nuruu Complex (Fig. 19a) was interpreted as timing the intrusion of a primitive continental magmatic arc (Buriánek et al., 2017). Widespread and generally island-arc related magmatism in the Lake Zone took place during the

Cambrian (c. 555–495 Ma), whereas at the western margin of the Lake Zone, a mid-Ordovician island-arc (c. 460 Ma) was recently found (Soejono et al., 2016).

Moreover, several studies of detrital zircons (dominant age peak at c. 520 Ma) from the Gorny Altai (Chen et al., 2015, 2016), Chinese Altai (Jiang et al., 2011; Long et al., 2010; Sun et al., 2008), Tseel (Jiang et al., 2012), Gobi Altai (Gibson et al., 2013) and the margin of the Baydrag microcontinent (Kröner et al., 2011) suggest an existence of a large Cambrian magmatic-arc system, both in western Mongolia and in the Gorny Altai.

However, it needs to be stressed that both ophiolite- and arc-related magmatic evolution of the units bordering the Precambrian Tuva-Mongolia, Zabkhan, and Baydrag microcontinental segments started at c. 570 Ma; however, the major period of the magmatic activity culminated at c. 510 Ma (Fig. 18b). In general, the late Neoproterozoic–Ordovician isotope province and corresponding crust-forming event were previously identified and well established in the central part of the CAOB (Kovalenko et al., 2004), the Lake Zone (Kovach et al., 2011) and Altay-Sayan region (Rudnev et al., 2013b). We suggest here, that the whole crust-forming event can be divided into two episodes (Dobretsov et al., 2003; Kozakov et al., 2013, 2015) and we focus here solely onto the younger, late Cambrian–Early Ordovician one.

Moreover, Neoproterozoic–Cambrian ophiolites and magmatic arc complexes have been described from the opposite side of the Baydrag

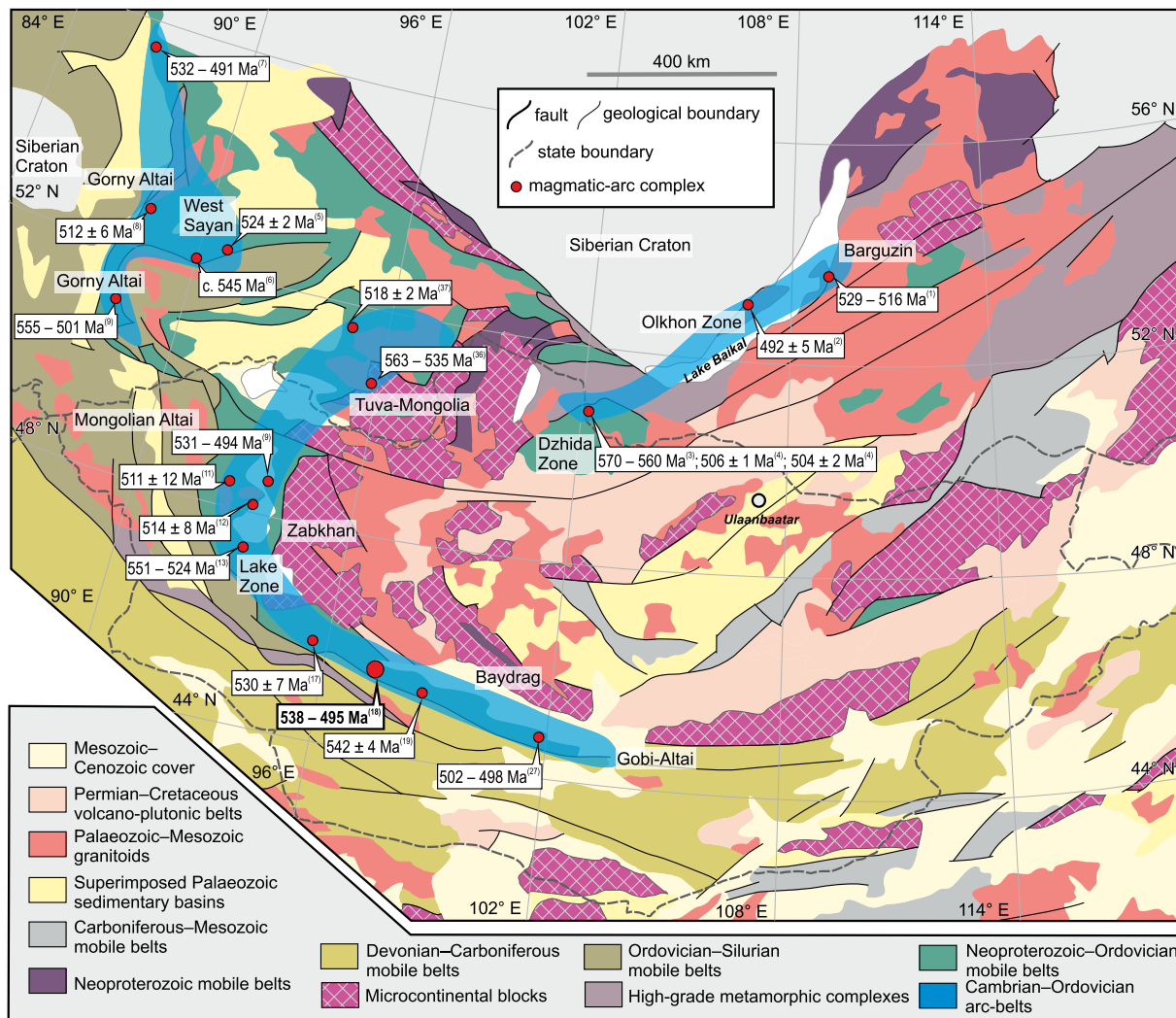


Fig. 17. Simplified tectonic map of the central CAOB depicting main lithotectonic domains (modified from Parfenov et al., 2003) and spatial distribution of Cambrian to Ordovician magmatic arcs; their zircon ages are also shown. Numbers in top-right corner of each box refer to references given in Fig. 18.

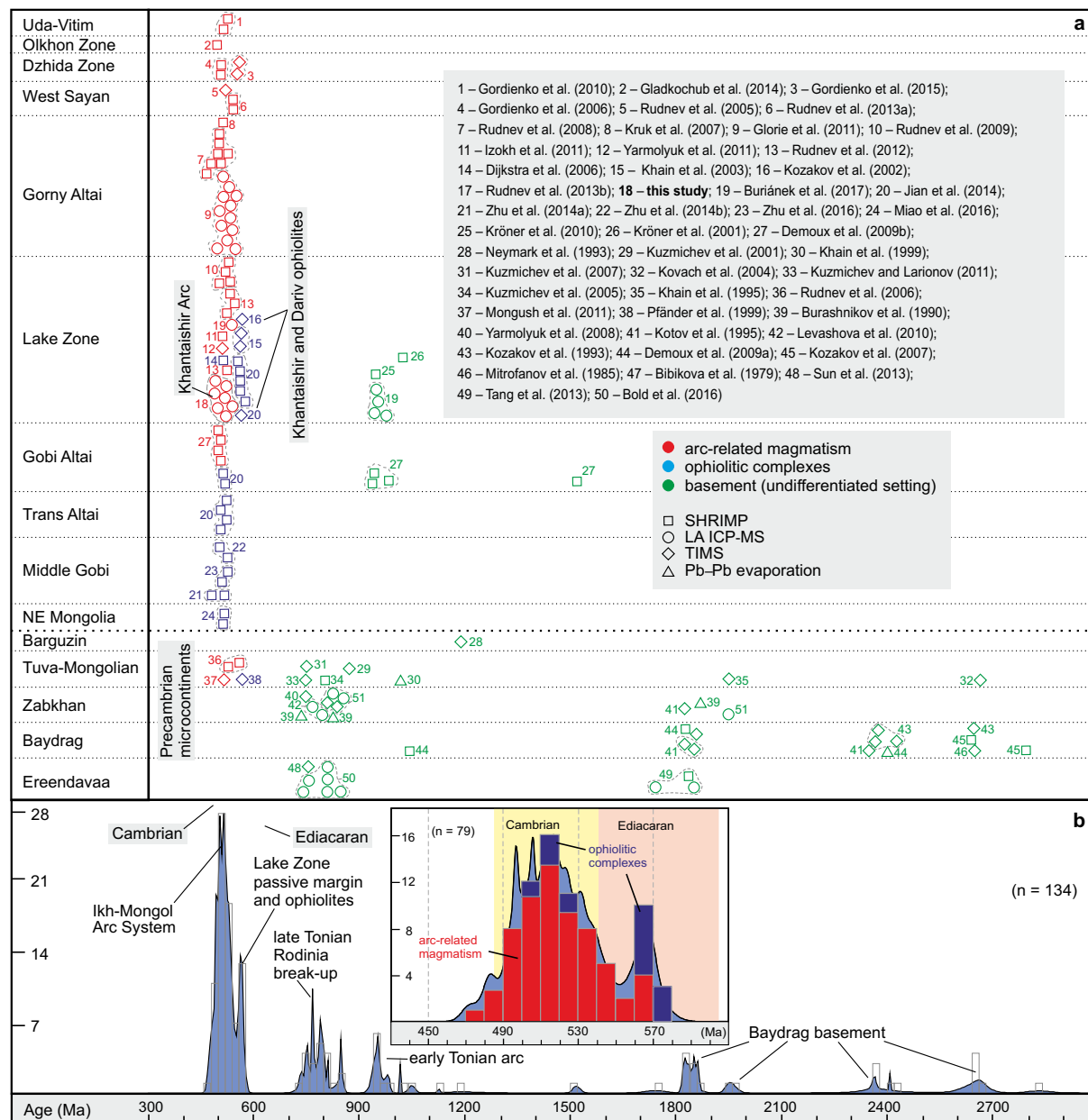


Fig. 18. (a) Correlation of U-Pb and Pb-Pb zircon ages arranged by individual microcontinents. For each, a range of basement ages, arc magmatism and ophiolites are given (in online version of this figure distinguished by colour). (b) – Frequency histograms and probability density plots of published zircon crystallization ages used in panel a, n – number of samples. Inset shows the detail of the main age peak. The density plots were produced by DensityPlotter (Vermeesch, 2012). Data sources: 1 – Gordienko et al. (2010); 2 – Gladkochub et al. (2014); 3 – Gordienko et al. (2015); 4 – Gordienko et al. (2006); 5 – Rudnev et al. (2005); 6 – Rudnev et al. (2013a); 7 – Rudnev et al. (2008); 8 – Kruck et al. (2007); 9 – Glorie et al. (2011); 10 – Rudnev et al. (2009); 11 – Izokh et al. (2011); 12 – Yarmolyuk et al. (2011); 13 – Rudnev et al. (2012); 14 – Dijkstra et al. (2006); 15 – Khain et al. (2003); 16 – Kozakov et al. (2002); 17 – Rudnev et al. (2013b); 18 – this study; 19 – Buriánek et al. (2017); 20 – Jian et al. (2014); 21 – Zhu et al. (2014a); 22 – Zhu et al. (2014b); 23 – Zhu et al. (2016); 24 – Miao et al. (2016); 25 – Kröner et al. (2010); 26 – Kröner et al. (2001); 27 – Demoux et al. (2009b); 28 – Neymark et al. (1993); 29 – Kuzmichev et al. (2001); 30 – Khain et al. (1999); 31 – Kuzmichev et al. (2007); 32 – Kovach et al. (2004); 33 – Kuzmichev and Larionov (2011); 34 – Kuzmichev et al. (2005); 35 – Khain et al. (1995); 36 – Rudnev et al. (2006); 37 – Mongush et al. (2011); 38 – Pfänder et al. (1999); 39 – Burashnikov (1990); 40 – Yarmolyuk et al. (2008); 41 – Kotov et al. (1995); 42 – Levashova et al. (2010); 43 – Kozakov et al. (1993); 44 – Demoux et al. (2009a); 45 – Kozakov et al. (2007); 46 – Mitrofanov et al. (1985); 47 – Bibikova et al. (1979); 48 – Sun et al. (2013); 49 – Tang et al. (2013); 50 – Bold et al. (2016).

Block as well (Demoux et al., 2009a; Kozakov et al., 2008, 2015; Jian et al., 2010; Kröner et al., 2011). This indicates the possible presence of an independent, (near?) contemporaneous and broadly parallel subduction zone there – again, this structure has not been a subject of the current study.

5.5. Synthesis and definition of the Ikh-Mongol Arc System

All the above data point to a major importance of ocean crust formation, subduction and associated magmatic activity within the

Neoproterozoic and early Palaeozoic oceanic system of the central CAOB (Fig. 18a). Unfortunately, direct correlation of these dismembered complexes is difficult and thus a potential continuation from the KMC to the eastern-central parts of the CAOB is, in part, speculative. Still, the studied KMC fits well into a belt of Cambrian arc-related magmatic complexes in terms of its position, composition and age (Fig. 18a–b). This belt, >1800 km in length, borders the outer margin of the Mongolian Precambrian ribbon continent, defining the western, external part of the Mongolian orocline (Xiao et al., 2015 and references therein) (Fig. 17). The spatial distribution indicates that many of the Cambrian

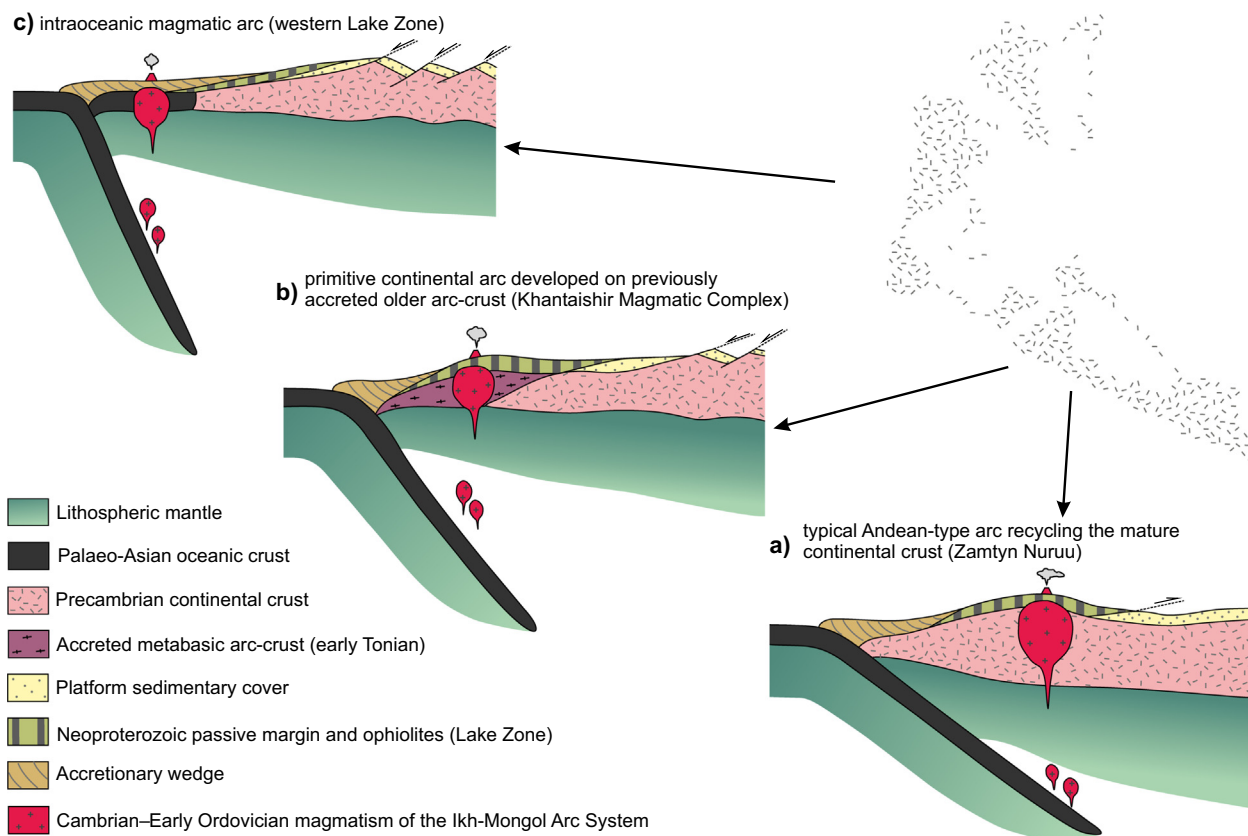


Fig. 19. Interpretative cross sections depicting different configurations of three known sections of the Ikh-Mongol Arc System. (a) Typical continental magmatic arc in the Zamtyr Nuruu founded on mature crust of the Baydrag Continent (Buriánek et al., 2017); (b) primitive continental arc developed on previously accreted older (early Tonian) arc in the Khantaishir Magmatic Complex (this study); (c) intraoceanic magmatic arc in the western Lake Zone (Rudnev et al., 2012; Soejono et al., 2016; Yarmolyuk et al., 2011).

to Ordovician magmatic complexes within this belt constituted a huge single subduction system.

This view agrees well with the concept of magmatic-arc systems, having operated in the Palaeo-Asian Ocean in late Neoproterozoic to Cambrian times (Dobretsov and Buslov, 2007; Şengör and Natal'in, 1996). Şengör et al. (1993) assumed the existence of a single and persistent Tuva-Mongol arc active over much of the early Palaeozoic. However, we argue that the main episode of magmatism and associated crustal growth was restricted to the interval of c. 530 to 490 Ma (Fig. 18b) and that the magmatic activity could have been related to a more complicated arc system, rather than to a single, continuous arc. Thus in order to avoid confusion, we coin the new term Ikh-Mongol Arc System for this giant Cambrian to early Ordovician structure.

In the quest for elucidating the petrogenesis of the Khantaishir segment of the Ikh-Mongol Arc System it is important to discuss the previous geological history of the Baydrag continental margin in the study area. There is growing evidence for an important early Tonian (c. 1000–850 Ma) subduction-related magmatism affecting the Palaeoproterozoic continental margin (Buriánek et al., 2017; Demoux et al., 2009b; Kozakov et al., 2014). In addition, the former authors showed that the Baydrag continental margin in the present-day Zamtyr Nuruu Range was the location of yet another (Cambrian) Andean-type subduction event. The magma sources of the Cambrian arc have been sought dominantly in the Palaeoproterozoic basement with a small contribution from the early Tonian arc (Fig. 19a).

Our data also fit a similar scenario; apart from the obvious mantle contribution, the KMC magmas also recycled the older, late Palaeoproterozoic mafic metaigneous arc crust (Fig. 19b). Based on Hf and Nd model ages, but lacking precise age data, we can only speculate that it could have been the same early Tonian Andean-type arc material as proposed by Buriánek et al. (2017). On the other hand, we found no

evidence for Baydrag basement-derived detritus except for the migmatite in the roof of the KMC that contains c. 750 Ma igneous-looking zircons. Similar ages were reported from extension-related rhyolite-andesite volcanic suite of the Baydrag Continent by Levashova et al. (2010, 2011). Some authors interpreted such a bimodal, extension-related igneous activity as a testimony of Rodinia break-up (Dobretsov et al., 2003; Yarmolyuk et al., 2008; Kheraskova et al., 2010).

The new data presented here improve the scenario proposed by Buriánek et al. (2017, their Fig. 17). The probability age distribution for arc-derived magmatic rocks and ophiolite complexes (Fig. 18b) shows that the Baydrag Continent formed at 2.7 to 1.8 Ga, followed by early Tonian active margin magmatism at around 950–930 Ma and late Tonian volcanism related to the Rodinia break-up at 800–700 Ma.

More importantly, we see a strong concentration of ages between 600 and 480 Ma that define two peaks: a narrow Ediacaran (with a c. 570 Ma maximum) and a wide Cambrian (c. 510 Ma). The former is interpreted in terms of ophiolites formation, back-arc and oceanic-arc magmatism of short-lived supra-subduction marginal basins finally obducted onto the Baydrag Continent in early Cambrian times (Khain et al., 2003; Štípká et al., 2010). The latter reflects voluminous arc magmatism affecting the entire Tuva-Mongol, Zabkhan and Baydrag continental margin, including the newly accreted units of the Lake Zone with ca. 570 Ma ophiolites.

Therefore it seems likely that the late Proterozoic ophiolite sequences and Precambrian continents formed a single, unified tectonic unit before the intrusion of Ikh-Mongol Arc System (Sal'nikova et al., 2001; Kovach et al., 2011; Bold et al., 2016; Buriánek et al., 2017). Depending on the exact position, the arc acquired a character of a typical Andean arc recycling the mature Palaeoproterozoic continental crust (e.g., Zamtyr Nuruu, Fig. 19a), of a primitive continental arc developed on previously accreted older (?early Tonian) arc crust (Khantaishir

Magmatic Complex, Fig. 19b) or of a typical intraoceanic arc (western Lake Zone, Fig. 19c).

In general, this paper represents a cautionary tale; the character of subduction (intraoceanic vs. Andean-type), and thus of the magma sources, may change dramatically along strike of an arc. This has grave consequences for models of crustal recycling in that the remelted recently accreted mafic arc-type contributions would be difficult to recognize by conventional (Hf-Nd) isotopic approaches and could easily be mistaken for a juvenile input (Kröner et al., 2014, 2017).

The Ikh-Mongol Arc System magmatism affected different regions of an extended continental margin in Cambrian to Early Ordovician times (Fig. 19). This magmatism heralded the onset of slab roll-back, related extension and formation of a giant accretionary sedimentary wedge forming the future Mongol Altai Terrane (Xiao and Santosh, 2014; Xiao et al., 2009b). Taken together, the Cambro-Ordovician Ikh-Mongol Arc System magmatism and associated formation of a giant accretionary sedimentary wedge represented the most important period of crustal growth in the Tuva-Mongolian realm of the CAOB.

6. Conclusions

The newly described Cambrian Khantaishir Magmatic Complex (KMC) occurs in the eastern Khantaishir Range (south-central Mongolia). Combined petrological and whole-rock geochemical research, complemented by *in-situ* U-Pb zircon ages and Hf isotopic compositions, yielded the following conclusions:

1. The KMC exhibits a section from deeper, ultramafic cumulates (coarse-grained Amp gabbros and hornblendites; c. 0.35–0.5 GPa) to shallower crustal levels with intermediate rock types (mainly Amp-Bt tonalites; c. 0.1–0.2 GPa).
2. U-Pb zircon dating provides evidence for long-lived Cambrian (538 ± 3 to 494 ± 3 Ma) magmatism, whereby the dominant mafic plutons mostly preceded the subordinate felsic igneous activity.
3. The (normal-) calc-alkaline geochemical signature and a characteristic enrichment in large-ion lithophile elements (LILE: including Li, Rb, K, Sr, and Pb) and U with Th relative to the high-field strength elements (HFSE: Nb and Ta) indicate an origin within an igneous arc.
4. The lack of significant zircon inheritance in the magmatic products and rather primitive zircon ϵ_{Hf} values ($> +3$ but for most samples $> +8$), as well as whole-rock Sr-Nd isotopic compositions imply that the arc was not founded on mature continental crust.
5. Even for the tonalite with the least radiogenic Hf, the two-stage whole-rock Nd and *in-situ* Hf-in-zircon crustal model ages preclude partial melting of metabasic crust older than c. 1.5 Ga.
6. Multiple intrusions of mafic magmas developed by fractional crystallization and/or accumulation of (Ol, Cpx), Amp + Bt, later joined by plagioclase. An important role is also ascribed to the magma mixing and to the exchange of xenocrysts/antecrysts between compositionally different melt batches derived from depleted mantle and lower crustal metabasic sources (remelting of the early Tonian arc?).
7. The KMC is only a small fragment of a belt of Cambrian-Ordovician arc-related magmatic complexes exceeding 1800 km in length – termed here the Ikh-Mongol Arc System. It decorates the outer margin of a chain of Precambrian microcontinents (Tuva-Mongolia, Zabkhan and Baydrag) that, together with accreted late Neoproterozoic marginal basins (Lake Zone), defines the western, external part of the Mongolian orocline.
8. We argue that the Cambro-Ordovician was the most important period of crustal growth in the Mongolian tract of the CAOB.

Supplementary data to this article can be found online at <https://doi.org/10.1016/j.gr.2017.10.003>.

Acknowledgements

The authors would like to thank Jitka Míková (Czech Geological Survey, Prague) for assistance with the Sr-Nd isotopic separations and Petr Gadas (Masaryk University, Brno) for help with the electron-microprobe analyses. The manuscript was improved significantly by detailed reviews of Wenjiao Xiao and Victor Kovach, and benefited from careful editorial work of Shoujie Liu. This research was financially supported by the Czech Science Foundation (GAČR) (P210/12/2205 and 17-17540S). The International Partnership (132744KYSB20160005) and the 100 Talents programs of the Chinese Academy of Sciences (both to Y.D.J.) are also acknowledged. This paper is dedicated to Prof. O. Gerel on occasion of her 75th birthday.

References

- Abdel-Rahman, A.M., 1994. Nature of biotites from alkaline, calc-alkaline and peraluminous magmas. *Journal of Petrology* 35, 525–541.
- Alonso-Perez, R., Müntener, O., Ulmer, P., 2009. Igneous garnet and amphibole fractionation in the roots of island arcs: experimental constraints on andesitic liquids. *Contributions to Mineralogy and Petrology* 157, 541–558.
- Andersen, D.J., Lindsley, D.H., Davidson, P.M., 1993. QUILF: a Pascal program to assess equilibria among Fe–Mg–Mn–Ti oxides, pyroxenes, olivine, and quartz. *Computers & Geosciences* 19, 1333–1350.
- Annen, C., Blundy, J.D., Sparks, R.S.J., 2006. The genesis of intermediate and silicic magmas in deep crustal hot zones. *Journal of Petrology* 47, 505–539.
- Arculus, R.J., 1987. The significance of source versus process in the tectonic controls of magma genesis. *Journal of Volcanology and Geothermal Research* 32, 1–12.
- Arndt, N.T., Goldstein, S.L., 1989. An open boundary between lower continental crust and mantle: its role in crust formation and crustal recycling. *Tectonophysics* 161, 201–212.
- Atherton, M., Petford, N., 1993. Generation of sodium-rich magmas from newly underplated basaltic crust. *Nature* 362, 144–146.
- Badarch, G., Cunningham, W.D., Windley, B.F., 2002. A new terrane subdivision for Mongolia: implications for the Phanerozoic crustal growth of Central Asia. *Journal of Asian Earth Sciences* 21, 87–110.
- Barbarin, B., 2005. Mafic magmatic enclaves and mafic rocks associated with some granitoids of the central Sierra Nevada Batholith, California: nature, origin, and relations with the hosts. *Lithos* 80, 155–177.
- Bateman, R., 1995. The interplay between crystallization, replenishment and hybridization in large felsic magma chambers. *Earth-Science Reviews* 39, 91–106.
- Beard, J.S., Ragland, P.C., Rushmer, T., 2004. Hydration crystallization reactions between anhydrous minerals and hydrous melt to yield amphibole and biotite in igneous rocks: description and implications. *The Journal of Geology* 112, 617–621.
- Belousova, E.A., Kostitsyn, Y.A., Griffin, W.L., Begg, G.C., O'Reilly, S.Y., Pearson, N.J., 2010. The growth of the continental crust: constraints from zircon Hf-isotope data. *Lithos* 119, 457–466.
- Bibikova, E.V., Gracheva, T.V., Makarov, V.A., Vorobjev, V.S., 1979. Geochronological borders for the southern part of East Transbaikalia from data of U-Pb method dating (in Russian). *Geochimiya* 2, 204–215.
- Blichert-Toft, J., Albarede, F., 1997. The Lu-Hf isotope geochemistry of chondrites and the evolution of the mantle–crust system. *Earth and Planetary Science Letters* 148, 243–258.
- Bold, U., Crowley, J.L., Smith, E.F., Sambuu, O., Macdonald, F.A., 2016. Neoproterozoic to early Paleozoic tectonic evolution of the Zavkhan Terrane of Mongolia: implications for continental growth in the Central Asian Orogenic Belt. *Lithosphere* 8, 729–750.
- Boynton, W.V., 1984. Cosmochemistry of the rare earth elements: meteorite studies. In: Henderson, P. (Ed.), *Rare Earth Element Geochemistry*. Elsevier, Amsterdam, pp. 63–114.
- Buchan, C., Pfänder, J., Kröner, A., Brewer, T.S., Tomurtogoo, O., Tomurhuu, D., Cunningham, D., Windley, B.F., 2002. Timing of accretion and collisional deformation in the Central Asian Orogenic Belt: implications of granite geochronology in the Bayankhongor Ophiolite Zone. *Chemical Geology* 192, 23–45.
- Burashnikov, V.V., 1990. Tectonics of the Urgamal Zone, Early Caledonides of Western Mongolia. Unpublished Ph.D. Thesis. Geological Institute, Russian Academy of Sciences, Moscow.
- Buriánek, D., Schulmann, K., Hrdličková, K., Hanžl, P., Janoušek, V., Gerdes, A., Lexa, O., 2017. Geochemical and geochronological constraints on distinct early-Neoproterozoic and Cambrian accretionary events along southern margin of the Baydrag Continent in western Mongolia. *Gondwana Research* 47, 200–227.
- Buslov, M.M., De Grave, J., 2015. Tectonics and geodynamics of the Altai-Sayan Foldbelt (southern Siberia). In: Kröner, A. (Ed.), *The Central Asian Orogenic Belt. Beiträge zur regionalen Geologie der Erde* vol. 32. Borntraeger Science Publishers, Stuttgart, pp. 93–154.
- Buslov, M.M., Saponova, I.Y., Watanabe, T., Obut, O.T., Fujiwara, Y., Iwata, K., Semakov, N.N., Sugai, Y., Smirnova, L.V., Kazansky, A.Y., 2001. Evolution of the paleo-Asian Ocean (Altai-Sayan region, Central Asia) and collision of possible Gondwana-derived terranes with the southern marginal part of the Siberian Continent. *Geosciences Journal* 5, 203–224.
- Buslov, M.M., Geng, H., Travin, A.V., Otgonbaatar, D., Kulikova, A.V., Ming, C., Stijn, G., Semakov, N.N., Rubanova, E.S., Abildaeva, M.A., Voitishuk, E.E., Trofimova, D.A., 2013. Tectonics and geodynamics of Gorny Altai and adjacent structures of the Altai-Sayan folded area. *Russian Geology and Geophysics* 54, 1250–1271.

- Carswell, D.A., Compagnoni, R. (Eds.), 2003. Ultrahigh Pressure Metamorphism. EMU Notes in Mineralogy vol. 5. Eötvös University Press, Budapest.
- Castro, A., Gerya, T.V., 2008. Magmatic implications of mantle wedge plumes: experimental study. *Lithos* 103, 138–148.
- Castro, A., Vogt, K., Gerya, T., 2013. Generation of new continental crust by sublithospheric silicic-magma reworking in arcs: a test of Taylor's andesite model. *Gondwana Research* 23, 1554–1566.
- Cervelli, P.F., Fournier, T.J., Freymueller, J.T., Power, J.A., Lisowski, M., Pauk, B.A., 2010. Geodetic constraints on magma movement and withdrawal during the 2006 eruption of Augustine Volcano. In: Power, J.A., Coombs, M.L., Freymueller, J.T. (Eds.), The 2006 Eruption of Augustine Volcano, Alaska. U.S. Geological Survey Professional Papers 1769, Reston, VA, pp. 427–452.
- Chen, M., Sun, M., Buslov, M.M., Cai, K., Zhao, G.C., Zheng, J.P., Rubanova, E.S., Voytishek, E.E., 2015. Neoproterozoic-middle Paleozoic tectono-magmatic evolution of the Gorny Altai Terrane, northwest of the Central Asian Orogenic Belt: constraints from detrital zircon U-Pb and Hf-isotope studies. *Lithos* 233, 223–236.
- Chen, M., Sun, M., Cai, K., Buslov, M.M., Zhao, G.C., Jiang, Y.D., Rubanova, E.S., Kulikova, A.V., Voytishek, E.E., 2016. The early Paleozoic tectonic evolution of the Russian Altai: implications from geochemical and detrital zircon U-Pb and Hf isotopic studies of meta-sedimentary complexes in the Charysh-Terekta-Ulagan-Sayan suture zone. *Gondwana Research* 34, 1–15.
- Chopin, C., 1984. Coesite and pure pyrope in high-grade blueschists from western Alps: a first record and some consequences. *Contributions to Mineralogy and Petrology* 86, 107–118.
- Clæsens, D.T., 1998. Coronas, reaction rims, symplectites and emplacement depth of the Rymmen Gabbro, Transscandinavian igneous belt, southern Sweden. *Mineralogical Magazine* 62, 743–757.
- Clemens, J.D., Stevens, G., 2012. What controls chemical variation in granitic magmas? *Lithos* 134–135, 317–329.
- Condie, K.C., Kröner, A., 2013. The building blocks of continental crust: evidence for a major change in the tectonic setting of continental growth at the end of the Archean. *Gondwana Research* 23, 394–402.
- Corfu, F., Hanchar, J.M., Hoskin, P.W.O., Kinny, P., 2003. Atlas of zircon textures. In: Hanchar, J.M., Hoskin, P.W.O. (Eds.), Zircon. Reviews in Mineralogy and Geochemistry 53. Mineralogical Society of America and Geochemical Society, Washington, pp. 469–503.
- Cornejo, P.C., Mahood, G.A., 1997. Seeing past the effects of re-equilibration to reconstruct magmatic gradients in plutons: La Gloria Pluton, central Chilean Andes. *Contributions to Mineralogy and Petrology* 127, 159–175.
- Davidson, J., Turner, S., Handley, H., Macpherson, C., Dosseto, A., 2007. Amphibole “sponge” in arc crust? *Geology* 35, 787–790.
- Davidson, J., Turner, S., Plank, T., 2013. Dy/Dy*: variations arising from mantle sources and petrogenetic processes. *Journal of Petrology* 54, 525–537.
- Davidson, J.P., Morgan, D.J., Charlier, B.L.A., Harlou, R., Hora, J.M., 2007. Microsampling and isotopic analysis of igneous rocks: implications for the study of magmatic systems. *Annual Review of Earth and Planetary Sciences* 35, 273–311.
- Debon, F., Le Fort, P., 1983. A chemical-mineralogical classification of common plutonic rocks and associations. *Transactions of the Royal Society of Edinburgh, Earth Sciences* 73, 135–149.
- Deering, C.D., Bachmann, O., 2010. Trace element indicators of crystal accumulation in silicic igneous rocks. *Earth and Planetary Science Letters* 297, 324–331.
- Demoux, A., Kröner, A., Badarch, G., Jian, P., Tomurhüü, D., Wingate, M.T.D., 2009a. Zircon ages from the Baydrag Block and the Bayankhongor Ophiolite Zone: time constraints on late Neoproterozoic to Cambrian subduction- and accretion-related magmatism in Central Mongolia. *The Journal of Geology* 117, 377–397.
- Demoux, A., Kröner, A., Liu, D., Badarch, G., 2009b. Precambrian crystalline basement in southern Mongolia as revealed by SHRIMP zircon dating. *International Journal of Earth Sciences* 98, 1365–1380.
- DePaolo, D.J., 1981. Trace element and isotopic effects of combined wallrock assimilation and fractional crystallization. *Earth and Planetary Science Letters* 53, 189–202.
- Dergunov, A.B. (Ed.), 2001. Tectonics, Magmatism, and Metallogeny of Mongolia. Routledge, London and New York.
- Dessimoz, M., Müntener, O., Ulmer, P., 2012. A case for hornblende dominated fractionation of arc magmas: the Chelan Complex (Washington Cascades). *Contributions to Mineralogy and Petrology* 163, 567–589.
- Didier, J., Barbarin, B. (Eds.), 1991a. Enclaves and Granite Petrology. Elsevier, Amsterdam.
- Didier, J., Barbarin, B., 1991b. The different types of enclaves in granites – nomenclature. In: Didier, J., Barbarin, B. (Eds.), Enclaves and Granite Petrology. Elsevier, Amsterdam, pp. 19–24.
- Dijkstra, A.H., Brouwer, F.M., Cunningham, W.D., Buchan, C., Badarch, G., Mason, P.R.D., 2006. Late Neoproterozoic proto-arc ocean crust in the Dariv Range, Western Mongolia: a supra-subduction zone end-member ophiolite. *Journal of the Geological Society (London)* 163, 363–373.
- Dobretsov, N.L., Buslov, M.M., 2007. Late Cambrian–Ordovician tectonics and geodynamics of Central Asia. *Russian Geology and Geophysics* 48, 71–82.
- Dobretsov, N.L., Buslov, M.M., Vernikovsky, V.A., 2003. Neoproterozoic to Early Ordovician evolution of the Paleo-Asian Ocean: implications to the break-up of Rodinia. *Gondwana Research* 6, 143–159.
- Dobretsov, N.L., Buslov, M.M., Yu, U., 2004. Fragments of oceanic islands in accretion-collision areas of Gorny Altai and Salair, southern Siberia, Russia: early stages of continental crustal growth of the Siberian Continent in Vendian–early Cambrian time. *Journal of Asian Earth Sciences* 23, 673–690.
- Dobrzhinetskaya, L.F., Faryad, S.W., Wallis, S., Cuthbert, S. (Eds.), 2011. Ultra-high Pressure Metamorphism. 25 years After the Discovery of Coesite and Diamond. Elsevier, Amsterdam.
- Domeier, M., Torsvik, T.H., 2014. Plate tectonics in the late Paleozoic. *Geoscience Frontiers* 5, 303–350.
- Droop, G.T.R., 1987. A general equation for estimating Fe^{3+} concentrations in ferromagnesian silicates using stoichiometric criteria. *Mineralogical Magazine* 51, 431–435.
- Dufek, J., Bergantz, G.W., 2005. Lower crustal magma genesis and preservation: a stochastic framework for the evaluation of basalt–crust interaction. *Journal of Petrology* 46, 2167–2195.
- Dymkova, D., Gerya, T., Burg, J.P., 2016. 2D thermomechanical modelling of continent–arc–continent collision. *Gondwana Research* 32, 138–150.
- Förster, H.-J., Tischendorf, G., Trumbull, R.B., 1997. An evaluation of the Rb vs. (Y + Nb) discrimination diagram to infer tectonic setting of silicic igneous rocks. *Lithos* 40, 261–293.
- Gibson, T.M., Myrow, P.M., Macdonald, F.A., Minjin, C., Gehrels, G.E., 2013. Depositional history, tectonics, and detrital zircon geochronology of Ordovician and Devonian strata in southwestern Mongolia. *GSA Bulletin* 125, 877–893.
- Gladkochub, D.P., Donskaya, T.V., Wingate, M.T.D., Poller, U., Kröner, A., Fedorovsky, V.S., Mazukabzov, A.M., Todt, W., Pisarevsky, S.A., 2008. Petrology, geochronology, and tectonic implications of c. 500 Ma metamorphic and igneous rocks along the northern margin of the Central Asian Orogen (Olkhon Terrane, Lake Baikal, Siberia). *Journal of the Geological Society (London)* 165, 235–246.
- Gladkochub, D.P., Donskaya, T.V., Fedorovsky, V.S., Mazukabzov, A.M., Sklyarov, E.V., Lavrenchuk, A.V., Lepekhina, E.N., 2014. Fragment of the early Paleozoic (~500 Ma) island arc in the structure of the Olkhon Terrane, Central Asian fold belt. *Doklady Earth Sciences* 457, 905–909.
- Glorie, S., De Grave, J., Buslov, M.M., Zhimulev, F.I., Izmer, A., Vandoorne, W., Ryabinin, A., van den Haute, P., Vanhaecke, F., Elburg, M.A., 2011. Formation and Palaeozoic evolution of the Gorny-Altaï-Altaï-Mongolia suture zone (South Siberia): zircon U/Pb constraints on the igneous record. *Gondwana Research* 20, 465–484.
- Goldstein, S.I., O'Nions, R.K., Hamilton, P.J., 1984. A Sm-Nd isotopic study of atmospheric dusts and particulates from major river systems. *Earth and Planetary Science Letters* 70, 221–236.
- Gordienko, I.V., Kovach, V.P., Gorokhovsky, D.V., Plotkina, Y.V., 2006. Composition, U-Pb age, and geodynamic setting of island-arc gabbroids and granitoids of the Dzhida Zone. *Russian Geology and Geophysics* 47, 948–955.
- Gordienko, I.V., Filimonov, A.V., Minina, O.R., Gornova, M.A., Medvedev, A.Y., Klimuk, V.S., Elbaev, A.L., Tomurtogoo, O., 2007. Dzhida island-arc system in the Paleoasian Ocean: structure and main stages of Vendian–Paleozoic geodynamic evolution. *Russian Geology and Geophysics* 48, 91–106.
- Gordienko, I.V., Bulgatov, A.N., Ruzhentsev, S.V., Minina, O.R., Klimuk, V.S., Vetrushskikh, L.I., Nekrasov, G.E., Lastochkin, N.I., Sitnikova, V.S., Metelkin, D.V., Goneger, T.A., Lepekhina, E.N., 2010. The late Riphean–Paleozoic history of the Uda-Vitim island arc system in the Transbaikalian sector of the Paleoasian Ocean. *Russian Geology and Geophysics* 51, 461–481.
- Gordienko, I.V., Gorokhovskiy, D.V., Elbaev, A.L., Bayanova, T.B., 2015. New data on the early Paleozoic gabbroid and granitoid magmatism age within the Dzhida Zone of Caledonides (southwestern Transbaikalia, North Mongolia). *Doklady Earth Sciences* 463, 817–821.
- Griffin, W.L., Pearson, N.J., Belousova, E., Jackson, S.E., van Achterbergh, E., O'Reilly, S.Y., Shee, S.R., 2000. The Hf isotope composition of cratonic mantle: LAM-MC-ICPMS analysis of zircon megacrysts in kimberlites. *Geochimica et Cosmochimica Acta* 64, 133–147.
- Grove, T.L., Till, C.B., Krawczynski, M.J., 2012. The role of H_2O in subduction zone magmatism. *Annual Review of Earth and Planetary Sciences* 40, 413–439.
- Guy, A., Schulmann, K., Janoušek, V., Štípká, P., Armstrong, R., Belousova, E., Dolgopolova, A., Seltmann, R., Lexa, O., Jiang, Y., Hanžl, P., 2015. Geophysical and geochemical nature of relaminated arc-derived lower crust underneath oceanic domain in southern Mongolia. *Tectonics* 34, 1030–1053.
- Hacker, B.R., Kelemen, P.B., Behn, M.D., 2011. Differentiation of the continental crust by relamination. *Earth and Planetary Science Letters* 307, 501–516.
- Hacker, B.R., Kelemen, P.B., Behn, M.D., 2015. Continental lower crust. *Annual Review of Earth and Planetary Sciences* 43, 167–205.
- Hart, S.R., Dunn, T., 1993. Experimental Cpx/melt partitioning of 24 trace elements. *Contributions to Mineralogy and Petrology* 113, 1–8.
- Hibbard, M.J., 1991. Textural anatomy of twelve magma-mixed granitoid systems. In: Didier, J., Barbarin, B. (Eds.), Enclaves and Granite Petrology. Elsevier, Amsterdam, pp. 431–444.
- Hibbard, M.J., 1995. Mixed magma rocks. *Petrography to Petrogenesis*. Prentice Hall, New Jersey, pp. 242–260.
- Hildreth, W., Moorbath, S., 1988. Crustal contributions to arc magmatism in the Andes of Central Chile. *Contributions to Mineralogy and Petrology* 98, 455–489.
- Holland, T.J.B., Blundy, J.D., 1994. Non-ideal interactions in calcic amphiboles and their bearing on amphibole-plagioclase thermometry. *Contributions to Mineralogy and Petrology* 116, 433–447.
- Hrdličková, K., Gerdes, A., Gilíková, H., Bat-Ulzii, D., Hanžl, P., 2010. Burd Gol Granite Massif as a product of the late Cambrian post-orogenic magmatism in the SE part of the Lake Zone, Gobi Altay, SW Mongolia. *Journal of Geosciences* 55, 369–386.
- Huppert, H.E., Sparks, R.S.J., 1988. The generation of granitic magmas by intrusion of basalt into continental crust. *Journal of Petrology* 29, 599–624.
- Hutchison, C.S., 1975. The norm, its variations, their calculation and relationships. *Schweizerische Mineralogische und Petrographische Mitteilungen* 55, 243–256.
- Izokh, A.E., Vishnevskii, A.V., Polyakov, G.V., Shelepaev, R.A., 2011. Age of picrite and picrodolerite magmatism in western Mongolia. *Russian Geology and Geophysics* 52, 7–23.
- Jacobsen, S.B., Wasserburg, G.J., 1980. Sm-Nd isotopic evolution of chondrites. *Earth and Planetary Science Letters* 50, 139–155.

- Jagoutz, O., Behn, M.D., 2013. Foundering of lower island-arc crust as an explanation for the origin of the continental Moho. *Nature* 504, 131–134.
- Jagoutz, O., Kelemen, P.B., 2015. Role of arc processes in the formation of continental crust. *Annual Review of Earth and Planetary Sciences* 43, 363–404.
- Jagoutz, O., Schmidt, M.W., 2012. The formation and bulk composition of modern juvenile continental crust: the Kohistan arc. *Chemical Geology* 298–299, 79–96.
- Janoušek, V., 2006. *Saturnin*, R language script for application of accessory-mineral saturation models in igneous geochemistry. *Geologica Carpathica* 57, 131–142.
- Janoušek, V., Moyen, J.F., 2014. Mass balance modelling of magmatic processes in *GCDkit*. In: Kumar, S., Singh, R.N. (Eds.), *Modelling of Magmatic and Allied Processes*. Society of Earth Scientists Series 83. Springer, Berlin, pp. 225–238.
- Janoušek, V., Bowes, D.R., Rogers, G., Farrow, C.M., Jelínek, E., 2000. Modelling diverse processes in the petrogenesis of a composite batholith: the Central Bohemian Pluton, Central European Hercynides. *Journal of Petrology* 41, 511–543.
- Janoušek, V., Braithwaite, C.J.R., Bowes, D.R., Gerdes, A., 2004. Magma-mixing in the genesis of Hercynian calc-alkaline granitoids: an integrated petrographic and geochemical study of the Sázava intrusion, Central Bohemian Pluton, Czech Republic. *Lithos* 78, 67–99.
- Janoušek, V., Farrow, C.M., Erban, V., 2006. Interpretation of whole-rock geochemical data in igneous geochemistry: introducing Geochemical Data Toolkit (*GCDkit*). *Journal of Petrology* 47, 1255–1259.
- Janoušek, V., Konopásek, J., Ulrich, S., Erban, V., Tajčmanová, L., Jeřábek, P., 2010. Geochemical character and petrogenesis of Pan-African Amspoort suite of the Boundary Igneous Complex in the Kaoko Belt (NW Namibia). *Gondwana Research* 18, 688–707.
- Janoušek, V., Moyen, J.F., Martin, H., Erban, V., Farrow, C., 2016. *Geochemical Modelling of Igneous Processes – Principles and Recipes in R Language. Bringing the Power of R to a Geochemical Community*. Springer-Verlag, Berlin, Heidelberg.
- Jian, P., Kröner, A., Windley, B.F., Shi, Y., Zhang, F., Miao, L., Tomurhuu, D., Zhang, W., Liu, D., 2010. Zircon ages of the Bayankhongor ophiolite mélange and associated rocks: time constraints on Neoproterozoic to Cambrian accretionary and collisional orogenesis in Central Mongolia. *Precambrian Research* 177, 162–180.
- Jian, P., Kröner, A., Jahn, B.M., Windley, B.F., Shi, Y., Zhang, W., Zhang, F., Miao, L., Tomurhuu, D., Liu, D., 2014. Zircon dating of Neoproterozoic and Cambrian ophiolites in West Mongolia and implications for the timing of orogenic processes in the central part of the Central Asian Orogenic Belt. *Earth-Science Reviews* 133, 62–93.
- Jiang, Y.D., Sun, M., Zhao, G.C., Yuan, C., Xiao, W.J., Xia, X.P., Long, X.P., Wu, F.Y., 2011. Precambrian detrital zircons in the early Paleozoic Chinese Altai: their provenance and implications for the crustal growth of central Asia. *Precambrian Research* 189, 140–154.
- Jiang, Y.D., Sun, M., Kröner, A., Tumurkhuu, D., Long, X.P., Zhao, G.C., Yuan, C., Xiao, W.J., 2012. The high-grade Tseel Terrane in SW Mongolia: an early Paleozoic arc system or a Precambrian slier? *Lithos* 142–143, 95–115.
- Johnson, K.T.M., 1998. Experimental determination of partition coefficients for rare earth and high-field-strength elements between clinopyroxene, garnet, and basaltic melt at high pressures. *Contributions to Mineralogy and Petrology* 133, 60–68.
- Kay, R.W., Kay, S.M., 1993. Delamination and delamination magmatism. *Tectonophysics* 219, 177–189.
- Kelemen, P.B., 1995. Genesis of high Mg# andesites and the continental crust. *Contributions to Mineralogy and Petrology* 120, 1–19.
- Kelemen, P.B., Behn, M.D., 2016. Formation of lower continental crust by relamination of buoyant arc lavas and plutons. *Nature Geoscience* 9, 197–205.
- Kemp, A.I.S., Hawkesworth, C.J., 2014. 4.11 – growth and differentiation of the continental crust from isotope studies of accessory minerals. In: Holland, H.D., Turekian, K.K. (Eds.), *Treatise on Geochemistry*, Second Edition Elsevier, Oxford, pp. 379–421.
- Khain, E.V., Neimark, I.A., Amelin Yu, V., 1995. The Caledonian stage of remobilization of the Precambrian basement of the Gargan block, the Eastern Sayan (isotopic geochronological data) (in Russian). *Doklady Akademii Nauk* 342, 776–780.
- Khain, E.V., Bibikova, E.V., Degtyarev, K., Gibsher, A.S., Didenko, A.N., Klochko, A.N., Ryttsk, E.Y., Sal'nikova, E.B., Fedotova, A.A., 1999. The Paleo-Asian Ocean in the Neoproterozoic and early Paleozoic: new isotope geochronological data. *Geological Development of Proterozoic Pericratonic and Palaeoceanic Structures of Northern Eurasia*, pp. 175–181 Abstract Volume. St. Petersburg.
- Khain, E.V., Bibikova, E.V., Sal'ikova, E.B., Kröner, A., Gibsher, A.S., Didenko, A.N., Degtyarev, K.E., Fedotova, A.A., 2003. The Palaeo-Asian Ocean in the Neoproterozoic and early Palaeozoic: new geochronologic data and palaeotectonic reconstructions. *Precambrian Research* 122, 329–358.
- Kheraskova, T.N., Bush, V.A., Didenko, A.N., Samygina, S.G., 2010. Breakup of Rodinia and early stages of evolution of the Paleoasiatic Ocean. *Tectonophysics* 44, 3–24.
- Kohn, M.J., Corrie, S.L., Markley, C., 2015. The fall and rise of metamorphic zircon. *American Mineralogist* 100, 897–908.
- Košler, J., Sylvester, P.J., 2003. Present trends and the future of zircon in geochronology: Laser ablation ICPMS. In: Hanchar, J.M., Hoskin, P.W.O. (Eds.), *Zircon. Reviews in Mineralogy and Geochemistry* 53. Mineralogical Society of America and Geochemical Society, Washington, pp. 243–275.
- Košler, J., Fonneland, H., Sylvester, P.J., Tubrett, M., Pedersen, R.B., 2002. U-Pb dating of detrital zircons for sediment provenance studies – a comparison of laser ablation ICPMS and SIMS techniques. *Chemical Geology* 182, 605–618.
- Kotov, A.B., Kozakov, I.K., Bibikova, E.V., Sal'nikova, E.B., Kirnozova, T.I., Kovach, V.P., 1995. Duration of regional metamorphic episodes in areas of polycyclic endogenic processes – a U-Pb geochronological study (in Russian). *Petrology* 3, 567–575.
- Kovach, V.P., Matukov, D.I., Berezhnaya, N.G., 2004. Tectonics of Precambrian mobile belts. The 32nd IGC Florence, Session: T31.01. 1263.
- Kovach, V.P., Yarmolyuk, V.V., Kovalenko, V.I., Kozlovskyi, A.M., Kotov, A.B., Terent'eva, L.B., 2011. Composition, sources, and mechanisms of formation of the continental crust of the Lake Zone of the Central Asian Caledonides. II. Geochemical and Nd isotope data. *Petrology* 19, 399–425.
- Kovalenko, D.V., Mongush, A.A., Ageeva, O.A., Eenzhin, G., 2014. Sources and geodynamic environments of formation of Vendian–early Paleozoic magmatic complexes in the Daribi Range, Western Mongolia. *Petrology* 22, 389–417.
- Kovalenko, V.I., Yarmolyuk, V.V., Kovach, V.P., Kotov, A.B., Kozakov, I.K., Sal'nikova, E.B., Larin, A.M., 2004. Isotope provinces, mechanisms of generation and sources of the continental crust in the Central Asian mobile belt: geological and isotopic evidence. *Journal of Asian Earth Sciences* 23, 605–627.
- Kozakov, I.K., Bibikova, E., Neymark, L.A., Kimozova, T.I., 1993. The Baydaric Block. In: Rudnik, B.A., Sokolov, Y.M., Filatova, L.I. (Eds.), *The Early Precambrian of the Central Asian Fold Belt*. Nauka, St. Petersburg, pp. 118–137.
- Kozakov, I.K., Sal'nikova, E.B., Khain, E.V., Kovach, V.P., Berezhnaya, N.G., Yakovleva, S.Z., Plotkina, Y.V., 2002. Early Caledonian crystalline rocks of the Lake Zone in Mongolia: formation history and tectonic settings as deduced from U-Pb and Sm-Nd datings. *Geotectonics* 36, 156–166.
- Kozakov, I.K., Sal'nikova, E.B., Wang, T., Didenko, A.N., Plotkina, Y., Podkovyrov, V.N., 2007. Early Precambrian crystalline complexes of the Central Asian microcontinent: age, sources, tectonic position. *Stratigraphy and Geological Correlation* 15, 121–140.
- Kozakov, I.K., Sal'nikova, E.B., Kovach, V.P., Yarmolyuk, V.V., Anisimova, I.V., Kozlovskii, A.M., Plotkina, Y.V., Myskova, T.A., Fedoseenko, A.M., Yakovleva, S.Z., Sugorakova, A.M., 2008. Vendian stage in formation of the early Caledonian superterrane in Central Asia. *Stratigraphy and Geological Correlation* 16, 360–382.
- Kozakov, I.K., Sal'nikova, E.B., Yarmolyuk, V.V., Kovach, V.P., Kozlovskii, A.M., Anisimova, I.V., Plotkina, Y., Fedoseenko, A.M., Yakovleva, S.Z., Erdenezhargal, C., 2013. Crustal growth stages in the Songino block of the Early Caledonian superterrane in Central Asia: I. Geological and geochronological data. *Petrology* 21, 203–220.
- Kozakov, I.K., Kovach, V.P., Bibikova, E.V., Kirnozova, T.I., Lykhin, D.A., Plotkina, Y., Tolmacheva, E.V., Fugzan, M.M., Erdenezhargal, C., 2014. Late Riphean episode in the formation of crystalline rock complexes in the Dzabkhan microcontinent: geological, geochronologic, and Nd isotopic-geochemical data. *Petrology* 22, 480–506.
- Kozakov, I.K., Kovach, V.P., Yakovleva, S.Z., Anisimova, I.V., Kozlovskiy, A.M., Fedoseenko, A.M., 2015. Main stages in the evolution and geodynamic setting of the South Hangay Metamorphic Belt, Central Asia. *Petrology* 23, 309–330.
- Kröner, A., Tomurtogoo, O., Badarch, G., Windley, B.F., Kozakov, I.K., 2001. New zircon ages and significance for crustal evolution in Mongolia. In: Sklyarov, E.V. (Ed.), *IGCP-440 Workshop*, Guidebook and Abstract Volume. Irkutsk, pp. 142–145.
- Kröner, A., Windley, B.F., Badarch, G., Tomurtogoo, O., Hegner, E., Jahn, B.M., Gruscha, S., Khain, E.V., Demoux, A., Wingate, M.T.D., 2007. Accretionary growth and crust formation in the Central Asian Orogenic Belt and comparison with the Arabian-Nubian Shield. In: Hatcher Jr., R.D., Carlson, M.P., McBride, J.H., Martínez Catalán, J.R. (Eds.), *4-D Framework of Continental Crust*. Geological Society of America Memoirs 200, pp. 181–209.
- Kröner, A., Lehmann, J., Schulmann, K., Demoux, A., Lexa, O., Tomurhuu, D., Štípková, P., Liu, D., Wingate, M.T.D., 2010. Lithostratigraphic and geochronological constraints on the evolution of the Central Asian Orogenic Belt in SW Mongolia: early Paleozoic rifting followed by late Paleozoic accretion. *American Journal of Science* 310, 523–574.
- Kröner, A., Demoux, A., Zack, T., Rojas-Agramonte, Y., Jian, P., Tomurhuu, D., Barth, M., 2011. Zircon ages for a felsic volcanic rock and arc-related early Palaeozoic sediments on the margin of the Baydrag microcontinent, Central Asian Orogenic Belt, Mongolia. *Journal of Asian Earth Sciences* 42, 1008–1017.
- Kröner, A., Kovach, V., Belousova, E., Hegner, E., Armstrong, R., Dolgopolova, A., Seltmann, R., Alexeiev, D.V., Hoffmann, J.E., Wong, J., Sun, M., Cai, K., Wang, T., Tong, Y., Wilde, S.A., Degtyarev, K.E., Rytsk, E., 2014. Reassessment of continental growth during the accretionary history of the Central Asian Orogenic Belt. *Gondwana Research* 25, 103–125.
- Kröner, A., Kovach, V., Alexeiev, D., Wang, K.L., Wong, J., Degtyarev, K., Kozakov, I., 2017. No excessive crustal growth in the Central Asian Orogenic Belt: further evidence from field relationships and isotopic data. *Gondwana Research* 50, 135–166.
- Kruk, N.N., Rudnev, S.N., Shokalsky, S.P., Babin, G.A., Kubida, M.L., Lepikhina, E.N., Kovach, V.P., 2007. Age and tectonic position of plagiogranites of Sarakoksha Massif (Altai Mountains) (in Russian). *Litosfera* 137–146.
- Kruk, N.N., Vladimirov, A.G., Babin, G.A., Shokalsky, S.P., Sennikov, N.V., Rudnev, S.N., Volkova, N.I., Kovach, V.P., Serov, P.A., 2010. Continental crust in Gorny Altai: nature and composition of protoliths. *Russian Geology and Geophysics* 51, 431–446.
- Kruk, N.N., Rudnev, S.N., Vladimirov, A.G., Shokalsky, S.P., Kovach, V.P., Serov, P.A., Volkova, N.I., 2011. Early–middle Paleozoic granitoids in Gorny Altai, Russia: implications for continental crust history and magma sources. *Journal of Asian Earth Sciences* 42, 928–948.
- Kusbach, V., Janoušek, V., Hasalová, P., Schulmann, K., Fanning, C.M., Erban, V., Ulrich, S., 2015. Importance of crustal relamination in origin of the orogenic mantle peridotite–high-pressure granulite association: example from the Náměšt' Granulite Massif (Bohemian Massif, Czech Republic). *Journal of the Geological Society (London)* 172, 479–490.
- Kuzmichev, A.B., Larionov, A.N., 2011. The Sarkhoi Group in East Sayan: Neoproterozoic (~770–800 Ma) volcanic belt of the Andean type. *Russian Geology and Geophysics* 52, 685–700.
- Kuzmichev, A.B., Bibikova, E.V., Zhuravlev, D.Z., 2001. Neoproterozoic (~800 Ma) orogeny in the Tuva-Mongolia Massif (Siberia): island arc–continent collision at the northeast Rodinia margin. *Precambrian Research* 110, 109–126.
- Kuzmichev, A.B., Kröner, A., Hegner, E., Dunyi, L., Yusheng, W., 2005. The Shishkhid ophiolite, northern Mongolia: a key to the reconstruction of a Neoproterozoic island-arc system in central Asia. *Precambrian Research* 138, 125–150.
- Kuzmichev, A.B., Sklyarov, E., Postnikov, A., Bibikova, E., 2007. The Oka Belt (Southern Siberia and northern Mongolia): a Neoproterozoic analog of the Japanese Shimanto Belt? *Island Arc* 16, 224–242.
- Lamb, M.A., Badarch, G., 2001. Paleozoic sedimentary basins and volcanic arc systems of southern Mongolia: new geochemical and petrographic constraints. In: Hendrix,

- S.M., Davis, A.G. (Eds.), Paleozoic and Mesozoic Tectonic Evolution of Central and Eastern Asia: From Continental Assembly to Intracontinental Deformation. Geological Society of America Memoirs 194, pp. 117–149.
- Lancaster, P.J., Storey, C.D., Hawkesworth, C.J., Dhuime, B., 2011. Understanding the roles of crustal growth and preservation in the detrital zircon record. *Earth and Planetary Science Letters* 305, 405–412.
- Larrea, P., França, Z., Lago, M., Widom, E., Galé, C., Ubide, T., 2013. Magmatic processes and the role of antecrysts in the genesis of Corvo Island (Azores Archipelago, Portugal). *Journal of Petrology* 54, 769–793.
- Leake, B.E., Woolley, A.R., Arps, C.E.S., Birch, W.D., Gilbert, M.C., Grice, J.D., Hawthorne, F.C., Kato, A., Kisch, H.J., Krivovichev, V.G., Linthout, K., Laird, J., Mandarino, J., Maresch, W.V., Nickel, E.H., Rock, N.M.S., Schumacher, J.C., Smith, J.C., Stephenson, N.C.N., Whittaker, E.J.W., Youzhi, G., 1997. Nomenclature of amphiboles: report of the Subcommittee on Amphiboles of the International Mineralogical Association Commission on New Minerals and Mineral Names. *Mineralogical Magazine* 61, 295–321.
- Lee, C.T., Anderson, D.L., 2015. Continental crust formation at arcs, the arclogite 'delamination' cycle, and one origin for fertile melting anomalies in the mantle. *Science Bulletin* 60, 1141–1156.
- Lee, C.T., Bachmann, O., 2014. How important is the role of crystal fractionation in making intermediate magmas? Insights from Zr and P systematics. *Earth and Planetary Science Letters* 393, 266–274.
- Lehmann, J., Schulmann, K., Lexa, O., Corsini, M., Kröner, A., Štípká, P., Tomurhuu, D., Otgonbator, D., 2010. Structural constraints on the evolution of the Central Asian Orogenic Belt in SW Mongolia. *American Journal of Science* 310, 575–628.
- Levashova, N.M., Kalugin, V.M., Gibbs, A.S., Yff, J., Ryabinin, A.B., Meert, J.G., Malone, S.J., 2010. The origin of the Bayardic microcontinent, Mongolia: constraints from paleomagnetism and geochronology. *Tectonophysics* 485, 306–320.
- Levashova, N.M., Meert, J.G., Gibbs, A.S., Grice, W.C., Bazhenov, M.L., 2011. The origin of microcontinents in the Central Asian Orogenic Belt: constraints from paleomagnetism and geochronology. *Precambrian Research* 185, 37–54.
- Liew, T.C., Hofmann, A.W., 1988. Precambrian crustal components, plutonic associations, plate environment of the Hercynian Fold Belt of Central Europe: indications from a Nd and Sr isotopic study. *Contributions to Mineralogy and Petrology* 98, 129–138.
- Long, X.P., Yuan, C., Sun, M., Xiao, W.J., Zhao, G.C., Wang, Y.J., Cai, K., Xia, X.P., Xie, L.W., 2010. Detrital zircon ages and Hf isotopes of the early Paleozoic flysch sequence in the Chinese Altai, NW China: new constrains on depositional age, provenance and tectonic evolution. *Tectonophysics* 480, 213–231.
- Lu, Z., Dzurisin, D., Biggs, J., Wicks, C., McNutt, S., 2010. Ground surface deformation patterns, magma supply, and magma storage at Okmok volcano, Alaska, from InSAR analysis: I. Intereruption deformation, 1997–2008. *Journal of Geophysical Research: Solid Earth* 115. <https://doi.org/10.1029/2009JB006969>.
- Ludwig, K.R., 2003. Isoplot/Ex Version 3.00. A Geochronological Toolkit for Microsoft Excel, User's Manual. Berkeley Geochronology Center Special Publications 4, Berkeley.
- Ludwig, K.R., 2012. Isoplot/Ex Version 3.75. A geochronological toolkit for Microsoft Excel, User's Manual. Berkeley Geochronology Center Special Publications 5, Berkeley.
- Lugnair, G.W., Marti, K., 1978. Lunar initial $^{143}\text{Nd}/^{144}\text{Nd}$: differential evolution line of the lunar crust and mantle. *Earth and Planetary Science Letters* 39, 349–357.
- Maierová, P., Schulmann, K., Lexa, O., Guillot, S., Štípká, P., Janoušek, V., Čadek, O., 2016. European Variscan orogenetic evolution as an analogue of Tibetan–Himalayan orogen – insights from petrology and numerical modeling. *Tectonics* 35, 1760–1780.
- Marinov, N.A., Zonenshain, L.P., Blagonravov, V.A. (Eds.), 1973. Geology of the Mongolian People's Republic. 2. Magmatism, Metamorphism, Tectonics (in Russian). Nedra, Moscow.
- Matsumoto, I., Tomurtogoo, O., 2003. Petrological characteristics of the Hantaishir Ophiolite Complex, Altai Region, Mongolia: coexistence of podiform chromitite and boninite. *Gondwana Research* 6, 161–169.
- McKenzie, D., O'Nions, R.K., 1991. Partial melt distributions from inversion of rare earth element concentrations. *Journal of Petrology* 32, 1021–1091.
- Miao, L., Baatar, M., Zhang, F., Anaad, C., Zhu, M.S., Yang, S., 2016. Cambrian Kherlen ophiolite in northeastern Mongolia and its tectonic implications: SHRIMP zircon dating and geochemical constraints. *Lithos* 261, 128–143.
- Mitrofanov, F.P., Bibikova, E.V., Gracheva, T.V., Kozakov, I.K., Sumin, L.V., Shuleshko, I.K., 1985. Archaean isotope age of tonalite ("grey") gneisses within the Caledonian structures of Central Mongolia (in Russian). *Doklady Akademii Nauk* 284, 670–674.
- Miyashiro, A., 1974. Volcanic rock series in island arcs and active continental margins. *American Journal of Science* 274, 321–355.
- Molina, J.F., Moreno, J.A., Castro, A., Rodríguez, C., Fershtater, G.B., 2015. Calcic amphibole thermobarometry in metamorphic and igneous rocks: new calibrations based on plagioclase/amphibole Al–Si partitioning and amphibole/liquid Mg partitioning. *Lithos* 232, 286–305.
- Mongkoltip, P., Ashworth, J.R., 1983. Quantitative estimation of an open-system symplectite-forming reaction: restricted diffusion of Al and Si in coronas around olivine. *Journal of Petrology* 24, 635–661.
- Mongush, A.A., Lebedev, V.I., Kovach, V.P., Sal'nikova, E.B., Druzhkova, E.K., Yakovleva, S.Z., Plotkina, Y., Zagornaya, N.Y., Travin, A.V., Serov, P.A., 2011. The tectonomagmatic evolution of structure-lithologic complexes in the Tannu-Ola Zone, Tuva, in the late Vendian–early Cambrian (from geochemical, Nd isotope, and geochronological data). *Russian Geology and Geophysics* 52, 503–516.
- Moore, J.G., Lockwood, J.P., 1973. Origin of comb layering and orbicular structure, Sierra Nevada Batholith, California. *Geological Society of America Bulletin* 84, 1–20.
- Morimoto, N., 1988. Nomenclature of pyroxenes. *Mineralogical Magazine* 52, 535–550.
- Mossakovskiy, A.A., Ruzhentsev, S.V., Samygina, S.G., Kheraskova, T.N., 1994. Central Asian fold belt: geodynamic evolution and formation history. *Geotectonics* 27, 445–474.
- Münntener, O., Kelemen, P.B., Grove, T.L., 2001. The role of H_2O during crystallization of primitive arc magmas under uppermost mantle conditions and genesis of igneous pyroxenites: an experimental study. *Contributions to Mineralogy and Petrology* 141, 643–658.
- Neymark, L.A., Rytsk, E.Yu., Rizvanova, N.G., 1993. Hercynian age and Precambrian crustal protolith for Barguzin granitoids of Angaro-Bitimskii Batholith (in Russian). *Doklady Akademii Nauk* 331, 726–729.
- O'Hara, M.J., 1977. Geochemical evolution during fractional crystallisation of a periodically refilled magma chamber. *Nature* 266, 503–507.
- Ota, T., Utsunomiya, A., Uchio, Y., Isozaki, Y., Buslov, M.M., Ishikawa, A., Maruyama, S., Kitajima, K., Kaneko, Y., Yamamoto, H., Katayama, I., 2007. Geology of the Gorny Altai subduction–accretion complex, southern Siberia: tectonic evolution of an Ediacaran–Cambrian intra-oceanic arc–trench system. *Journal of Asian Earth Sciences* 30, 666–695.
- Otamendi, J.E., Ducea, M.N., Bergantz, G.W., 2012. Geological, petrological and geochemical evidence for progressive construction of an arc crustal section, Sierra de Valle Fértil, Famatinian Arc, Argentina. *Journal of Petrology* 53, 761–800.
- Parfenov, L.M., Khanchuk, A.I., Badarch, G., Miller, R.J., Naumova, V.V., Nokleberg, W.J., Ogasawara, M., Prokopiev, A.V., Yan, H., 2003. Preliminary Northeast Asia geodynamics map, sheet 2, scale 1:5,000,000. US Geological Survey Open-File Report 03-205.
- Paterson, S.R., Žák, J., Janoušek, V., 2008. Growth of complex sheeted zones during recycling of older magmatic units into younger: Sawmill Canyon area, Tuolumne Batholith, Sierra Nevada, California. *Journal of Volcanology and Geothermal Research* 177, 457–484.
- Pearce, J.A., 1982. Trace element characteristics of lavas from destructive plate boundaries. In: Thorpe, R.S. (Ed.), *Andesites: Orogenic Andesites and Related Rocks*. John Wiley & Sons, Chichester, pp. 525–548.
- Pearce, J.A., 2008. Geochemical fingerprinting of oceanic basalts with applications to ophiolite classification and the search for Archean oceanic crust. *Lithos* 100, 14–48.
- Pearce, J.A., 2014. Immobile element fingerprinting of ophiolites. *Elements* 10, 101–108.
- Pearce, J.A., Peate, D.W., 1995. Tectonic implications of the composition of volcanic arc magmas. *Annual Review of Earth and Planetary Sciences* 23, 251–285.
- Peccerillo, A., Taylor, S.R., 1976. Geochemistry of Eocene calc-alkaline volcanic rocks from the Kastamonu area, Northern Turkey. *Contributions to Mineralogy and Petrology* 58, 63–81.
- Pfänder, J., Jochum, K.P., Todt, W., Kröner, A., 1999. Relationships between the mantle, lower crust and upper crust within the Agardagh-Tes Chem ophiolite, Central Asia: evidence from petrologic, trace element, and isotopic data. *Ophioliti* 24, 151–152.
- Pistone, M., Blundy, J.D., Brooker, R.A., 2015. Textural and chemical consequences of interaction between hydrous mafic and felsic magmas: an experimental study. *Contributions to Mineralogy and Petrology* 171, 1–21.
- Plank, T., Kelley, K.A., Zimmer, M.M., Hauri, E.H., Wallace, P.J., 2013. Why do mafic arc magmas contain ~4 wt% water on average? *Earth and Planetary Science Letters* 364, 168–179.
- Powell, R., 1984. Inversion of the assimilation and fractional crystallization (AFC) equations: characterization of contaminants from isotope and trace element relationships in volcanic suites. *Journal of the Geological Society (London)* 141, 447–452.
- Rapp, R.P., Watson, E.B., 1995. Dehydration melting of metabasalt at 8–32 kbar: implications for continental growth and crust–mantle recycling. *Journal of Petrology* 36, 891–931.
- Rapp, R.P., Norman, M.D., Laporte, D., Yaxley, G.M., Martin, H., Foley, S.F., 2010. Continent formation in the Archean and chemical evolution of the cratonic lithosphere: melt–rock reaction experiments at 3–4 GPa and petrogenesis of Archean Mg-diorites (sanukitoids). *Journal of Petrology* 51, 1237–1266.
- Ridolfi, F., Renzulli, A., Puerini, M., 2010. Stability and chemical equilibrium of amphibole in calc-alkaline magmas: an overview, new thermobarometric formulations and application to subduction-related volcanoes. *Contributions to Mineralogy and Petrology* 160, 45–66.
- Roberts, M.P., Clemens, J.D., 1993. Origin of high-potassium, calc-alkaline, I-type granitoids. *Geology* 21, 825–828.
- Rojas-Agramonte, Y., Kröner, A., Demoux, A., Xia, X., Wang, W., Donskaya, T., Liu, D., Sun, M., 2011. Detrital and xenocrystic zircon ages from Neoproterozoic to Palaeozoic arc terranes of Mongolia: significance for the origin of crustal fragments in the Central Asian Orogenic Belt. *Gondwana Research* 19, 751–763.
- Rudnev, S.N., Babin, G.A., Vladimirov, A.G., Krusk, N.N., Shokalsky, S.P., Borisov, S.M., Travin, A.V., Levchenkov, O.A., Terleev, A.A., Kuibida, M.L., 2005. Geologic setting, age, and geochemical model of the formation of West Sayan plagiogranitoids. *Geologiya i Geofizika* 46, 170–187.
- Rudnev, S.N., Vladimirov, A.G., Ponomarchuk, V.A., Bibikova, E.V., Sergeev, S.A., Plotkina, Y.V., Bayanova, T.B., 2006. The Kaakhem polychronous granitoid batholith, eastern Tuva: composition, age, sources, and geodynamic setting (in Russian). *Litosfera* 200, 3–33.
- Rudnev, S.N., Borisov, S.M., Babin, G.A., Levchenkov, O.A., Makeev, A.F., Serov, P.A., Matukov, D.I., Plotkina, Y., 2008. Early Paleozoic batholiths in the northern part of the Kuznetsk Alatau: composition, age, and sources. *Petrology* 16, 395–419.
- Rudnev, S.N., Izokh, A.E., Kovach, V.P., Shelepaev, R.A., Terent'eva, L.B., 2009. Age, composition, sources, and geodynamic environments of the origin of granitoids in the northern part of the Ozernaya Zone, western Mongolia: growth mechanisms of the Paleozoic continental crust. *Petrology* 17, 439–475.
- Rudnev, S.N., Izokh, A.E., Borisenko, A.S., Shelepaev, R.A., Orihashi, Y., Lobanov, K.V., Vishnevsky, A.V., 2012. Early Paleozoic magmatism in the Bumbat–Hairhan area of the Lake Zone in western Mongolia (geological, petrochemical, and geochronological data). *Russian Geology and Geophysics* 53, 425–441.
- Rudnev, S.N., Babin, G.A., Kovach, V.P., Kiseleva, V.Y., Serov, P.A., 2013a. The early stages of island-arc plagiogranitoid magmatism in Gornaya Shoriya and West Sayan. *Russian Geology and Geophysics* 54, 20–33.

- Rudnev, S.N., Kovach, V.P., Ponomarchuk, V.A., 2013b. Vendian–early Cambrian island-arc plagiogranitoid magmatism in the Altai-Sayan folded area and in the Lake Zone of western Mongolia (geochronological, geochemical, and isotope data). *Russian Geology and Geophysics* 54, 1272–1287.
- Rudnick, R.L., Gao, S., 2003. The composition of the continental crust. In: Holland, H.D., Turekian, K.K. (Eds.), *Treatise on Geochemistry 3, The Crust* (ed. R.L. Rudnick). Elsevier-Pergamon, Oxford, pp. 1–64.
- Sal'nikova, E.B., Kozakov, I.K., Kotov, A.B., Kröner, A., Todt, W., Bibikova, E.V., Nutman, A., Yakovleva, S.Z., Kovach, V.P., 2001. Age of Palaeozoic granites and metamorphism in the Tuvino-Mongolian Massif of the Central Asian Mobile Belt: loss of a Precambrian microcontinent. *Precambrian Research* 110, 143–164.
- Schulmann, K., Lexa, O., Janoušek, V., Lardeaux, J.M., Edel, J.B., 2014. Anatomy of a diffuse cryptic suture zone: an example from the Bohemian Massif, European Variscides. *Geology* 42, 275–278.
- Sengör, A.M.C., Natal'in, B.A., 1996. Turkic-type orogeny and its role in the making of the continental crust. *Annual Review of Earth and Planetary Sciences* 24, 263–337.
- Sengör, A.M.C., Natal'in, B.A., Burtman, V.S., 1993. Evolution of the Altaiid tectonic collage and Palaeozoic crustal growth in Eurasia. *Nature* 364, 299–307.
- Shand, S.J., 1943. *Eruptive Rocks. Their Genesis, Composition, Classification, and Their Relation to Ore-Deposits With a Chapter on Meteorite*. John Wiley & Sons, New York.
- Shervais, J.W., 1982. Ti-V plots and the petrogenesis of modern and ophiolitic lavas. *Earth and Planetary Science Letters* 59, 101–118.
- Sisson, T.W., 1994. Hornblende–melt trace-element partitioning measured by ion microprobe. *Chemical Geology* 117, 331–344.
- Smith, D.J., 2014. Clinopyroxene precursors to amphibole sponge in arc crust. *Nature Communications* 5. <https://doi.org/10.1038/ncomms5329>.
- Söderlund, U., Patchett, P.J., Vervoort, J.D., Isachsen, C.E., 2004. The ^{176}Lu decay constant determined by Lu-Hf and U-Pb isotope systematics of Precambrian mafic intrusions. *Earth and Planetary Science Letters* 219, 311–324.
- Soejono, I., Burianek, D., Svojková, M., Žáček, V., Čáp, P., Janoušek, V., 2016. Mid-Ordovician and Late Devonian magmatism in the Togtokhinchil Complex: new insight into the formation and accretionary evolution of the Lake Zone (western Mongolia). *Journal of Geosciences* 61, 5–23.
- Solgadi, F., Sawyer, E.W., 2008. Formation of igneous layering in granodiorite by gravity flow: a field, microstructure and geochemical study of the Tuolumne Intrusive Suite at Sawmill Canyon, California. *Journal of Petrology* 49, 2009–2042.
- Spandler, C., Pirard, C., 2013. Element recycling from subducting slabs to arc crust: a review. *Lithos* 170–171, 208–223.
- Steiger, R.H., Jäger, E., 1977. Subcommission on Geochronology: convention on the use of decay constants in geo- and cosmochronology. *Earth and Planetary Science Letters* 36, 359–362.
- Štípká, P., Schulmann, K., Lehmann, J., Corsini, M., Lexa, O., Tomurhuu, D., 2010. Early Cambrian eclogites in SW Mongolia: evidence that the Paleo-Asian Ocean suture extends further east than expected. *Journal of Metamorphic Geology* 28, 915–933.
- Sun, L.X., Ren, B.F., Zhao, F.Q., Ji, S.P., Geng, J.Z., 2013. Late Paleoproterozoic magmatic records in Erguna Massif: evidence from the zircon U-Pb dating of granitic gneisses (in Chinese with English abstract). *Geological Bulletin of China* 32, 341–352.
- Sun, M., Yuan, C., Xiao, W.J., Long, X.P., Xia, X.P., Zhao, G.C., Lin, S.F., Wu, F.Y., Kröner, A., 2008. Zircon U-Pb and Hf isotopic study of gneissic rocks from the Chinese Altai: progressive accretionary history in the early to middle Palaeozoic. *Chemical Geology* 247, 352–383.
- Sun, S.S., McDonough, W.F., 1989. Chemical and isotopic systematics of oceanic basalts: implications for mantle composition and processes. In: Saunders, A.D., Norry, M. (Eds.), *Magmatism in the Ocean Basins*. Geological Society of London Special Publications 42, pp. 313–345.
- Tang, J., Xu, W.L., Wang, F., Wang, W., Xu, M.J., Zhang, Y.H., 2013. Geochronology and geochemistry of Neoproterozoic magmatism in the Erguna Massif, NE China: petrogenesis and implications for the breakup of the Rodinia supercontinent. *Precambrian Research* 224, 597–611.
- Tatsumi, Y., 2005. The subduction factory: how it operates in the evolving Earth. *GSA Today* 15, 4–10.
- Tatsumi, Y., Eggins, S., 1995. Subduction Zone Magmatism. *Frontiers in Earth Sciences*. Blackwell, Cambridge, Mass.
- Taylor, S.R., 1967. The origin and growth of continents. *Tectonophysics* 4, 17–34.
- Taylor, S.R., McLennan, S.M., 1995. The geochemical evolution of the continental crust. *Reviews in Geophysics* 33, 241–265.
- Taylor, S.R., McLennan, S.M., 2009. *Planetary Crusts: Their Composition, Origin and Evolution*. Cambridge University Press, Cambridge.
- Turner, S.P., Stüwe, K., 1992. Low-pressure corona textures between olivine and plagioclase in unmetamorphosed gabbros from Black Hill, South Australia. *Mineralogical Magazine* 56, 503–509.
- Vermeesch, P., 2012. On the visualisation of detrital age distributions. *Chemical Geology* 312–313, 190–194.
- Vernon, R.H., 1984. Microgranitoid enclaves in granites – globules of hybrid magma quenched in a plutonic environment. *Nature* 309, 438–439.
- Volkova, N.I., Sklyarov, E.V., 2007. High-pressure complexes of Central Asian Fold Belt: geologic setting, geochemistry, and geodynamic implications. *Russian Geology and Geophysics* 48, 83–90.
- Watson, E.B., Harrison, T.M., 1983. Zircon saturation revisited: temperature and composition effects in a variety of crustal magma types. *Earth and Planetary Science Letters* 64, 295–304.
- Weaver, B.L., Tarney, J., 1984. Empirical approach to estimating the composition of the continental crust. *Nature* 310, 575–577.
- Whitney, D.L., Evans, B.W., 2010. Abbreviations for names of rock-forming minerals. *American Mineralogist* 95, 185–187.
- Wiebe, R.A., 1996. Mafic-silicic layered intrusions: the role of basaltic injections on magmatic processes and the evolution of silicic magma chambers. *Transactions of the Royal Society of Edinburgh, Earth Sciences* 87, 233–242.
- Wiebe, R.A., Collins, W.J., 1998. Depositional features and stratigraphic sections in granitic plutons: implications for the emplacement and crystallization of granitic magma. *Journal of Structural Geology* 20, 1273–1289.
- Wilhem, C., Windley, B.F., Stampfli, G.M., 2012. The Altaids of Central Asia: a tectonic and evolutionary innovative review. *Earth-Science Reviews* 113, 303–341.
- Windley, B.F., Alexeev, D., Xiao, W.J., Kröner, A., Badarch, G., 2007. Tectonic models for accretion of the Central Asian Orogenic Belt. *Journal of the Geological Society (London)* 164, 31–47.
- Witt-Eickschen, G., Seck, H.A., 1991. Solubility of Ca and Al in orthopyroxene from spinel peridotite: an improved version of an empirical geothermometer. *Contributions to Mineralogy and Petrology* 106, 431–439.
- Wood, D.A., 1980. The application of a Th-Hf-Ta diagram to problems of tectonomagmatic classification and to establishing the nature of crustal contamination of basaltic lavas of the British Tertiary volcanic province. *Earth and Planetary Science Letters* 50, 11–30.
- Xia, X.P., Sun, M., Geng, H.Y., Sun, Y., Wang, Y.J., Zhao, G.C., 2011. Quasi-simultaneous determination of U-Pb and Hf isotope compositions of zircon by excimer-laser-ablation multiple-collector ICPMS. *Journal of Analytical Atomic Spectrometry* 26, 1868–1871.
- Xiao, W.J., Santosh, M., 2014. The western Central Asian Orogenic Belt: a window to accretionary orogenesis and continental growth. *Gondwana Research* 25, 1429–1444.
- Xiao, W.J., Windley, B.F., Badarch, G., Sun, S., Li, J., Qin, K., Wang, Z., 2004. Palaeozoic accretionary and convergent tectonics of the southern Altaids: implications for the growth of Central Asia. *Journal of the Geological Society (London)* 161, 339–342.
- Xiao, W.J., Windley, B.F., Huang, B.C., Han, C.M., Yuan, C., Chen, H.L., Sun, M., Sun, S., Li, J.L., 2009a. End-Permian to mid-Triassic termination of the accretionary processes of the southern Altaids: implications for the geodynamic evolution, Phanerozoic continental growth, and metallogeny of Central Asia. *International Journal of Earth Sciences* 98, 1189–1217.
- Xiao, W.J., Windley, B.F., Yuan, C., Sun, M., Han, C.M., Lin, S.F., Chen, H.L., Yan, Q.R., Liu, D.Y., Qin, K.Z., Li, J.L., Sun, S., 2009b. Paleozoic multiple subduction–accretion processes of the southern Altaids. *American Journal of Science* 309, 221–270.
- Xiao, W.J., Windley, B.F., Sun, S., Li, J.L., Huang, B., Han, C.M., Yuan, C., Sun, M., Chen, H., 2015. A tale of amalgamation of three Permo-Triassic collage systems in Central Asia: oroclines, sutures, and terminal accretion. *Annual Review of Earth and Planetary Sciences* 43, 477–507.
- Yakubchuk, A., 2004. Architecture and mineral deposit settings of the Altaiid orogenic collage: a revised model. *Journal of Asian Earth Sciences* 23, 761–779.
- Yanshin, A.L., 1965. Tectonic structure of Eurasia (in Russian). *Geotektonika* 5, 3–35.
- Yarmolyuk, V.V., Kovalenko, V.I., Anisimova, I.V., Sal'nikova, E.B., Kovach, V.P., Kozakov, I.K., Kozlovsky, A.M., Kudryashova, E.A., Kotov, A.B., Plotkina, Y., Terent'eva, L.B., Yakovleva, S.Z., 2008. Late Riphean alkali granites of the Zabhan microcontinent: evidence for the timing of Rodinia breakup and formation of microcontinents in the Central Asian Fold belt. *Doklady Earth Sciences* 420, 583–588.
- Yarmolyuk, V.V., Kovach, V.P., Kovalenko, V.I., Sal'nikova, E.B., Kozlovskii, A.M., Kotov, A.B., Yakovleva, S.Z., Fedoseenko, A.M., 2011. Composition, sources, and mechanism of continental crust growth in the Lake Zone of the Central Asian Caledonides: I. Geological and geochronological data. *Petrology* 19, 55–78.
- Yogodzinski, G.M., Lees, J.M., Churikova, T.G., Dorendorf, F., Wörner, G., Volynets, O.N., 2001. Geochemical evidence for the melting of subducting oceanic lithosphere at plate edges. *Nature* 409, 500–504.
- Žák, J., Paterson, S.R., Janoušek, V., Kabele, P., 2009. The Mammoth Peak sheeted complex, Tuolumne Batholith, Sierra Nevada, California: a record of initial growth or late thermal contraction in a magma chamber? *Contributions to Mineralogy and Petrology* 158, 447–470.
- Zandt, G., Gilbert, H., Owens, T.J., Ducea, M., Saleeby, J., Jones, C.H., 2004. Active foundering of a continental arc root beneath the southern Sierra Nevada in California. *Nature* 431, 41–46.
- Zhang, Y., Sun, M., Yuan, C., Xu, Y., Long, X.P., Tomurhuu, D., Wang, C., He, B., 2015. Magma mixing origin for high Ba-Sr granitic pluton in the Bayankhongor area, central Mongolia: response to slab roll-back. *Journal of Asian Earth Sciences* 113, 353–368.
- Zhu, M.S., Baatar, M., Miao, L., Anaad, C., Zhang, F., Yang, S., Li, Y., 2014a. Zircon ages and geochemical compositions of the Manlay ophiolite and coeval island arc: implications for the tectonic evolution of South Mongolia. *Journal of Asian Earth Sciences* 96, 108–122.
- Zhu, M.S., Miao, L., Baatar, M., Zhang, F., Anaad, C., Yang, S., Li, Y., 2014b. Zircon ages and geochemical data of the Biluuutin ovoo ophiolite: implication for the tectonic evolution of South Mongolia. *International Geology Review* 56, 1769–1782.
- Zhu, M.S., Miao, L., Baatar, M., Zhang, F., Anaad, C., Yang, S., Li, X., 2016. Early Paleozoic oceanic inliers and reconstruction of accretionary tectonics in the Middle Gobi region, Mongolia: evidence from SHRIMP zircon U-Pb dating and geochemistry. *Journal of Asian Earth Sciences* 127, 300–313.
- Zonenshain, L.P., 1973. The evolution of Central Asiatic geosynclines through sea-floor spreading. *Tectonophysics* 19, 213–232.
- Zonenshain, L.P., Kuzmin, M.I., 1978. The Khan-Taishir ophiolitic complex of Western Mongolia, its petrology, origin and comparison with other ophiolitic complexes. *Contributions to Mineralogy and Petrology* 67, 95–109.
- Zonenshain, L.P., Kuzmin, M.I., Moralev, V.M., 1976. *Global Tectonics, Magmatism and Metallogeny* (in Russian). Nedra, Moscow.
- Zorin, Y., 1999. *Geodynamics of the western part of the Mongolia–Okhotsk collisional belt, Trans-Baikal region (Russia) and Mongolia*. *Tectonophysics* 306, 33–56.